Project ID: TPF-5(352) - 0092-19-19

USE OF RECYCLED MATERIALS AS MECHANICALLY STABILIZED EARTH (MSE) RETAINING WALL REINFORCED BACKFILLS
PHASE II: LARGE-SCALE TESTING

Project ID: TPF-5(352) - 0092-19-15

MSE: RCA-GEOTEXTILE INTERACTION "TUFA"

Authors:

Azin Mardani
Royal Military College of Canada
21am105@queensu.ca

Aiyoub Abbaspour, Ph.D.
George Mason University
aabbaspo@gmu.edu

Burak F. Tanyu, Ph.D.
George Mason University
btanyu@gmu.edu

Greg Siemens, Ph.D.
Royal Military College of Canada
siemensg@queensu.ca

William J. Likos, Ph.D.
University of Wisconsin-Madison
likos@wisc.edu

DRAFT – September 16, 2022

Recycled Materials Resource Center
University of Wisconsin-Madison
Madison, WI 53706 USA

PREFACE

The overall goal of this project is to facilitate use of recycled materials in reinforced backfills for mechanically stabilized earth (MSE) retaining wall construction. Activities described in this report represent Phase II of a larger effort that has been previously documented in a Recycled Materials Resource Center (RMRC) report (Soleimanbeigi et al., 2016) and related journal and conference publications (Yin et al., 2016, Yin et al., 2017; Soleimanbeigi and Likos, 2019; Soleimanbeigi et al., 2019; Soleimanbeigi et al., 2022). Phase II includes collaboration among three research institutions: the University of Wisconsin-Madison (UW), the Royal Military College of Canada (RMC), and George Mason University (GMU). This report documents RMRC projects TPF-5(352) - 0092-19-19 (PI: W. Likos) and TPF-5(352) - 0092-19-19 (PI: B. Tanyu) administered through UW and GMU, respectively.

The Phase I project effort was designed to address many of the critical aspects in beneficial use of recycled materials for construction applications, with emphasis on use of recycled concrete aggregate (RCA) and recycled asphalt pavement (RAP) in MSE wall construction. This included a comprehensive literature review for a wide range of recycled materials, an overview of MSE wall design and performance, and a laboratory experimental testing program focused on mechanical and hydraulic properties of RCA and RAP in the context of MSE walls. Laboratory experiments were conducted using representative samples of RCA and RAP to assess internal shear strength, geosynthetic interface strength, creep potential, temperature dependent shear strength, and drainage/filtration performance of RCA-geosynthetic systems. Results from the Phase I effort indicate that RCA and RAP are potentially suitable materials for use as MSE wall backfill from a mechanical property perspective, but that comprehensively assessing hydraulic performance for MSE applications requires more detailed investigation with careful consideration of physical scale and flow conditions.

The Phase II effort described in this report was conducted to evaluate the suitability of RCA in MSE wall applications from a hydraulic (drainage/clogging) perspective, and specifically when the system is reinforced with woven geotextiles. Previous studies from the GMU research team (e.g., Abbaspour et al., 2018; Abbaspour and Tanyu, 2019a; Abbaspour and Tanyu, 2019b; Tanyu and Abbaspour, 2020) show that hydraulic performance of RCA-geotextile systems can be affected by one of two major clogging phenomena (physical and/or chemical) depending on the environment and fluid flow conditions. Physical clogging is predominant in saturated fluid environments under continuous flow conditions, as the pore water more likely remains chemically under-saturated with respect to minerals that precipitate tufa. Such conditions inhibit formation or deposition of precipitate and, in some cases, can even lead to the dissolution of readily soluble minerals in the RCA material. On the other hand, the relatively large seepage forces associated with saturated flow systems can cause fines within RCA to migrate onto geotextiles in contact with the RCA and reduce their ability to permeate water. Gradation of the RCA and permittivity of the geotextile are thus important factors affecting migration of fines and associated physical clogging. Chemical clogging (precipitate formation), on the other hand, tends to dominate in environments characterized by periodic flow conditions with repeated cycles of wetting and drying, which is more typical of MSE wall conditions in field applications. Calcareous tufa (calcium-based crystals that may grow on the geotextile) is derived by diagenetic calcite precipitation (Abbaspour and Tanyu, 2019b), followed by evaporative precipitate formations, dominantly gypsum, that becomes

active due to wetting and drying cycles. Tufa deposition within the geotextile filaments can lead to a reduction in filtration capacity of the RCA/geotextile system.

The overall goal of the Phase II effort documented herein has been to closely replicate field conditions in terms of scale (i.e., large-scale experiments), flow conditions (i.e., multidimensional 2-D, 3-D flow), and wetting-drying cycles. Two sets of complementary experiments were designed to investigate hydraulic performance of RCA-woven geotextile systems: one that replicates a large-scale MSE wall structure through physical modeling conducted at the Royal Military College of Canada's MSE wall testing facility and the other as a series of large-scale column tests used to evaluate one-dimensional vertical flow conditions under conditions identical to the large-scale MSE wall experiment. Numerical seepage models were developed to understand hydraulic behavior in the wall experiments and to generalize the flow phenomena for different boundary conditions. In both experimental set-ups the following conditions were simulated:

- The gradation of the RCA was selected and processed to have minimum fines content. Based on previous findings, this was necessary to create a scenario where the potential for physical clogging does not become the leading mechanism for clogging, thereby maximizing the potential for understanding chemical clogging and the conditions that lead to it;

- Spacing between the reinforcement geotextiles was selected to be as close to each other as allowed in GRS-IBS systems, thereby providing a worst-case scenario in terms of potential clogging;

- The aggregate within the RCA was selected to contain calcium-based compounds, thereby providing a worst case scenario in terms of chemical clogging.

Findings from this study demonstrate that with proper gradation, RCA could be considered as backfill for MSE walls even if the reinforcements are woven geotextiles. This is anticipated to provide rationale for the next and final step of evaluations where actual MSE wall(s) is constructed in real field applications and subject to natural environmental conditions over a long period of time. In that final step, the focus would be on evaluating the potential for chemical clogging.

This report consists of five chapters. Chapter 1 provides an introduction to the problem and motivation for the research, including background information on mechanical and hydraulic performance of RCA in MSE wall applications. Chapter 2 summarizes materials and methods adopted for the large-scale MSE wall testing and column testing programs. Chapter 3 summarizes results obtained from the MSE wall and column tests and from forensic measurements made using geotextiles exhumed from the tests. Chapter 4 describes a complimentary numerical seepage modeling program conducted to extend the observations from the large-scale MSE wall test. Finally, Chapter 5 provides a summary of conclusions and recommendations for implementation.

References Cited

Abbaspour, A., Tanyu, B.F., Aydilek, A.H., Dayioglu, A.Y., 2018. Methodology to evaluate hydraulic compatibility of geotextile and RCA in underdrain systems. *Geosynthetics International* 25, 67–84. https://doi.org/10.1680/jgein.17.00034

Abbaspour, A., Tanyu, B.F., 2019a. Evaluate hydraulic compatibility of geotextile and RCA in underdrain systems under turbulent flow regime, in: *Geosynthetics Conference 2019*. IFAI, Houston, Texas, U.S.A.

Abbaspour, A., Tanyu, B.F., 2019b. Tufa precipitation from Recycled Concrete Aggregate (RCA) over geotextile: Mechanism, composition, and affecting parameters. *Construction and Building Materials* 196, 317–329. https://doi.org/10.1016/j.conbuildmat.2018.10.146

Soleimanbeigi, A., Likos, W.J., Tanyu, B., and Aydilek, A.H., 2016, "Recycled materials as backfill for mechanically stabilized earth walls," Recycled Materials Resource Center Report.

Soleimanbeigi, A., and Likos, W.J., 2019, "Mechanical properties of recycled concrete aggregate and recycled asphalt pavement reinforced with geosynthetics," *Proc. Geo-Congress 2019*, Philadelphia, PA. https://doi.org/10.1061/9780784482087.026.

Soleimanbeigi, A., Tanyu, B., Aydilek, A., Florio, P., Abbaspour, A., Aliconas, Y., Likos, W.J., 2019, "Evaluation of recycled concrete aggregate as backfill for geosynthetic-reinforced MSE walls," *Geosynthetics International*, https://doi.org/10.1680/jgein.19.00025.

Soleimanbeigi, A., Özocak, A., Li, B., Akmaz, E., Dayioglu, A.Y., Tanyu, B.F., Aydilek, A.H., Likos, W.J., 2022, "Mechanical and hydraulic compatibility of RAP with geosynthetics used in MSE walls," *Geosynthetics International*, https://doi.org/10.1680/jgein.21.00016.

Tanyu, B., Abbaspour, A., 2020. Evaluation of Use of Crushed Hydraulic Cement Concrete (CHCC) as an Additive to Base Course/Subbase Material (Final Report No. Final Report No. FHWA/VTRC 21-R12). Virginia Transportation Research Council, George Mason University, Charlottesville, VA. https://doi.org/10.13140/RG.2.2.32533.96483/2

Yin, J., Soleimanbeigi, A., Warren, B., Likos, W.J., Edil, T.B., 2016, "Creep behavior of recycled asphalt pavement compacted at elevated temperatures," *Proc. ASCE Geotechnical and Structural Engineering Congress*, Phoenix, AZ. https://doi.org/10.1061/9780784479742.119.

Yin, J. Soleimanbeigi, A., Likos, W.J., Edil, T.B., 2017, "Effect of temperature on creep behavior of compacted recycled asphalt pavements," *Journal of Geotechnical and Geoenvironmental Engineering*, 143(4): 06016028, 10.1061/(ASCE)GT.1943-5606.0001636.

TABLE OF CONTENTS

LIST OF TABLES

LIST OF FIGURES

CHAPTER 1: INTRODUCTION

1.1 Mechanically Stabilized Earth Walls

A Mechanically Stabilized Earth (MSE) wall (Figure 1.1) is a vertical or near vertical earth retaining structure consisting of three major components: facing panels, reinforcement, and select backfill (Rathje *et al.*, 2006). MSE walls offer economic and technical advantages over conventional types of retaining walls (e.g. Gravity, Semi-Gravity, Cantilever and Counterfort), including less site preparation requirements, reduction of right-of-way acquisition and stability for wall-heights over 30 m. Geosynthetic reinforced MSE walls are often the least expensive choice for most wall heights (Koerner et al. 2000).

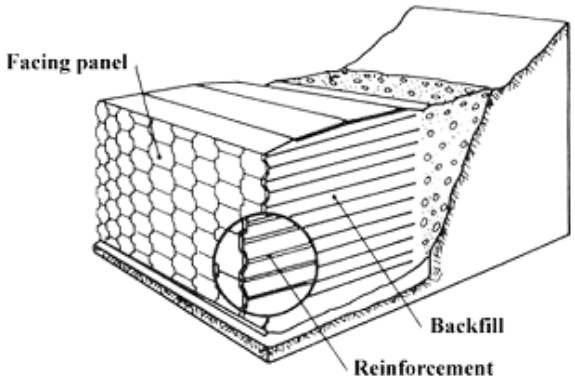

Figure 1.1 Schematic view of a mechanically stabilized earth wall

1.2 MSE Wall Components

The most critical components of a MSE wall are the selected backfill and reinforcements. The facing component is important for aesthetical purposes, but contributes little to the overall stability of the MSE wall system. The components of the MSE walls are discussed below:

1.2.1 Selected Backfill

Backfill materials can be natural or recycled materials that meet design criteria established by regulatory agencies (e.g. AASHTO, FHWA, state DOTs, etc.). The backfill used in MSE walls consists of coarse-grained material with low fines content (less than 15%) (AASHTO 2010; Anderson et al. 2012). The selection of backfill material considers the long-term performance of the wall system. The material shall offer good drainage, and thus the hydraulic conductivity of a selected material must be high enough to allow water to percolate freely though the backfill. Excessive amounts of fines can reduce the hydraulic conductivity of a given coarse material, thus contributing to long-term performance issues of the wall (Elias et al. 2001; Rathje et al 2006). Based on the AASHTO T-27 criteria discussed by Berg et al. (2009), to obtain reasonable drainage, the fines content of the selected material for reinforced fill shall have no more than 15% fines (as

determined from passing No. 200 sieve) and 60% fine sand size particles (as determined from particles passing No. 40 sieve). The plasticity index of the material shall be less than 6.

Potential corrosion of metal reinforcements can be enhanced if water is retained by poorly draining backfill. For this reason, the use of material with high water absorption potential such as clay and silt is not recommended as backfill (Elias et al. 2001; Berg et al. 2009). Corrosion is a concern when the MSE wall system utilizes metal reinforcements because it can result in sudden failure of the wall system (FHWA 2009; Anderson et al. 2012).

The mechanical stability of the wall depends, in part, on the mechanical properties of the backfill. The material should yield adequate angle of internal friction allowing high shear strength against horizontal pressures imposed by the soil mass (Elias et al. 2001; Rathje et al. 2006; Berg et al. 2009). The selected backfill should also develop sufficient interface friction with the reinforcement. Well-graded and less angular materials yield higher values of dry unit weight during compaction (FHWA 2009). Materials compacted at low dry unit weight and low water content can experience significant settlement upon wetting (Basma et al. 1992; Rathje et al. 2006; Berg et al. 2009).

An additional deformation mechanism of concern in MSE walls is creep if the backfill is a material with high creep potential such as recycled asphalt pavement (RAP) or recycled asphalt shingles (RAS) (Soleimanbeigi et al. 2014, 2015). This behavior will be more enhanced at higher temperatures. The use of materials susceptible to creep is usually not recommended for backfill because they affect the long-term stability of the wall, leading to excess deformation of the MSE wall system (Rathje et al. 2006).

1.2.2 Reinforcements

The function of reinforcements is to provide shear strength to the backfill against the lateral earth pressure. Reinforcements used in MSE walls can be classified as extensible and inextensible (Koerner 2005; Das 2008). Inextensible reinforcements show deformation at failure much less than the deformability of the soil. Steel strips and bar mats are examples of inextensible reinforcement. Extensible reinforcements, on the other hand, show deformation at failure equal to, or greater than the deformability of the soil. Geotextiles, geogrids and woven steel wire mesh are extensible reinforcements (Koerner 2005; Das 2008; Berg et al. 2009).

Geotextiles are made from geosynthetic fibers, fashioned into a flexible, porous fabric. Geotextiles can be made into woven and nonwoven patterns (Koerner 1994). The weaving process makes two sets of parallel filaments into a planar surface by systematically interlacing them to produce woven geotextiles. Nonwoven geotextiles, on the other hand, are produced by matting geosynthetic fibers together in a random or organized manner. After the placement of the fibers, these filaments are chemically, thermally or mechanically bonded (Holtz et al. 1998; Koerner et al. 2005; Das 2007). In MSE wall applications, woven geotextiles are typically used for reinforcements as they have much higher tensile strength. Nonwoven geotextiles are typically used to provide drainage along the facing and behind and underneath reinforced zones (Berg et al., 2009).

Geogrids are made with polypropylene (PP) or polyethylene (PET) (high-modulus plastic materials) into wide, grid-like shape. The apertures (e.g. opening between the longitudinal and transverse ribs) of geogrids are large enough to allow passage of backfill material from one side to another. Manufacturing of geogrids can be done with different process: extruded, woven and welded (Das, 2007; Koerner 2005; Holtz et al. 1998). Geogrids can be further engineered in uniaxial or biaxial strength directions. Geogrids are usually stiff and the apertures allow interlocking with surrounding backfill material (Das 2007). Samples of different types of geosynthetics are shown in Figure 1.2.

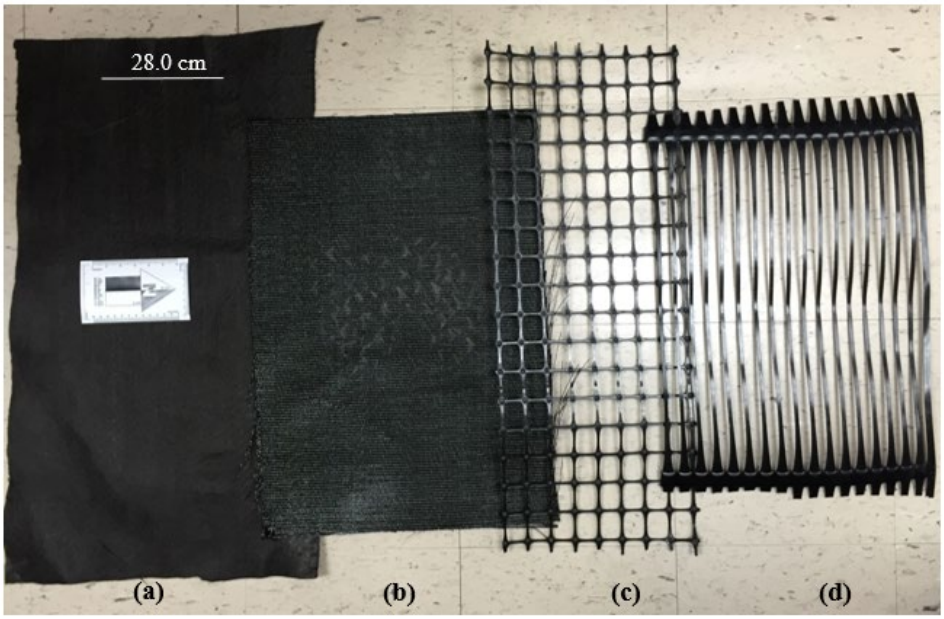

Figure 1.2 Geosynthetic reinforcement samples: (a) nonwoven geotextile, (b) woven geotextile, (c) biaxial geogrid, and (d) uniaxial geogrid.

Metallic reinforcements are generally made of steel and are susceptible to corrosion. Corrosion protection is achieved by galvanization but epoxy coating is also common. The primary types of metal reinforcements used in MSE wall applications are flat ribbed strips (Elias et al. 2009) and welded wire metal mats (Bilgin et al. 2014).

The type of reinforcement to be used in a given backfill depends on specific MSE wall applications, environmental conditions, expected loads, and the properties of the backfill material. Criteria regarding the general design are governed by codes that consider resistance according to various failure modes (Berg et al. 2009; Anderson et al. 2012; Elias et al. 2001). The efficiency of reinforcements depends on reinforcement length, reinforcement-to-panel-connection, as well as friction between the soil and the reinforcement face or ribs. Other factors, such as compaction and the facing system, affect the efficacy of a given reinforcement against horizontal movement. The type of reinforcement must be further analyzed based on its intrinsic properties such as creep potential, corrosion potential, ultra violet (UV) resistance and biodegradation susceptibility. These

properties are material dependent. The selected backfill material will also affect some of these intrinsic properties such as corrosion and biodegradation (Berg at al. 2009).

1.3 Recycled Materials as MSE Backfill

As noted above, backfill materials behind MSE walls must fulfill several engineering functions. They are required: (*i*) to have adequate shear strength to ensure stability within the backfill and interaction with the reinforcement (pullout resistance), (*ii*) to provide free drainage to reduce hydrostatic pore water pressure, (*iii*) to have adequate compaction characteristics to ensure minimal compressibility, (*iv*) to have satisfactory long-term (creep) characteristics to minimize excessive deformations, and (*v*) to be minimally corrosive to ensure the long-term integrity of reinforcement materials.

For these reasons, coarse-grained soils are generally favored for MSE construction because they can provide free drainage (when the amount of fines is small), have greater friction angles than fine-grained soils, and tend to yield smaller deformations when correctly compacted. This limitation on material type, however, can significantly increase the cost of construction on some projects because of the cost of transporting select material to the construction site when local select fill is not available. In most cases, the cost of select backfill material dominates the total cost of MSE wall construction (Rathje *et al.*, 2006).

At the same time, industrial operations and construction activities create granular materials that must be disposed. Producers of such materials must pay transportation costs, as well as disposal fees, to discard these materials. One solution is to recycle these materials and use them as alternative reinforced backfill. Throughout the U.S. and Canada, substantial amounts of recycled asphalt pavement (RAP) and recycled concrete aggregate (RCA) are being produced through reconstruction activities. Granular industrial byproducts such as foundry sand/slag, bottom ash, and iron/steel slag are also produced in large quantities. The use of recycled materials in engineering applications presents economic and environmental benefits. The disposal of these materials in landfills is costly and presents potential environmental issues for air and groundwater (Elias et al 2001; Rathje et al. 2006). If these materials were used as reinforced backfill for MSE walls, transportation and disposal costs associated with construction could be greatly reduced, translating into significant savings for state departments of transportation. Furthermore, such activities would promote sustainable construction, preserve natural resources, and reduce the carbon footprint and need for landfill disposal in highway construction.

Common recycled materials used in civil engineering applications include Recycled Concrete Aggregate (RCA), Recycled Asphalt Pavement (RAP), Bottom Ash (BA), Fly Ash (FA), Recycled Asphalt Shingles (RAS) and Foundry Sand (FDS). These materials have been used as base coarse for roadways, backfill for Mechanically Stabilized Earth (MSE) walls, aggregates for construction of highways and embankments, and the production of new asphalt and cement (FHWA 2004a; Anderson et al. 2009; Soleimanbeigi et al. 2015). RAP and RCA are the most extensively recycled construction materials used in the United States to date (Edil et al. 2012). Over 140 million tons of RCA (EPA 2015) and 75.8 million tons of RAP (NAPA 2014) are produced per year. According to the National Asphalt Pavement Association (NAPA), 99.0% of RAP waste is recycled (NAPA 2014).

1.4 Mechanical and Hydraulic Properties of RCA

1.4.1 Mechanical Properties of RCA: Summary of Previous Research

RCA differs from natural aggregates in composition (e.g. presence of mortar). It is more angular and has rougher surface than its virgin aggregate counterparts (Griffiths et al. 2002, Juan et al. 2009; Rathje et al. 2006; Soleimanbeigi et al. 2015). These physical characteristics are believed to augment the friction angle of RCA (Tatsuoka et al. 2005; Rathje et al. 2006). RCA is susceptible to higher-than-normal particle breakdown which can potentially increase the amount of fines (e.g. particles passing No. 200 sieve), thus reducing hydraulic conductivity and altering the material's compaction characteristics (Rathje et al 2006).

RCA particles have rough surfaces and angular shape, with a mix of natural aggregates and cement mortar (Anderson et al. 2009). The material is acquired from the reconstruction or demolition of pavements, airport runways, bridge structures and buildings (Rathje et al. 2006). The production of RCA is analogous to the production of natural aggregates (e.g. limestone, granite, etc.). It differs on the need to separate reinforcing steel and sealants which were added to the concrete for structural reinforcements, and materials that become mingled with the concrete waste during demolition (e.g. wood chips, plastics, tiles, and glass) (Kuo et al. 2002; Rathje et al. 2006). The final RCA product is then stored according to particle sizes. RCA can also be recycled in-situ using mobile plants and the material is usually reincorporated into the roadway (FHWA 2004a; Rathje et al. 2006).

Typical ranges for physical and mechanical properties of RCA are summarized in Table 1.1. Parameters reported include grain size indices, material composition, absorption, specific gravity, dry unit weight, water content, angle of internal friction, cohesion, and hydraulic conductivity.

1.4.2 Hydraulic Properties of RCA: Summary of Previous Research

Previous research has shown that RCA is an adequate reinforced backfill for MSE walls from a mechanical perspective, although its potentially marginal hydraulic conductivity requires additional drainage to be provided. High pH and potentially high chloride or sulfate content often associated with RCA leachate can cause corrosion of aluminum or galvanized steel reinforcing members, particularly in the presence of high moisture contents resulting from poor drainage (Popova et al., 1998; FHWA, 2000). Another unresolved issue is the potential precipitation of tufa ($CaCO_3$), which can clog filter fabrics and further inhibit adequate backfill drainage (Rathje et al., 2006).

The George Mason University (GMU) Sustainable Geo Infrastructure (SGI) research team has been involved in conducting extensive evaluations of the use of recycled concrete to create unbound aggregate for geo-structures since 2013. Brief descriptions of what has been conducted and learned over the years by the SGI group are summarized below.

Table 1.1 Range of typical engineering properties for RCA

Property	RCA (typical)
USCS	GW, GP, SW, SP, SC
AASHTO	A-1-a, A-1-b
Fines Content (%)	3.2 - 12.8
Mortar/Asphalt/Clay (%)	37.0 – 65.0
Absorption (%)	5.0 - 6.5
Specific gravity G_s	2.24 - 2.72
$\gamma_{d,\,max}$ (kN/m^3)	17.5 - 19.2
ω_{opt} (%)	8.7 - 11.9
Friction angle ϕ' (degrees)	41 - 63
Cohesion c' (kPa)	0 - 55.2
Hyd. Cond. k (cm/s)	7.1×10^{-4} - 1.8×10^{-3}

During the first phase; the SGI team designed and conducted extensive laboratory-scale tests to understand the chemical behavior and leaching characteristics of unbound aggregate created from recycled concrete. The source of the concrete used for these studies has been a mixture of materials including but not limited to demolished buildings, storm water drainage features such as concrete curb and gutter systems, aged roadways, and newly produced concrete that is left over from any given project (i.e., referred as wash out). In previous studies, recycled concrete aggregate (RCA) was created with different typical base course gradations and the extent of the potential for physical clogging was investigated via long-term filtration tests in fully saturated and continuous flow conditions. These tests have primarily focused on evaluating the physical compatibility between the RCA and nonwoven geotextiles used to construct sub drains for highways and roadways. Research efforts for these investigations have been funded by the Virginia Transportation Research Council (VTRC) and the findings have been published by Abbaspour et al. (2018); Abbaspour and Tanyu (2019a); and Tanyu and Abbaspour (2020).

The second phase of the SGI team investigations consisted of simulations of tufa precipitations from RCA in the laboratory. These efforts were funded by National Science Foundation (NSF) and consisted of simulations of the nonwoven geotextile/RCA interactions under unsaturated flow conditions (Tanyu and Abbaspour, 2020).

The third phase of the SGI team investigations involved a collaboration between the University of Wisconsin and the University of Maryland and focused on evaluating the physical clogging potential of typical woven geotextiles used to reinforce Mechanically Stabilized Earth (MSE) walls when RCA is considered as the reinforced aggregate. This study was funded by the Recycled Materials Resource Center (RMRC) and the RCA in this study had a gradation that contained about 8% fines.

The fourth phase of the SGI team investigations is an ongoing field simulation of an actual road section constructed using RCA and various mixtures of RCA and V.A. as the base course. The test sections include sub drains similar to the VDOT UD-4 edge drains (VDOT, 2008, 2016) that are installed in real highway projects (consisting of perforated pipe, course aggregate embedment, and a nonwoven geotextile wrapping). These efforts are being funded by VTRC and parts of the study have also been supplemented by the funds from RMRC.

1.4.3 Statement of the Problem

Based on the findings of previous studies, changes in hydraulic performance of RCA-geotextile systems can be dominantly affected by each one of two major clogging phenomena (physical and chemical) depending on the environment and flow conditions. Physical clogging is dominant in a saturated environment with continuous flow conditions as the permeant water remains under-saturated with respect to minerals that form RCA tufa. Such conditions inhibit the formation or deposition of precipitants and in some cases can even lead to dissolution of readily soluble minerals in the RCA material. On the other hand, seepage forces can cause some of the fines within RCA to migrate onto the geotextile and reduce the ability of the geotextile to permeate water (herein referred to as filtration capacity) through the RCA/geotextile interface. Gradation of the RCA and the permittivity characteristics of the geotextile thus play important factors to minimize the migration of fines. Creating RCA gradation with high internal stability (minimal potential for fines migration) will minimize the suffusion susceptibility and the concerns associated with physical clogging. Evaluation of grain size distribution of an RCA base layer that has been in service for some time allows the evaluation of the internal stability conditions of the initially selected gradation and susceptibility of a such layer to the occurrence of suffusion (Abbaspour et al., 2018; Abbaspour and Tanyu, 2019a).

On the other hand, the periodic flow conditions and cycles of wetting and drying, which are more typical of field conditions, significantly favor the occurrence of chemical clogging rather than physical clogging. Calcareous tufa (calcium-based crystals that may grow on the geotextile) is derived by diagenetic calcite precipitation (Abbaspour and Tanyu, 2019b), followed by evaporative precipitate formations, dominantly gypsum, that becomes active due to wetting and drying cycles. Tufa deposition within the geotextile filaments can lead to a reduction in filtration capacity of the RCA/geotextile system.

Observations from investigations with nonwoven geotextiles show that reduction in filtration capacity is unlikely to occur to an extent that creates no-flow conditions (a complete physical clogging of the system). Similarly, although chemical precipitations have been noted, the magnitude of the chemical clogging mechanisms was not observed in previous studies to be significant enough to pose a detrimental threat to the service life of the underdrain system. However, it was determined that the possibility of both physical and chemical clogging needs to be investigated any time RCA is considered for use with geotextiles, and such evaluations must take place during the design and double-checked during construction to prevent failures due to serviceability. To allow such evaluations, the SGI team has developed two models that were designed to evaluate the hydraulic compatibility of RCA and drainage geotextiles based on both physical and chemical clogging mechanisms. A clogging criterion (hydraulic conductivity ratio) is introduced based on long-term filtration tests under a saturated condition in which the clogging

is dominantly controlled by a physical phenomenon. Additionally, a tufa precipitation kinetics model was developed to estimate the reduction in infiltration rates of the RCA/geotextile system under unsaturated and periodic rainfall events (wet/dry cycles in which the chemical phenomenon is dominant). The former condition (saturated flow in a base layer) may occur in a real-life application in case of very high intensity and long duration of rainfall events. Whereas the latter condition was found to be prevalent during low-intensity and periodic rainfall events (especially seasonal changes in summer, autumn, and winter).

The occurrences of physical clogging in woven geotextile installed in an MSE wall with RCA material backfill were studied as part of the research conducted for the Recycled Material Research Center (RMRC) with the GMU team as one of the collaborators (Soleimanbeigi et al., 2016, 2019). Soleimanbeigi et al. (2016, 2019) used the same type of woven geotextile as the current research reported herein and tested the occurrence of physical clogging by a set of long-term filtration tests under saturated conditions. The RCA material tested in this set of experiments was a well-graded material (also known as VDOT 21-A gradation in accordance with Adams et al., 2012) with a maximum particle size of 38.1 mm (1.5 inches) and over 7.7% fines (passing No. 200 sieve). It was observed that the woven geotextile is prone to loss of serviceability due to the physical migration of RCA fines. Even though the no-flow condition was never observed, the evaluation of the pre- and post-filtration pore size distribution of woven geotextiles revealed that all openings larger than 0.5 mm were filled with RCA fines, significantly reducing the serviceability of the RCA/woven geotextile system. This indicated that further investigation for the chemical clogging may not be as important because under these conditions the system may already clog due to physical clogging.

Overall findings from all of the SGI team studies can be summarized as follows:

- RCA is a recycled material and factors such as the duration of the aging prior to use, the selected gradation to create the aggregate course, source of the rock type for the aggregate pieces within RCA all play important factors.

- Physical clogging concerns can significantly be eliminated by selecting the appropriate gradation of the RCA for the intended use of the specific geotextile that is being considered.

- Chemical precipitations may occur but there are ways to reduce the impact by selecting RCA gradations with minimal percent fines content and appropriate geotextile properties.

1.5 Research Approach

The research described in this report was developed to complement previous efforts to characterize mechanical properties of RCA and the hydraulic performance of RCA-Geotextile systems under idealized conditions. The overall goal of the Phase II effort described herein has been to closely replicate field conditions in terms of scale (i.e., large-scale experiments), flow conditions (i.e., 2-D, 3-D flow), and wetting-drying cycles. Two sets of complementary experiments were designed to investigate hydraulic performance of RCA-woven geotextile systems: one that replicates a large-scale MSE wall structure through physical modeling conducted at the Royal Military College

of Canada's MSE wall testing facility and the other as a series of large-scale column tests used to evaluate one-dimensional vertical flow conditions under conditions identical to the large-scale MSE wall. Numerical models were conducted to understand the larger hydraulic behavior in the wall experiments and to generalize the flow phenomena for different boundary conditions. In both experimental set-ups the following conditions were simulated:

- The gradation of the RCA was selected and processed to have minimum fines content. Based on previous findings, this was necessary to create a scenario where the potential for physical clogging does not become the leading mechanism for clogging, thereby maximizing the potential for understanding chemical clogging and the conditions that lead to it;

- Spacing between the reinforcement geotextiles were selected to be as close to each other as allowed in GRS-IBS systems, thereby providing a worst-case scenario in terms of potential clogging;

- The aggregate within the RCA was selected to contain calcium-based compounds, thereby providing a worst case scenario in terms of chemical clogging.

The one-dimensional column experiments were constructed in a 1-ft (0.3-m) diameter circular column with a height of 4 ft (1.2 m). The large-scale MSE wall was constructed to the same height (1.2 m) with a 3.3 m × 6 m backfill area. Both tests were constructed in lifts comprising 8 layers 150 mm thickness. Woven geotextile reinforced layers were used in 6 layers from the second to the seventh layer.

Five rainfall events were periodically carried out over 36 days for both the MSE wall system and the column systems to simulate rainfall-induced wetting-drying events. Rainfall events ranged from 1-inch to 2.5 inches. The first two cycles were performed in 2 stages of 1.5 in and 1 in and the last wetting cycle was applied as one step of 2.5 inches of water. After each wetting cycle, the systems were left to drain for approximately 10 days. Internal moisture migration for the MSE wall system was monitored using TDRs as well as boundary measurements of outflow and temperature / relative humidity.

CHAPTER 2: LARGE-SCALE WALL AND COLUMN TESTING PROGRAM

2.1 MSE Wall Testing Facility

Large-scale physical model tests were conducted at the Royal Military College of Canada (RMC) indoor MSE wall testing facility (e.g., Bathurst et al., 2000). The facility (Fig. 2.1) allows soil retaining wall structures that are as large as 3.6 m high by 3.4 m wide with backfill extending to a distance of 6 m from the front edge of the facility. The backfill and wall facing are seated on a rigid concrete foundation. The bacfill material is laterally contained between two parallel reinforced concrete counterfort walls bolted to the structural laboratory floor. A series of hollow steel sections at the top of the facility confine a series of air bags that can be used to apply a uniform surcharge (up to 150 kPa) to the entire backfill surface. The toe of full-scale wall models is located at the front of the test facility. The back of the soil mass is restrained by a series of rigid reinforced concrete bulkheads at the opposite end of the test facility. Plane-strain conditions are encouraged by covering the interior side-walls of the test facility with multiple layers of lubricated polyethylene sheeting. The test facility allows full-scale walls to be constructed, infiltrated, surcharged, excavated, and monitored in a controlled indoor laboratory environment. For the tests conducted herien, a sprinlker system was installed above the backfill surface to apply cycles of simulated rainfall with controlled duration and volume, followed by drying cycles obrained trhough draiange and evaporation.

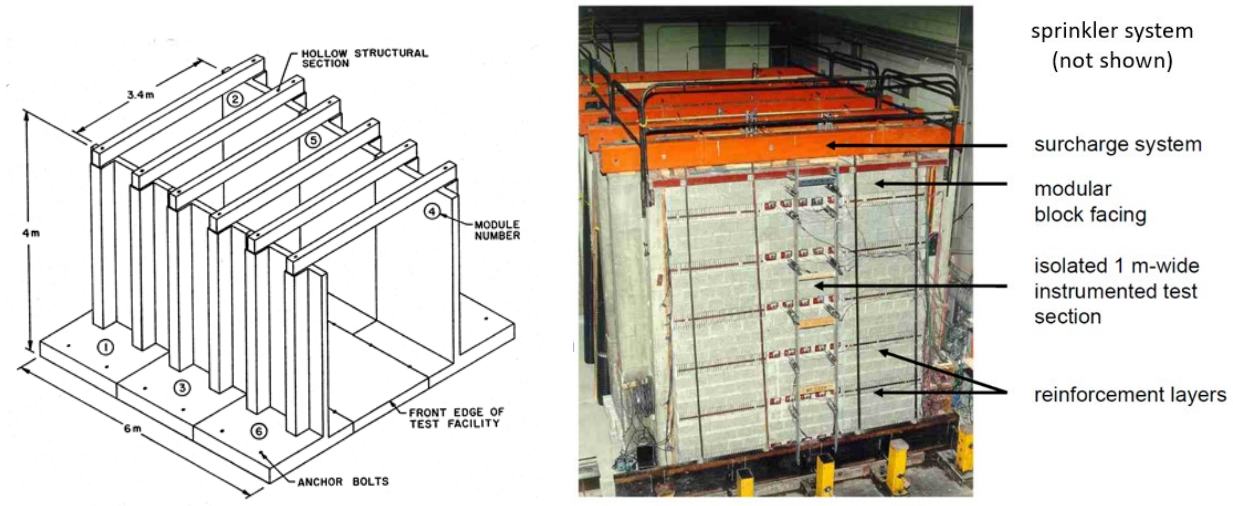

Figure 2.1 RMC Full-Scale MSE Wall Testing Facility (Bathurst et al., 2000). Note: the photo shown (b) is from a previous experiment.

2.2 Overall Layout of Large-Scale MSE Wall Test

Figure 2.2 illustrates the overall design and layout for the large-scale MSE wall tests. The MSE wall was constructed using processed RCA (Section 2.2) that was placed and compacted in eight lifts (0.15 m) to a total backfill height of 1.2 m. The width and depth of the backfill were 3.3 m and 6.0 m, respectively. Woven geotextile reinforced layers (Section 2.3) were used in six layers commencing from the top of lift 2 to the top of lift 7. Masonry concrete blocks (Section 2.4) were used as facing material. An overhead sprinkler system (Section 2.9) was designed and constructed to apply a controlled volume of water with controlled duration to the surface of the backfill with outflow water collected at the toe of the wall face. Internal and external instrumentation (Section 2.7) was placed to measure backfill moisture content, ponding water at the base, geotextile strains, horizontal and vertical toe loads, earth pressure at the base of the backfill, pH and Electrical-conductivity (EC) of the inflow and outflow water, and outflow water volume. Each of these components of the test set up are described in the following sections.

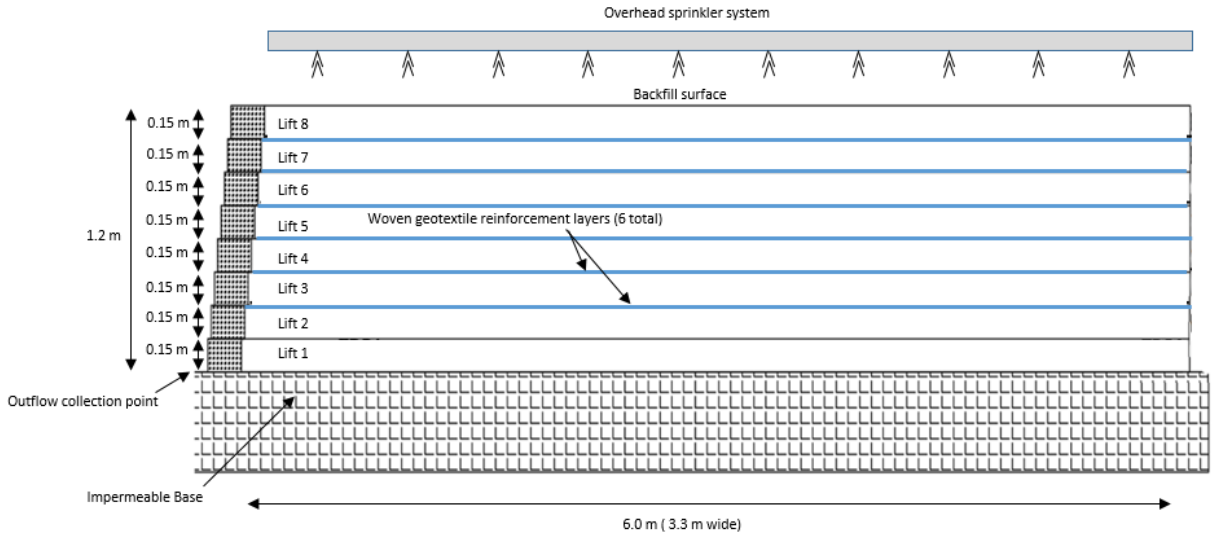

Figure 2.2 Overall schematic of large-scale MSE wall test.

2.3 RCA Backfill

2.3.1 Backfill Processing

Several AASHTO gradations for RCA were considered for use in the large-sale test wall based on previous experience and considering the RCA material used during Phase 1 of this study (Soleimanbeigi et al., 2016). In that study, tests were conducted using RCA with 7-8% fines and 100% passing the 1.5-inch sieve. The AASHTO No.8 gradation corresponding to these criteria, was thus first considered for replication in the Phase II large-scale tests. After extensive searching in and around 100 miles of RMC over a time period of 9 months, however, no economical source for AASHTO No. 8 could be found.

Rather, raw (unprocessed) RCA material was processed to meet the maximum and minimum specifications for AASTHO No 8 and AASHTO No 89. Processing (Figure 2.3) included washing and removal of fines through screens as well as vibration sieving to remove the larger particles. The processed material was subjected to regular grain-size distribution analysis, which all fall within the combined AASTHO specification.

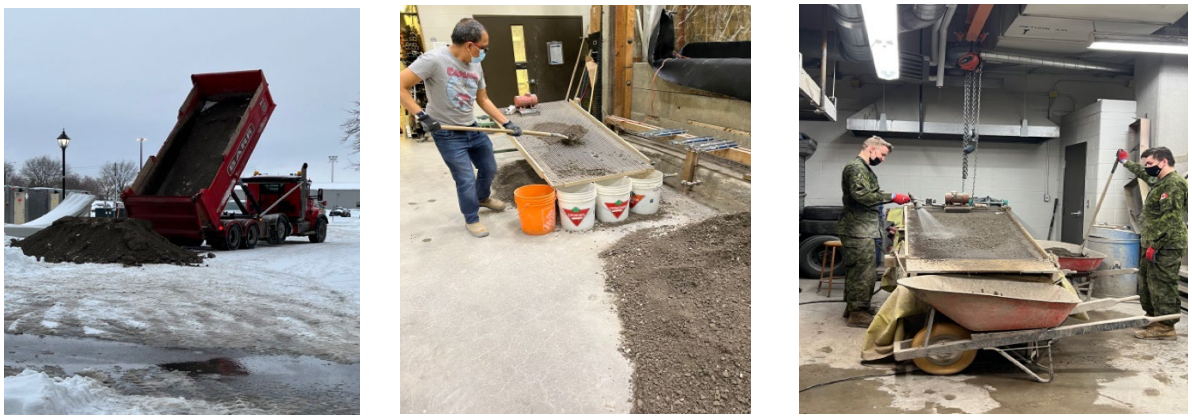

Figure 2.3 Photographs of processing efforts to manufacture RCA backfill: (a) unprocessed RCA, (b) sieving and (c) washing to remove coarse and fine-grained fractions.

2.3.2 Backfill Grain-Size and Index Properties

The final specification for the RCA backfill used in this study is shown in Table 2.1 and Figure 2.4 along with grain-size distribution testing performed during processing. The final specification utilized combined AASHTO No 8 and No. 89 specifications. The material has 100% passing the 1/2-inch sieve with less than 5% passing the No. 16 sieve.

Grain size distributions measured for various processing batches (see multiple curves in Figure 2.3) were constrained within the AASHTO specification ranges and produced ranges of coefficient of uniformity (C_u) and coefficient of curvature (C_c) as $1.6 < C_u < 2.05$ and $0.08 < C_c < 0.24$. The processed RCA classifies as poorly graded gravel (GP) using the Unified Soil Classification System (ASTM D2487). Values for the specific gravity of the solids (G_s) and absorption of the RCA material are 2.56 and 1.77, respectively, as determined following ASTM C 127-12. Hydraulic conductivity (k) was measured using the ASTM D 2434-19 method. The results showed k = 4.7 cm/sec, which is within the typical range for more general poorly graded gravel material.

Table 2.1. AASHTO No. 89, No. 8, and Processed RCA Gradation

Sieve Size	AASHTO No. 89	AASHTO No. 8	Processed RCA specification
½ inch (12.5 mm)	100% passing	100% passing	100% passing
3/8” inch (9.5 mm)	90-100% passing	85-100% passing	85-100% passing
No. 4 (4.75 mm)	20-55% passing	10-40% passing	10-55% passing
No. 8 (2.36 mm)	5-30% passing	0-10% passing	0-30% passing
No. 16 (1.18 mm)	0-10% passing	0-5% passing	0-10% passing
No. 50 (0.3mm)	0-5% passing	-	0-5% passing

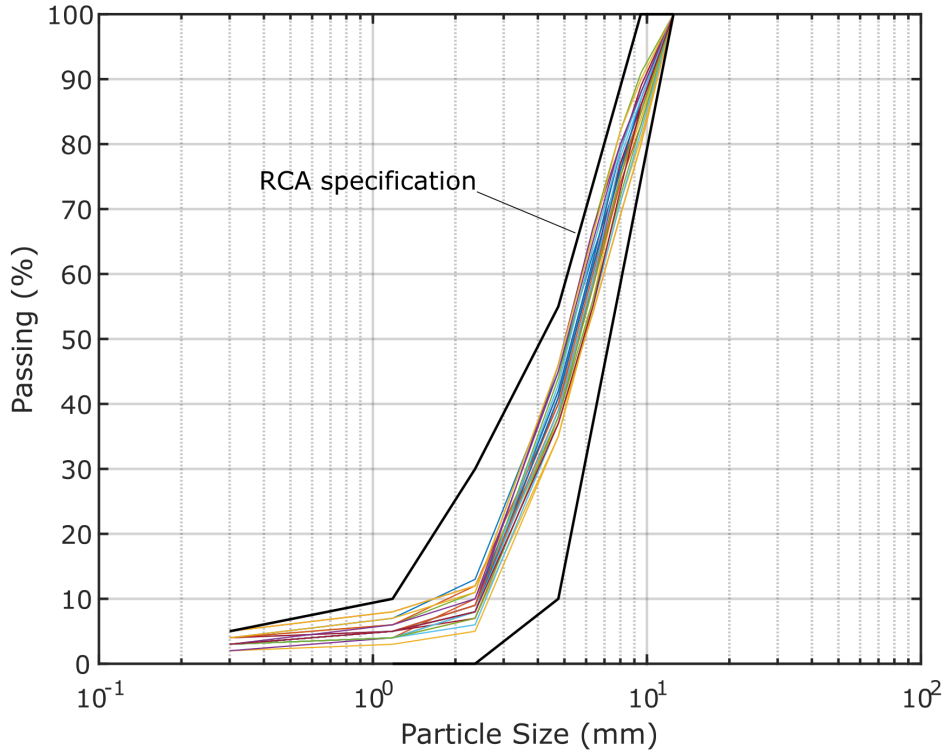

Figure 2.4 RCA backfill specification and grain-size distribution measurements

2.3.3 Proctor Compaction Testing

Standard proctor compaction testing was performed regularly during processing of the RCA backfill. Typical results are shown in Figure 2.5. A maximum dry density of 1.72 g/cm^3 at 8.84% moisture content was evaluated from the results.

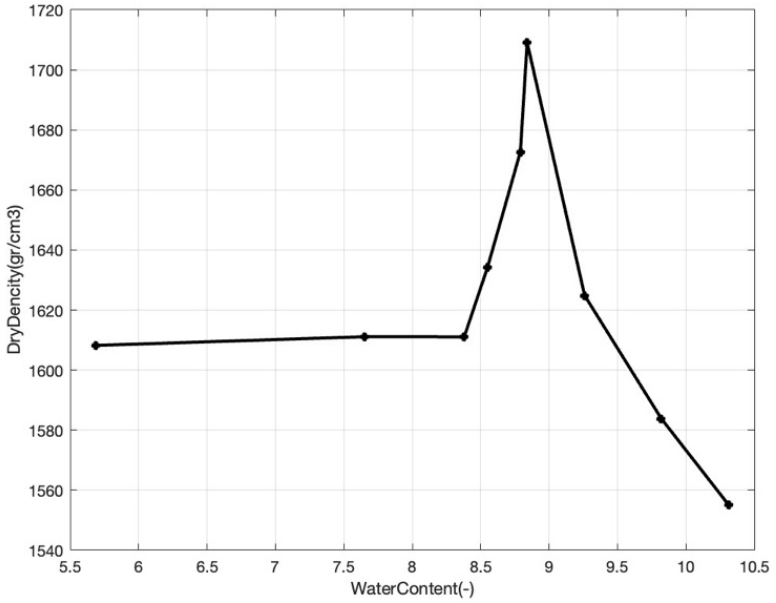

Figure 2.5 Typical Standard proctor results for processed RCA backfill

2.3.4 Water Retention Curves

Water retention curves (WRC) for the RCA and the geotextile reinforcement (described subsequently) are shown in Figure 2.6. The WRC for the reinforcement was measured using a process described by Chuang Lin (Spring 2019). The WRC for the RCA was estimated from unpublished research reports with a similar grain-size distribution. Both are typical of their respective materials and were used for numerical seepage modeling described in Chapter 4.

2.3.5 RCA Mortar Content

The measured mortar content (MC) of RCA particles was obtained using the acid treatment procedure as described by Abbaspour et al. (2016). In this method, the RCA material is soaked in 3M hydrochloric acid for 24 hours to dissolve the cement paste attached to the rock particles. After acid treatment, the material is washed, oven-dried, and measured for weight loss. Generally, the weight loss values decrease with each cycle until become insignificant (less than 1% by weight). At this point, the testing is terminated and the percentage of total weight loss to the initial sample weight is reported as the MC of the material. However, the parent rock of the RCA material used in this study is found to be of calcareous nature (limestone and dolostone) due to the geology of

the source (Ontario, Canada). Therefore, the weight loss of material after each cycle remained significant (more than 10% by weight) and did not seem to be decreasing. Therefore, the test was terminated after six cycles, and the total weight loss is reported herein. The mortar content determined using these procedures is 75.1%

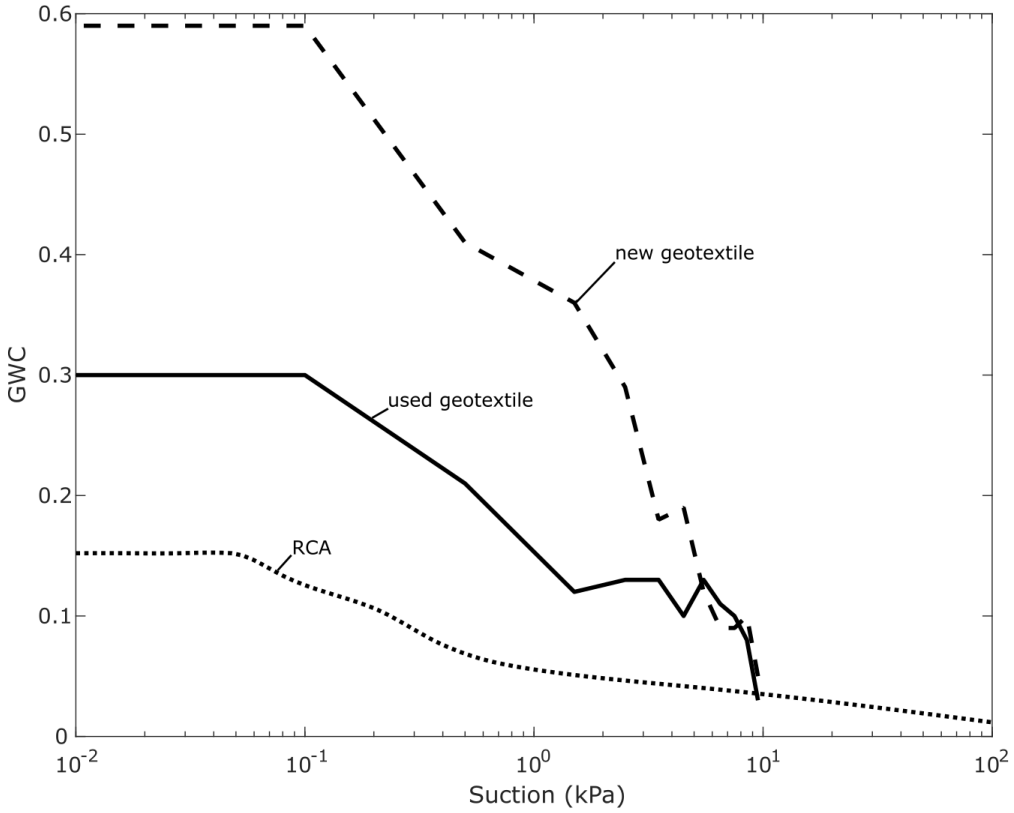

Figure 2.6 Water retention curves for RCA backfill and reinforcement

2.4 Geosynthetic Reinforcement

A woven Mirafi® HP570 geotextile (Figure 2.7) was used as reinforcement for this project, both in the large-scale MSE wall and column tests. Factory-measured properties are summarized in Table 2.2. This type of geotextile is composed of high-tenacity polypropylene yarns woven into a network so that the yarns retain their relative position. Mirafi® HP570 geotextile is inert to biological degradation and resistant to naturally encountered chemicals, alkalis, and acids. TenCate Geosynthetics Americas is accredited by Geosynthetic Accreditation Institute – Laboratory Accreditation Program (GAI-LAP).

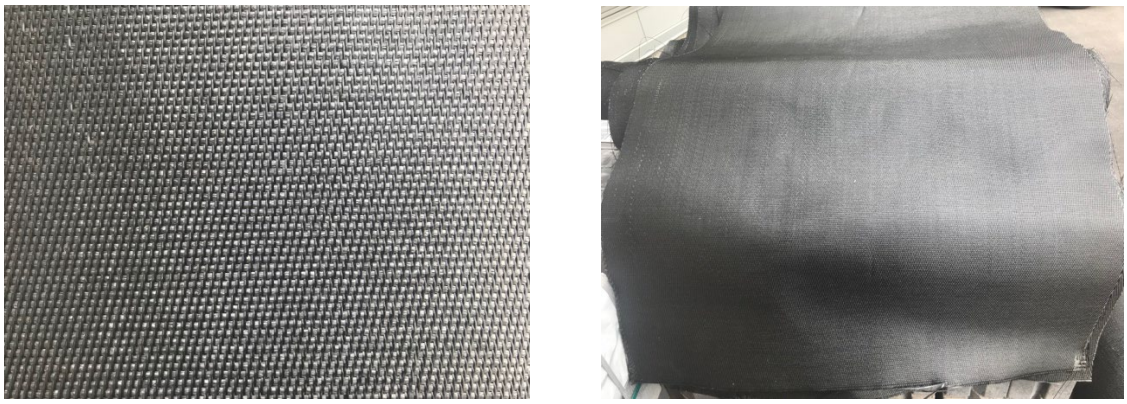

Figure 2.7 Photograph of geotextile reinforcement

Table 2.2 Geotextile Properties

Mechanical Properties	**Test Method**	**Unit**	**Minimum Average Roll Value**	
			MD	**CD**
Tensile Strength (at ultimate)	ASTM D4595	lbs/ft (kN/m)	4800 (70.0)	4800 (70.0)
Tensile Strength (at 5% strain)	ASTM D4595	lbs/ft (kN/m)	2400 (35.0)	3000 (43.8)
			Minimum Roll Value	
Flow Rate	ASTM D4491	gal/min/ft^2 (l/min/m^2)	30 (1222)	
Permittivity	ASTM D4491	sec^{-1}	0.5	
			Maximum Opening Size	
Apparent Opening Size (AOS)	ASTM D4751	U.S. Sieve (mm)	30 (0.60)	
			Minimum Test Value	
UV Resistance (at 500 hours)	ASTM D4355	% strength retained	80	
Physical Properties	**Unit**	**Roll Size**		
Roll Dimensions (length x width)	ft (m)	15 x 300 (4.5 x 91)	17 x 265 (5.18 x 80.8)	
Roll Area	yd^2 (m^2)	500 (418)	500 (418)	

2.5 MSE Wall Facing and Geotextile Connection

Masonry concrete blocks (10 cm × 20 cm × 30 cm) were used as facing material for the MSE wall. The blocks are manufactured with structural interlocking from the bottom to the top (Figure 2.8). The first row of blocks was placed on a metal plate with six steel bearing rollers underneath to facilitate lateral movements. During construction, the geotextile was laid between two blocks with a connection made by pinch bolts in front of the facing blocks (Figure 2.9).

Figure 2.8 Photograph of masonry concrete facing blocks

Figure 2.9 Geotextile installation between facing blocks

2.6 Backfill Compaction

Processed RCA was stored in large bags and moved into place using a large crane for compaction. The RCA was placed and compacted using the same procedures for all layers of backfill. The material was compacted in a total of 8 layers having 150 mm thickness to a total backfill height of 1.2 m. Each lift was leveled using a laser before and after compaction. All layers were compacted using hand tamping with a 5-kg square plate (250 mm × 250 mm) and a lightweight jumping jack tamper compactor (Wacker model ES 45 Y) (Figure 2.10). The hand tamping compactor was used to compact material extending approximately one meter from the wall face. The remaining five meters of the backfill were compacted using the jumping jack compactor. Lighter compaction was used near the face to minimize the effects of compaction on the wall face consistent with field compaction procedures (Berg et al., 2009).

Figure 2.10 Compaction equipment: (a) hand tamping compactor and (b) lightweight jumping jack tamper compactor

The material was compacted to optimum density determined from Standard Proctor tests on representative samples. To compact the RCA to reach the optimum dry density, the drop height of the manual compactor was 200 mm for four consecutive drops, and it was performed three times (12 drops total). A Troxler 3411-B nuclear densimeter surface moisture density gauge (backscatter mode) was used to measure the density and moisture content of the material. Measurements were made on the surface of each lift at nine points in different locations (face, middle, and back of the

backfill) to obtain dry density and moisture content. Average measured values of moisture content and maximum dry density were verified within 95% of the optimum dry density for each layer.

2.7 Sidewall Friction and Base Treatment

A lubricant polyethylene sheet system developed at RMC (e.g., Nelson 2005) was used to minimize sidewall and lateral friction, thus closely replicating plane strain conditions in the wall facility. A composite layer consisting of a Plexiglas sheet and three layers of polyethylene sheeting were used to create this system (Figure 2.11). Grease was used between the layers to increase lubrication and the sheets were stretched to prevent wrinkles. As noted subsequently, the majority of instrumentation was placed in the backfill at the centerline of the backfill to minimize boundary effects on the measurements. An impermeable membrane was also placed to cover the base and lower 6 inches of the sidewalls to collect infiltration water. The membrane was formed in a fashion to create a gutter in front of the wall under the facing such that outflow water could be collected and measured regularly during wetting-drying cycles.

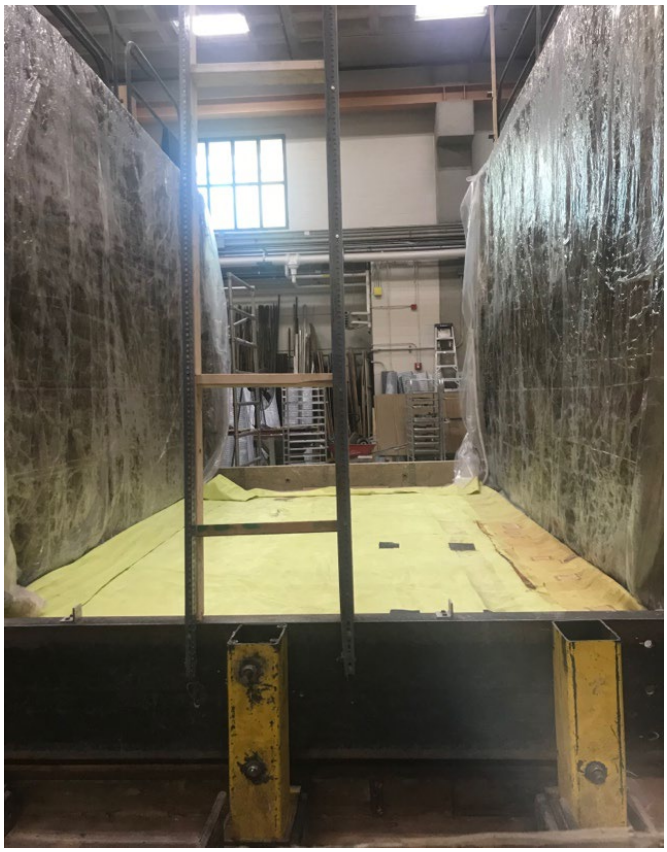

Figure 2.11 Sidewall treatment with lubricated polyethylene sheets (clear) and impermeable membrane (yellow) covering the base of the facility to collect infiltration water

2.8 Instrumentation

The overall instrumentation layout is shown in Figure 2.12 and is summarized in Table 2.3. All instruments were calibrated before and during the construction of the wall. Instrumentation was installed in the backfill (and externally) to obtain the following measurements:

- Moisture content (TDR probes, fiber optics);
- Ponding water at the base (open standpipes);
- Geotextile strains;
- Horizontal and vertical toe loads;
- Earth pressure at the base of the backfill;
- PH and Electrical-conductivity (EC) of inflow and outflow water;
- Outflow water volume

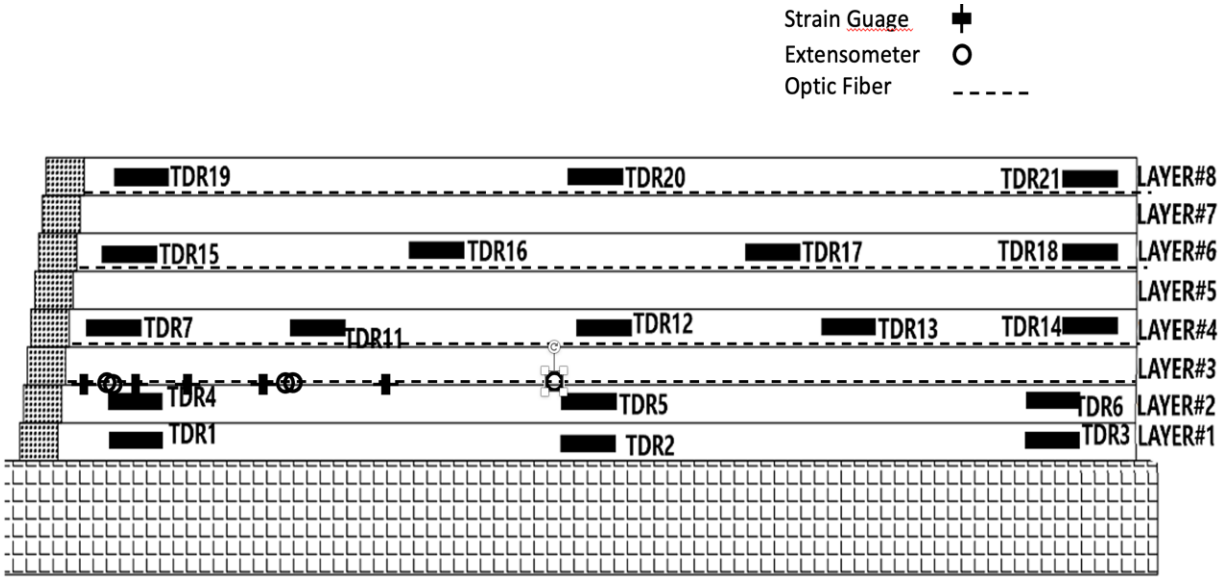

Figure 2.12 Layout of instruments and approximate locations in the RCA backfill.

Three data acquisition systems were used to monitor and record data during all phases of the project (before and during construction, during and after running wetting-drying cycle tests, and during post-test excavation). An Agilent 34980A data acquisition system combined with 34980A Bench Link Data Logger data acquisition software was used to obtain data from the stress and strain recorder instruments. A Campbell Scientific CR1000 and TDR 100 was used to collect moisture content measurements from TDR sensors buried in backfill. Luna software was used to record fiber optic readings. A personal computer (PC) with i5-4590 CPU, 3.30GHz, 4 Core(s) processor, and 8GB of RAM was connected to the Agilent and CR1000 units. A laptop was used to control the Luna software.

Table 2.3 Instrumentation summary

	Instrument	Purpose	Number of instruments	Manufacturer
Facing	Potentiometer (LVDTs)	Footing movement	5	Penny and Giles
	Toe load rings	Horizontal load at footing	6	Homemade
	Toe load cell	Vertical load at footing	18	Intertechnology Inc / Hoskin Scientific / homemade
Soil	Earth pressure cells	Soil pressure	7	Geokon EP4500
	Standpipes - piezometer	Water level	2	homemade
	TDR probes	Moisture content	18	Campbell Scientific
	Fiber optics	Moisture and water flow	4	Luna
	Thermometer and Humidity control	Temperature and Humidity	1	Govee
Reinforcement	Strain Gauges	Local strain in reinforcement	5	Showa Measuring Instruments
	Extensometers	global strain in reinforcement	5	Penny and Giles
Total			71	

2.8.1 Volumetric Water Content

A series of CS645 time-domain reflectometry (TDR) probes were used to measure the water content of the soil in different layers and positions inside the RCA backfill. This probe consists of a Santoprene head, three-pointed rods, and a standard RG58 cable. The length of each TDR rod is 7.5 cm, allowing the probe to be used in very high electrical conductivity soils or in laboratory column applications (maximum soil bulk electrical conductivity of 5 deciSiemens/meter). The RG58 cable is suitable for lengths up to 15 meters (50 ft) as measured from the tips of the probe's rods to the reflectometer. TDR probes are the sensors of the TDR measurement system and are inserted or buried in the medium to be measured. The probes are a waveguide extension on the end of the coaxial cable. Reflections of the applied signal along the waveguide occur where there

are impedance changes. The impedance value is related to the geometrical configuration of the probe (size and spacing of rods) and is inversely related to the dielectric constant of the surrounding material. A change in the volumetric water content of the medium surrounding the probe causes a change in the dielectric constant. This is registered as a change in probe impedance which affects the shape of the reflection. The shape of the reflection contains information used to determine water content and soil bulk electrical conductivity.

TDRs were placed in one of two configurations, as shown in Figure 2.13. In the lower layers (lifts 1 and 2), TDRs were placed in direct contact with the backfill in order to monitor changes in moisture content as the wetting front passed and during the drying cycle. In the upper layers, TDRs were placed inside small permeable bags filled with sand. The relatively finer grain sand has greater capillarity and thus retains water for a longer time. This was necessary such that the TDR, which can only be read every 2 minutes, can be used to detect a passing wetting front. All TDRs were calibrated in the medium with which they were in direct contact (i.e., RCA or sand).

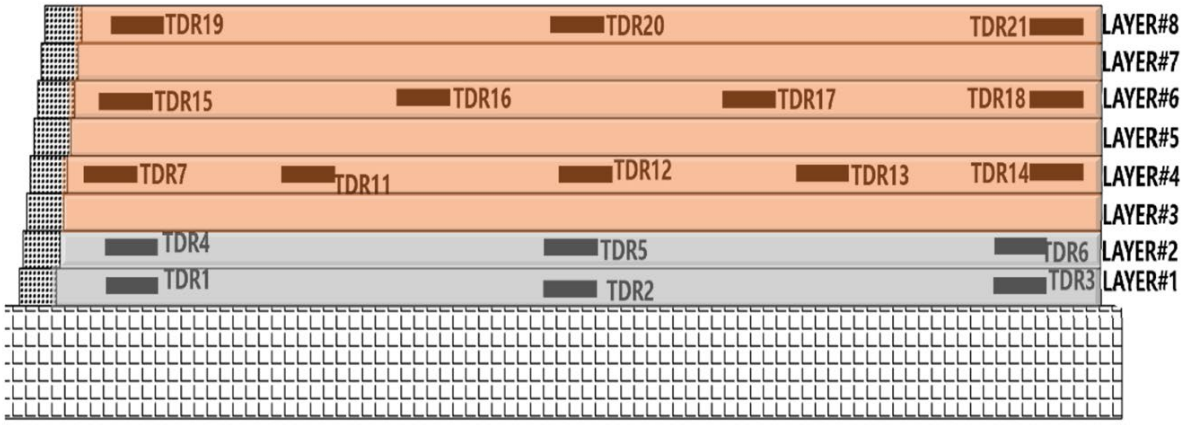

Figure 2.13 Approximate locations of TDR probes. Probes were placed along the centerline of the backfill (not to scale).

2.8.2 Standpipes

Two open standpipes were used in two different locations at 3.5 m and 5.0 m from the back of the wall to measure any ponding of water on the impermeable base of the MSE wall. Two water level indicators were placed inside the standpipes that make audible and visual notifications when they detect water. Water level indicators consist of a probe, a cable with laser-marked graduations, and a cable reel.

2.8.3 Environmental Sensors

The primary variables controlling evaporation rates during drying is the ambient temperature, relative humidity, and wind in the laboratory environment. Thus, a fan was set up to blow air over the top of the facility during drying. Temperature and relative humidity were monitored using a smart thermo-hygrometer model (H5179 Govee.)

2.8.4 Reinforcement Strains

Because of the focus of the research on wetting-drying cycles only the first layer of geotextile was instrumented for mechanical response. For this layer, the geotextile was divided into 3 parts with an overlap to simulate the plane strain condition for the strain gauges and extensometers. Strain gauges and extensometers were used to measure local and global strains respectively. They were mounted in the longitudinal direction to read the strains caused by outward movement of the wall face and probable failure planes through the geotextile. For this purpose, type strain gauges were used. To bond them to the geotextile, X-60 Adhesive glue and a five-minute glue were used underneath and on top of the gauge to make sure they will not detach. Then a layer of silicone was placed to make the system waterproof. Strain gauges were mounted at defined locations on top of the geotextile. They were connected to the D/A system selecting the 4-wire ohm function in the software to measure uniform axial strains.

2.8.5 Vertical Earth Pressure

Seven Geokon EP4500 earth pressure cells (EPC) were used to measure the vertical earth pressure due to the weight of the backfill along the base of the wall. The EPCs were placed at the base of the wall using Plaster of Paris to level and waterproof them.

2.8.6 Horizontal Toe Loads

Six toe load rings were used to record the movements of the toe caused by transferring the horizontal loads from the facing column above it. After calibration, they were installed between a beam bolted to the ground of the laboratory and the beam under the first row of facing blocks. The rollers under the facing blocks caused the horizontal and vertical loads decoupled. These 6 rollers were the reason that the horizontal component of the load was measured roughly separately from the vertical component. The aluminum load rings have four strain gauges attached to the bridge circuit to record the load at the connection to the ring. The capacity of the toe load rings is 22kN each and powered by a 5 VDC power supply.

2.8.7 Vertical Toe Loads

To measure the vertical load caused by the facing blocks, a series of 18 load cells in different capacities were used. After calibration, they placed directly on top of the foundation under a metal plate to apple the whole load by the blocks uniformly. The bolts inside the load cells were leveled

to touch the plate perfectly as the zero situation. 4 types of load cells in 4 different capacities proper to a different location in the aspect of applied load were used. one being a Canister type load cell models C62H1K-10P3 in 4.5 kN capacity and C62H-3K-10P3 in 13.5 kN capacity manufactured by Intertechnology Inc; the other one is a disk compression load cell (manufactured by Hoskin Scientific) which have 22 kN capacity. A third type was a homemade load cell that has four strain gauges attached to a steel disk when the compression load is applied to the disk.

2.8.8 Fiber Optic Moisture Sensors

Fiber optic sensors provide high density measurements of either strain or temperature. In this research an attempt was made to use fiber-optic (FO) based high-density temperature measurements to detect the passing wetting front and potentially cooling during evaporation. Figure 2.14 shows a typical layout and a photograph of an installed FO sensor. Four 45-m reels of fiber optics were used on top of layers 2, 3, 5, and 7. They were attached to the geotextile and transected the layer in six segments. A fiber optic reader, provided by LUNA, is used to detect strains in the fiber optic sensor at high resolution. In this test, cold water from the rainfall event was anticipated to induce a detectable thermal response from the fiber optics. However, the post-processing was unsuccessful. Typical data and a brief explanation is provided in Appendix A.

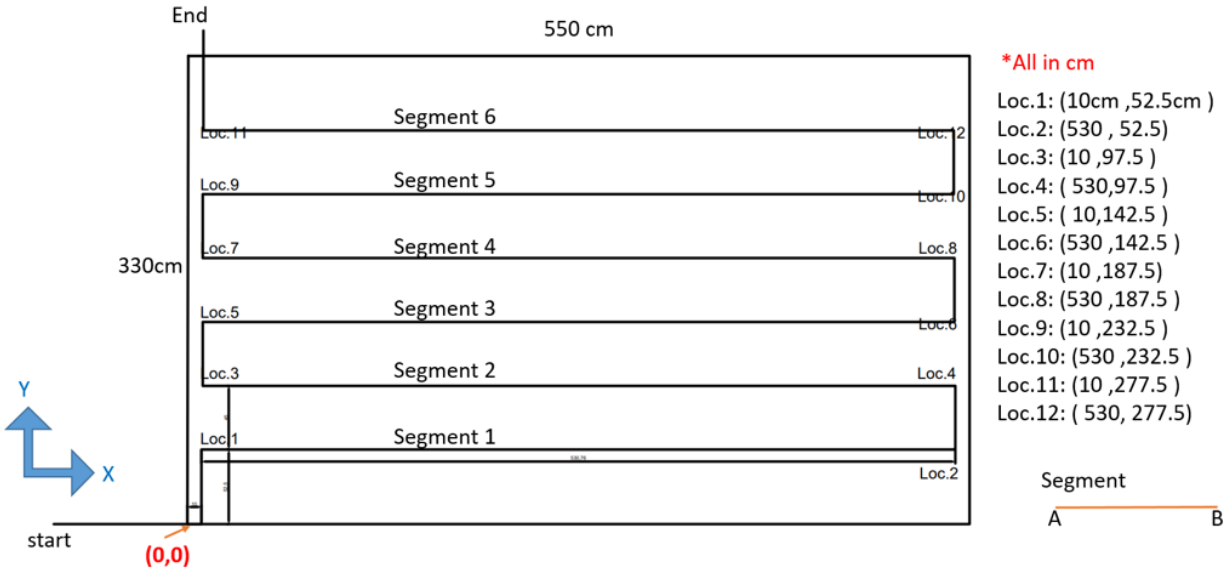

(a)

(b)

Figure 2.14 (a) Typical fiber optic layout on a reinforcement layer and (b) photograph showing fiber optic cable attached to reinforcement.

2.8.9 Chemical Analysis

The pH and total dissolved solids (TDS) of outflow water collected during wetting events were measured using pH and conductivity/TDS meter probes. Concentrations of dissolved calcium and sulfate ions (Ca^{2+} and SO_4^{2-}) were measured using inductively coupled plasma optical emission spectroscopy (ICP-OES), as these ions are identified as the dominant contributor to RCA tufa formation during the previous laboratory studies (Abbaspour and Tanyu, 2019b, 2021).

2.9 Wall Construction

The general MSE wall construction sequence was as follows:

- Outflow collection system: A 1-m × 0.5-m wooden box was built in front of the wall face to collect outflow water. The box was sealed using a plastic sheet and silicone to form a small dam in front of the wall face to collect outflow water draining from the toe and other probable points of the wall face (e.g., facing block seams).
- Support for face instrumentation: A metal beam was welded to the floor to support three metal H columns to install the potentiometer LVDTs used for measuring horizontal movements of the wall face.
- Facing blocks: A series of concrete blocks were placed as the facing in front of the wall.
- Backfill: RCA material was screened, washed, stored, and placed inside the wall using an overhead crane. The RCA was spread by hand and compacted.
- Compaction: Water was added to the RCA to reach the optimum moisture content determined via Standard Proctor compaction testing. Initially 200 mm of soil was laid out evenly and then compacted to for a final lift thickness of 150 mm. For this purpose, the electric jumping jack was used for four passes and a hand compactor performed 4 passes of compaction for the first

meter of backfill close to the face of the wall. The height of the manual compactor plate drops was approximately 300 mm.

- Soil density and moisture content measurements: At the surface of each compacted layer, 9 points were selected to check the moisture content and the bulk density of the material to ensure that all points have a value of dry density greater than 95% Standard Proctor. A Troxler 3411-B nuclear densimeter was used in the backscatter mode for these measurements. The RCA was recompacted if it did not achieve moisture and density values in the specified range.
- Reinforcement placement and facing connections: Geotextiles were placed after compaction and placement of the instrumentation inside the lifts. They were locked between the facing blocks and bolted to the previous block using metal strips. Geotextile was divided into three parts with 100mm overlap for the first layer (instrumented layer), and for the other layers, they were placed as a one-piece sheet on top of the soil folded at lateral and back sides to enforce water passing through them vertically.

2.10 Wetting and Drying Cycles

A wooden frame (Figure 2.15) was built and a series of connected sprinklers (Figure 2.16) in ten rows were used as a rainfall system. All sprinklers were adjusted before the tests to ensure they applied a uniformly distributed rate of flow to the backfill surface.

Figure 2.15 Wooden frame to support backfill sprinkler system

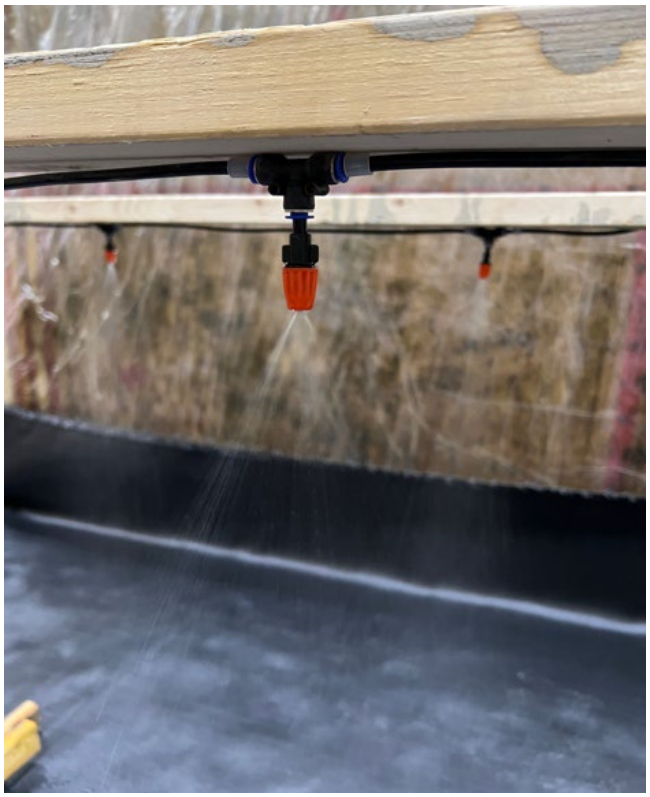

Figure 2.16 Sprinkler nozzle used to apply wetting events to backfill surface

Three wetting-drying cycles were applied to the walls in a series of five discreet events. Table 2.4 summarizes the timing of rainfall events and drying periods applied to the MSE wall system. Five rainfall events were applied ranging from 1”-2.5” of water. After the rainfall events, drying periods of between 1 and 13 days were allowed for drainage and evaporation. During this time a commercial fan passed air over the top of the wall to enhance evaporation.

2.11 Post-Test Excavation, Sampling and Analysis

2.11.1 Geotextile Sampling

Excavation was initiated after the wetting-drying cycles were complete. Geotextile samples were carefully exhumed in 9 locations and at various depths of the backfill (Figure 2.17). Pre-excavations were made as 2 ft. × 2 ft. square holes, from which 12-inch × 12-inch geotextile samples were exhumed. Nine RCA samples at each layer were also taken to measure moisture content and grain size distribution at these locations. After air-drying on a shelf the geotextile samples were carefully packaged and shipped to GMU for analysis. In total, a set of 54 geotextile samples were exhumed. Figure 2.18 shows a schematic location of the exhumed samples from all 6 layers of the large-scale experiment. Two locations were also chosen at each layer for determination of sand cone density. During the excavation, optic fibers, TDRs, and other instruments were retrieved and stored.

Table 2.4 Sequence of Wetting-Drying Cycles

Start of event	End of event	Elapsed time since first wetting (days)	Event
2022-May-04 10:33	2022-May-04 10:58	0-0.02	1st wetting event – 1”
2022-May-04 10:58	2022-May-05 13:10	0.02-1.11	Drying cycle
2022-May-05 13:10	2022-May-05 13:48	1.11-1.14	2nd wetting event – 1.5”
2022-May-05 13:48	2022-May-16 9:41	1.14-11.98	Drying cycle
2022-May-16 9:41	2022-May-16 10:17	11.98-12.0	3rd wetting event – 1”
2022-May-16 10:17	2022-May-17 9:53	12.0-13.0	Drying cycle
2022-May-17 9:53	2022-May-17 10:32	13.0-13.02	4th wetting event – 1.5”
2022-May-17 10:32	2022-May-30 13:48	13.02-26.1	Drying cycle
2022-May-30 13:48	2022-May-30 14:58	26.1-26.2	5th wetting event – 2.5”
2022-May-30 14:58	2022-June-09 10:00	26.2-36.0	Drying cycle
2022-June-09 10:00	2022-July-06 11:00	36.0-63.0	Deconstruction

(a)

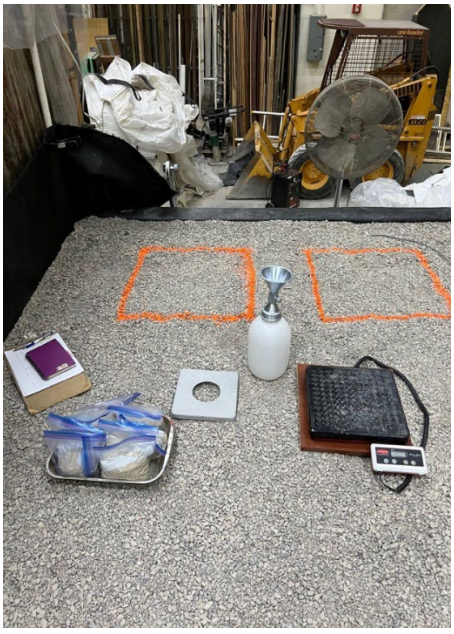

(b)

(c)

(d)

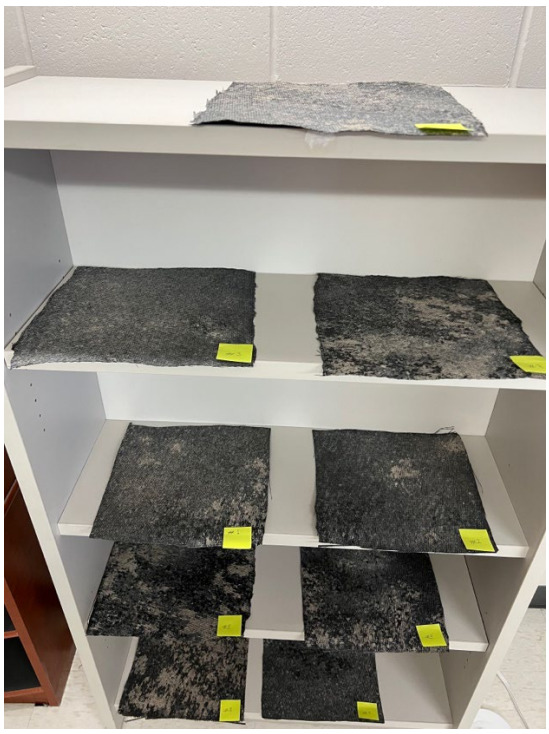

(e)

Figure 2.17 Exhumation of geotextile samples: (a) marking sample locations; (b) sand cone density measurements; (c) pre-excavation of samples; (d) brushing, cutting and exhuming samples; (e) air drying exhumed samples prior to shipment

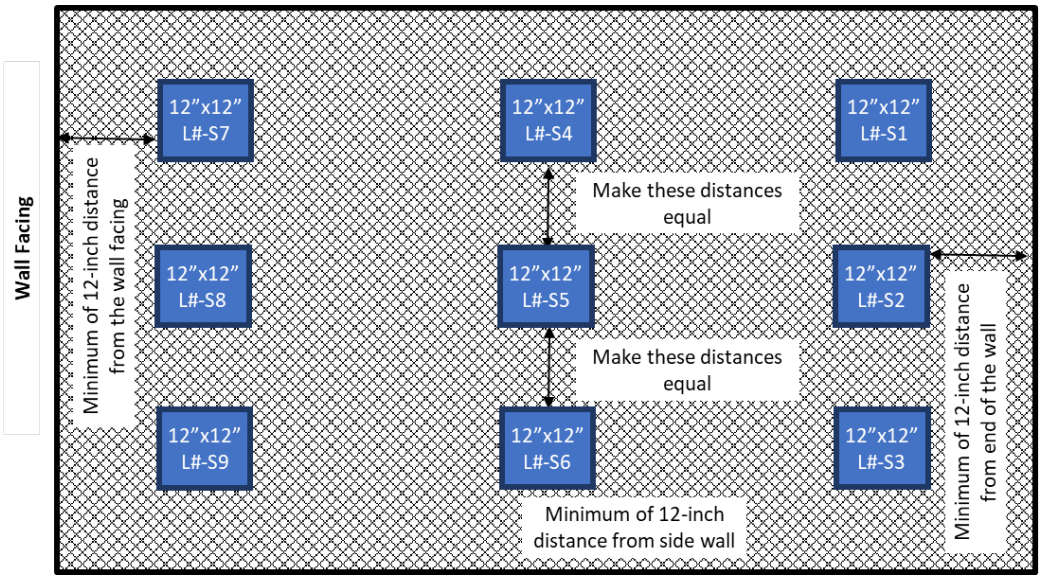

Figure 2.18 Schematic plan view of locations of the exhumed woven geotextile samples (same for all 6 layers) used in large-scale wall simulation

All geotextile samples shipped to GMU were inspected to select the most representative samples for further analyses. Based on the screening, samples from the middle of all geotextile layers (samples identified as L1-S5 through L6-S5) were selected for this purpose (8 samples). Considering that all samples were selected from almost the same location in each layer of the experiment, this approach was followed to also allow the investigation of the observed changes in infiltration properties of the geotextiles (if any) based on the height of the large-scale test.

It is reasonable to assume that lower layers having a higher amount of RCA material on top will be exposed to higher concentrations of leached ions and potentially can experience higher degrees of tufa precipitation. Therefore, an additional 2 samples from the mid-section of layer 5 (samples identified as L5-S2 and L5-S8) were selected for further investigations in order to evaluate the effect of boundary conditions (by the face of the wall and towards the back end of the backfill) on the occurrence of clogging phenomena. The reason for selecting layer 5 samples over layer 6 samples is that the geotextile reinforcement placed in layer 6 was cut in 1.5 m stripes prior to placement over RCA material. Although cutting the geotextile might not affect its mechanical behavior in the wall (in terms of tensile stress and strain), this layer is considered unsuitable for purposes of studying flow conditions. Therefore, the study focused on the samples from layer 5 instead of layer 6. All samples were evaluated for both permittivity tests and microscopic imaging as the dimensions of the samples (approximately 30 cm × 30 cm or 12 in. × 12 in.) were large enough to extract samples without compromising their integrity.

The total number of samples selected for detailed evaluation was 10 even though the scope of the GMU proposal submitted to RMRC requires an in-depth evaluation of 6 samples. The GMU team was able to investigate additional samples because of the timely shipment of the samples by the RMC team.

2.12 Column Tests

Parallel to the test conducted by the RMC team, the GMU team constructed a column test with the same height (1.22 cm) and reinforcement configuration at the GMU's laboratory. Figure 2.20 shows the photo and the layout of the experimental set-up.

The materials used in the construction of the column test (processed RCA and woven geotextile) were shipped to the GMU laboratory by the RMC team. Therefore, these materials were the same materials used in the construction of the large-scale experimentation simulating an MSE wall. The column consisted of a chamber with an inner diameter of 15.25 mm (6 inches). The first layer of RCA material was placed at the height of 30.50 cm (12 inches) followed by six (6) layers of 15.25 mm (6 inches) high. Woven geotextiles were placed in between each layer and glued to the inside of the column chamber with silicone glue. This method was used to fix each layer of geotextile and create a barrier on the edges of the geotextile samples to prevent sidewall leakage as previously demonstrated by Abbaspour and Tanyu (2021).

Three cycles of rain events were conducted on the column similar to the large-scale test. The flowchart in Figure 2.21 summarizes the sequence of the wetting and drying cycles and the tests conducted during and after the termination of the test.

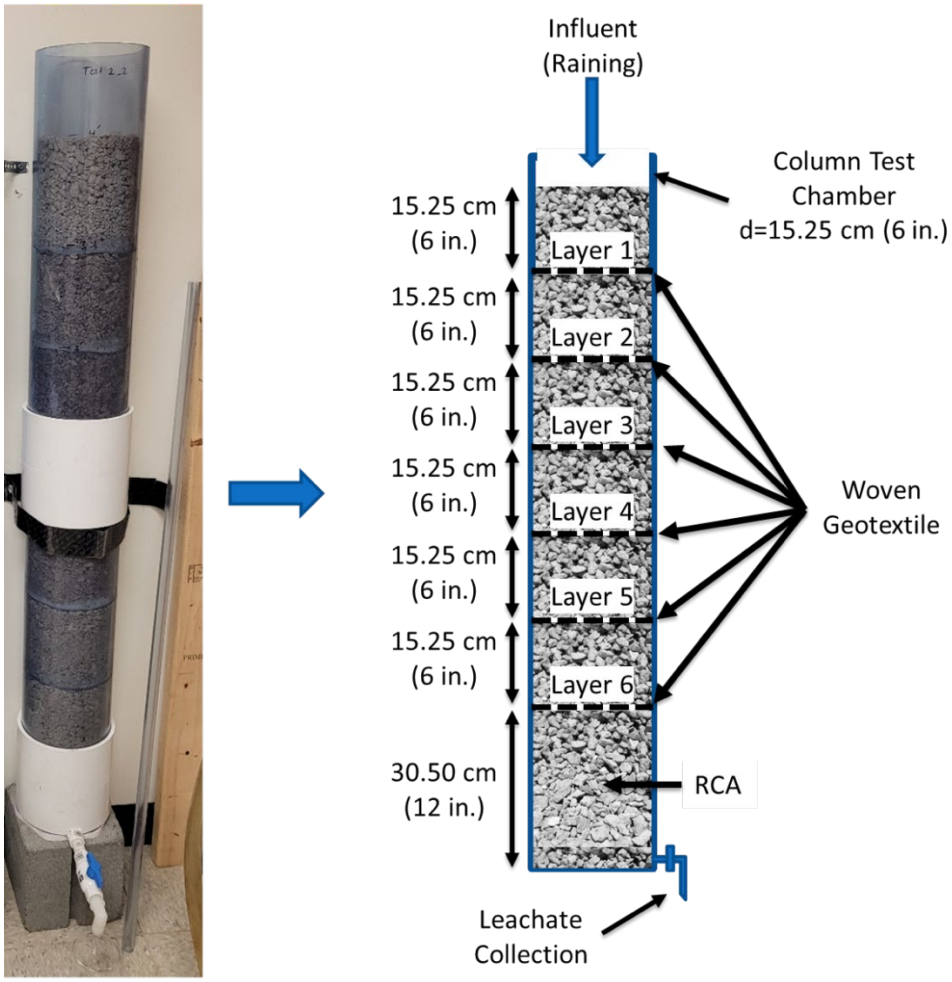

Figure 2.20 Photograph and schematic section of the GMU column test

Exhumed geotextile samples from the column experiments were divided into two groups and each group of samples was used only for one set of analyses. Therefore, geotextile samples from layers 2, 4, and 6 (identified as CT-L2, CT-L4, and CT-L6) were selected for chemical clogging evaluations by means of microscopic imaging and image analysis. Samples exhumed from layers 1, 3, and 5 were selected (identified as CT-L1, Ct-L3, and CT-L5) for permittivity tests. As the samples are selected from equally spaced layers, the intention was to correlate the number of layers above each sample to the changes in properties of the geotextile samples (if any).

Exhumed geotextile samples from the column test were circular with a diameter of 15.25 mm (6 in.) and used for permittivity tests and microscopic imaging. As pointed out by Abbaspour et al. (2018), it is not possible to run both permittivity tests and microscopic imaging on the same geotextile samples exhumed from a given column experiment as samples lose their integrity during the process.

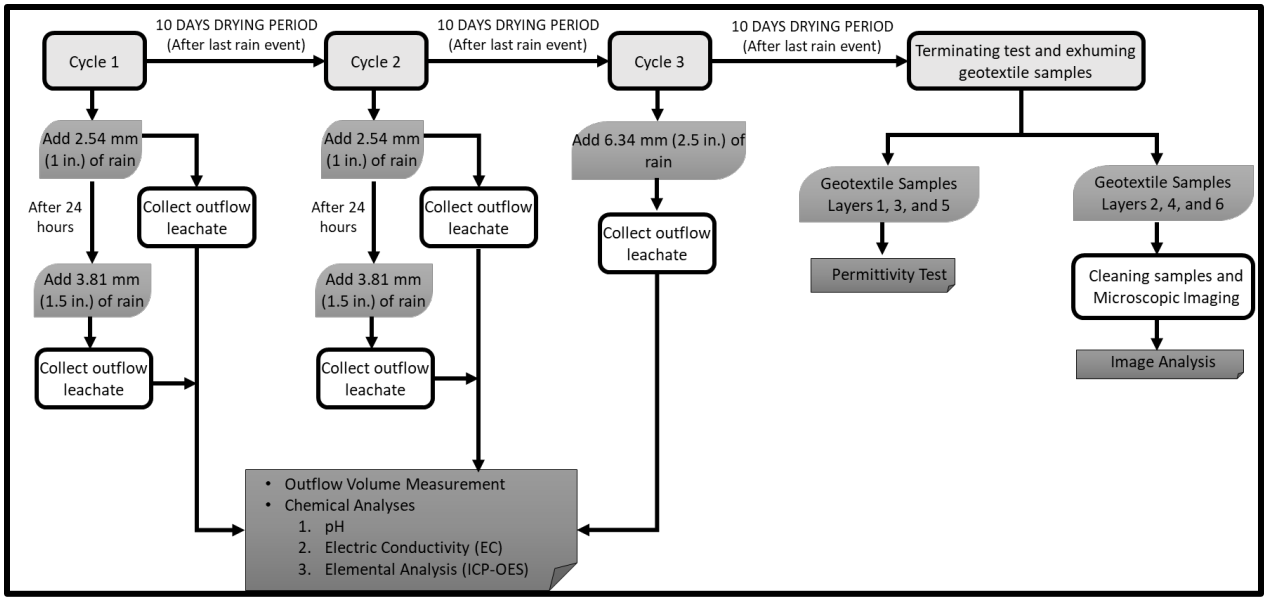

Figure 2.21 Flowchart of the sequence of wet/dry cycles and testing program for column test

2.13 Permittivity of Exhumed Geotextiles

The permittivity of virgin and exhumed geotextiles was determined following the procedures prescribed in ASTM D4491. Circular samples were cut from the larger samples (exhumed from the large-scale wall test) but the samples from the column test were used as is. Samples were soaked for a minimum of 24 hours before being placed into the permittivity test chamber. Tests were started with an applied head of 10 mm until flow was stabilized. After which applied head was increased in 10 mm increments to measure the permittivity of the samples at higher flow discharges.

2.14 Microscopic Imaging of Exhumed Geotextiles

The geotextile samples were cleaned prior to microscopic imaging by initially air-drying. The surface of the geotextile was cleaned using an archeologist brush and smooth air blow technique. After removing all of the loose particles, the remaining residuals were further evaluated under a microscope to determine whether the residuals have the known morphology of the RCA tufa (a result of chemical precipitation) or they resemble the deposits due to particle migration and entrapment (physical clogging). For all of the samples evaluated in this study, the observed deposits over the geotextile surfaces were determined to be dried RCA mud or RCA particle residuals. These deposits were easily removed using the same brushing and air-blowing technique.

After cleaning the samples, microscopic imaging was conducted using a Leica M125 C microscope (Figure 2.19) with a built-in 5 MP HD digital camera. These images were analyzed using Leica LAS X software. This process included removing the noise (in the form of reflections on the sample surface) and applying multiple image-enhancing filters as described by Abbaspour and Tanyu (2021). After enhancing the picture, the image was analyzed to include binary pixels that

could be quantified by the software. This allowed the surface area covered with precipitate deposition and marked as white pixels to be identified and quantified based on the calculated unit surface of various areas.

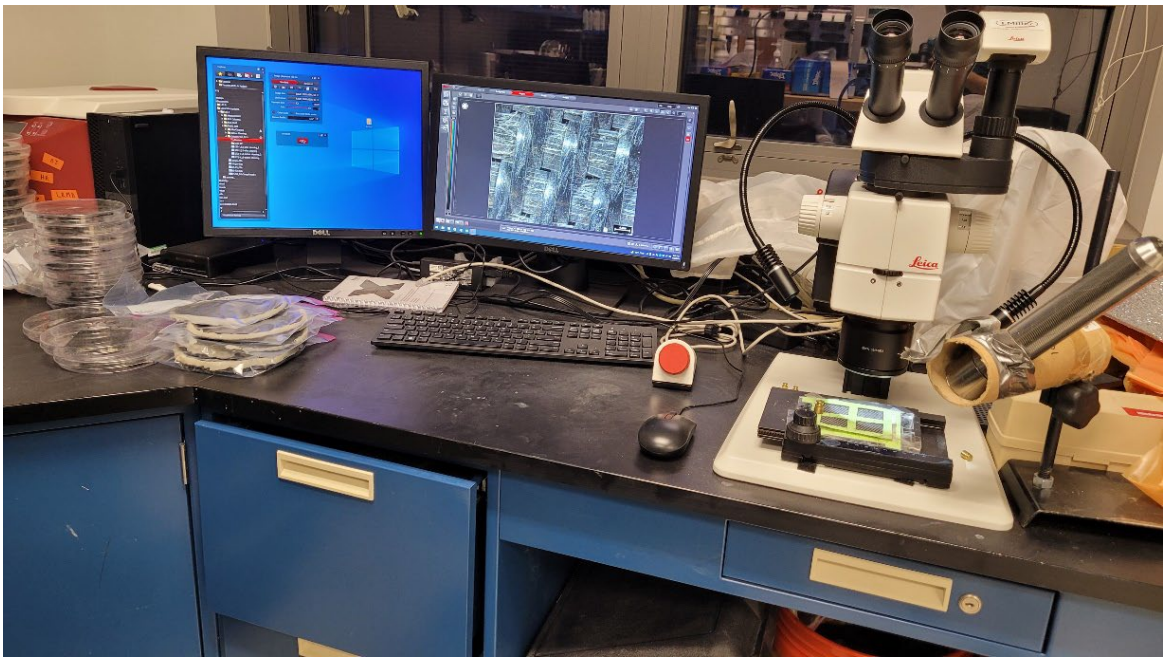

Figure 2.19 Leica M125 C microscope with a built-in 5 MP HD digital camera with a geotextile sample under analysis

CHAPTER 3: EXPERIMENTAL RESULTS

3.1 RCA Compaction: MSE Wall Construction and Excavation

Figure 3.1 shows compaction conditions (dry density) for the RCA backfill in the MSE wall test as obtained by Troxler gauge testing and sand cone measurements during construction and excavation, respectively. Results indicate that greater than 95% standard proctor density (1,624 kg/m^3) was achieved in all layers and that the wetting-drying test sequence did not significantly modify the backfill density. Figure 3.2 shows gravimetric moisture content readings taken during construction. Average moisture varies from ~6% near the top of the backfill surface, increasing to ~8.2% near the base of the wall. The decrease in moisture near the surface is attributed to surface evaporation during the construction sequence.

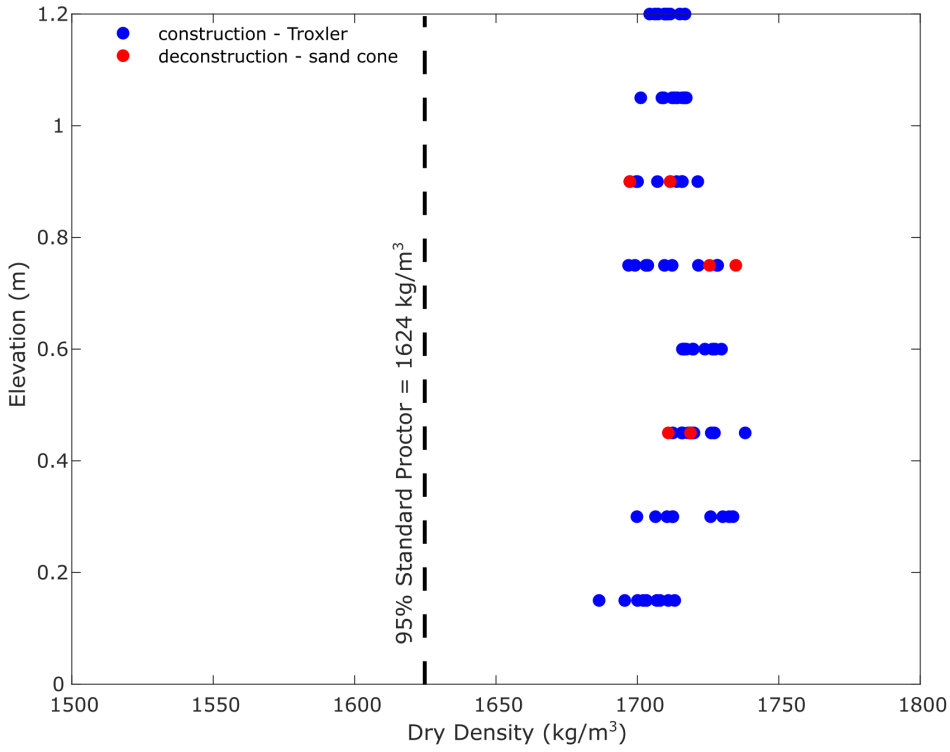

Figure 3.1 Compaction measurements during construction and excavation of the MSE test wall.

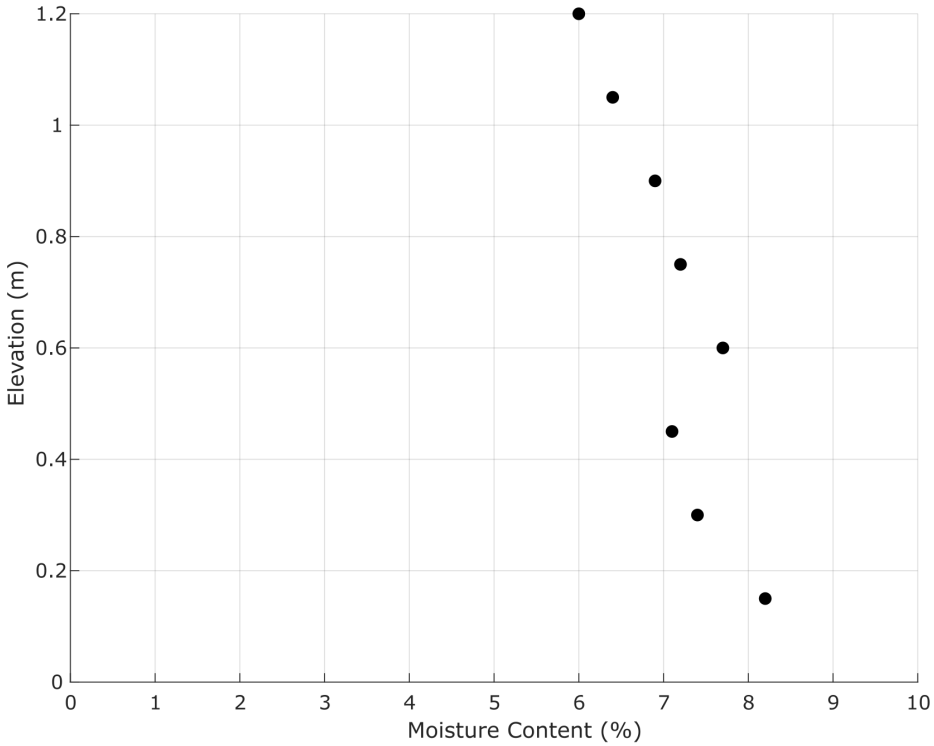

Figure 3.2 Average moisture content measurements during construction

3.2 Boundary Measurements during Wetting-Drying Cycles

3.2.1 Water Outflow

For each rainfall event the wetting front proceeded through the backfill and outflow was collected at the toe of the wall. Figure 3.3 shows cumulative inflow at the backfill surface and cumulative outflow throughout the experiment. The first and third rainfall events proceeded similarly. In both cases most of the water was retained within the backfill with only minor quantities of outflow collected over the next day. The second and fourth rainfall events also proceeded similarly. Almost immediately after initiation of wetting, measurable outflow at the toe occurred. Significant outflow occurred for the next two to three days and then tailed off during the drying cycle. To investigate the effect of larger rainfall, the fifth rain event of 2.5" was completed in a single step. Almost simultaneously outflow was recorded and significant outflow continued for the next two days before tailing off for the following nine days.

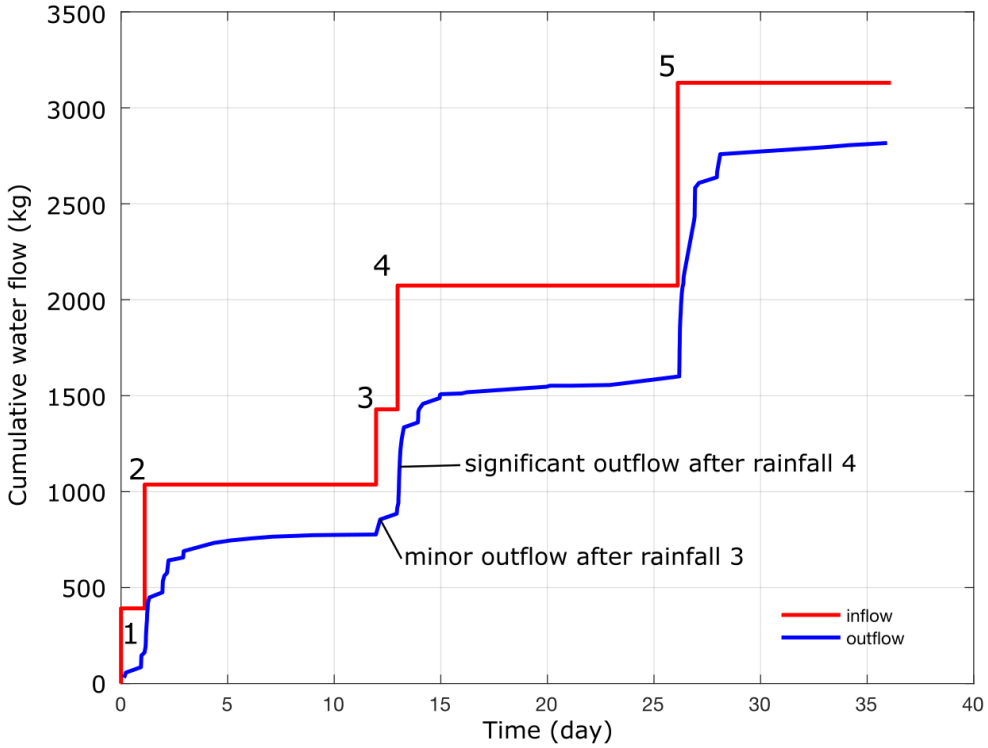

Figure 3.3 Inflow and outflow of water measured at the boundaries.

3.2.2 Chemical Analysis of Outflow

Chemical analysis of the outflow water was periodically performed. During and after each rainfall event, 50-ml leachate samples were collected from the outflow every hour in the first six hours. After this period, samples were taken every six hours. These samples were analyzed for pH and EC. Results plotted in Figure 3.4 and 3.5 show pH beginning at 12.45 and spiking up to over 12.6 with initial outflow following the larger rainfall events. After the peak, pH decreases non-linearly to less than 11.4 after both the 2nd and 4th rainfall events. EC measurements were initially approximately 4 mS but then decreases as outflow continued. Following the subsequent initial rainfall after the drying cycles, the EC increased again for the higher outflow period and then decreased along with the lower outflow volumes.

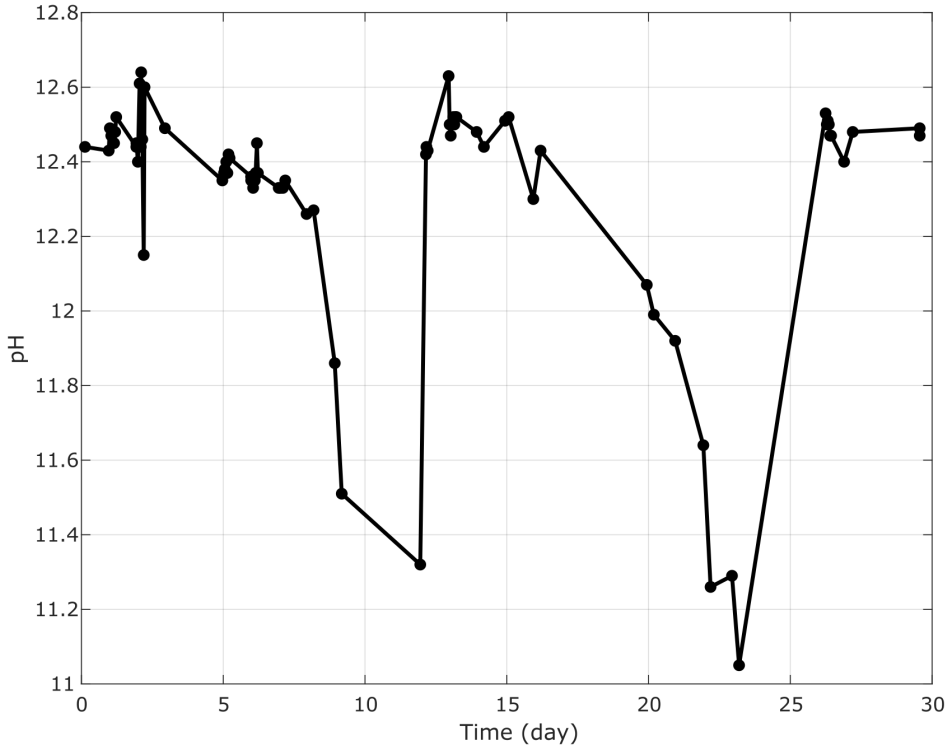

Figure 3.4 pH values of outflow samples

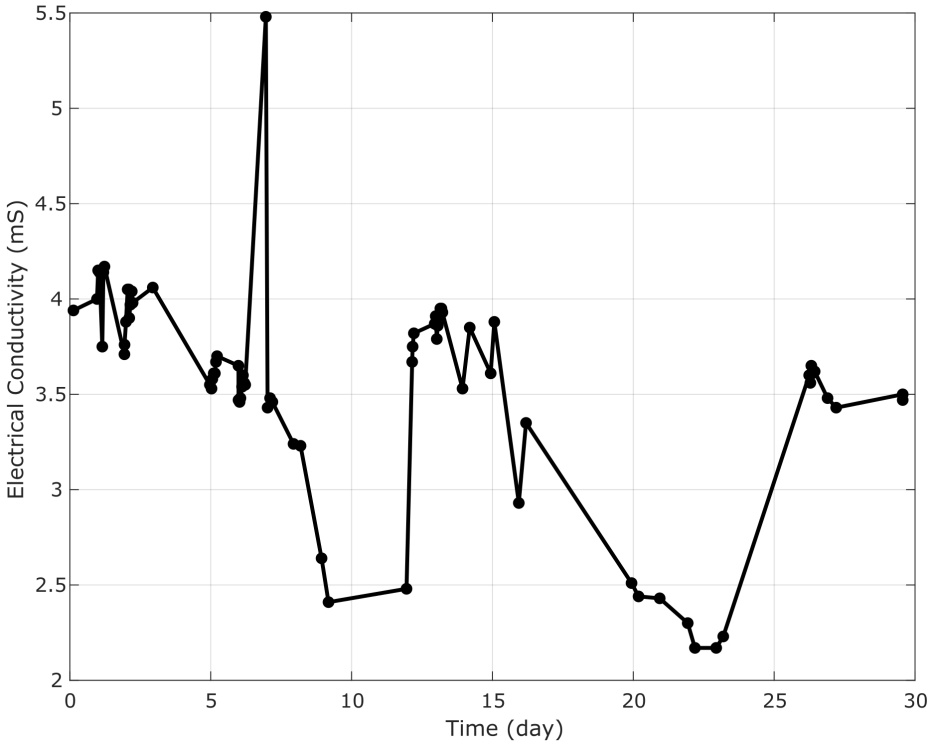

Figure 3.5 EC values of outflow samples

3.2.3 Environmental Conditions

Temperature and relative humidity records at the top surface of the wall are plotted in Figures 3.6 and 3.7 respectively. Ambient temperature remained between 20 and 24 ºC. Relative humidity above the backfill surface was close to 100% during rainfall events, with some response due to evaporation of the upper backfill layer during the drying period. The large fan located next to the wall refreshed the local air above the wall surface to maximize evaporation potential and induce drying of the backfill. Temporary increases in temperature coincide with the opening of the external doors due to operational requirements of RMC research.

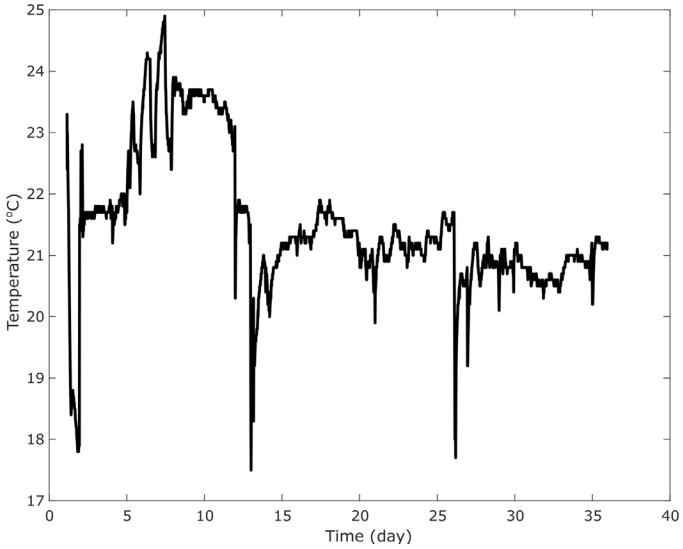

Figure 3.6 Air temperature above the MSE wall backfill

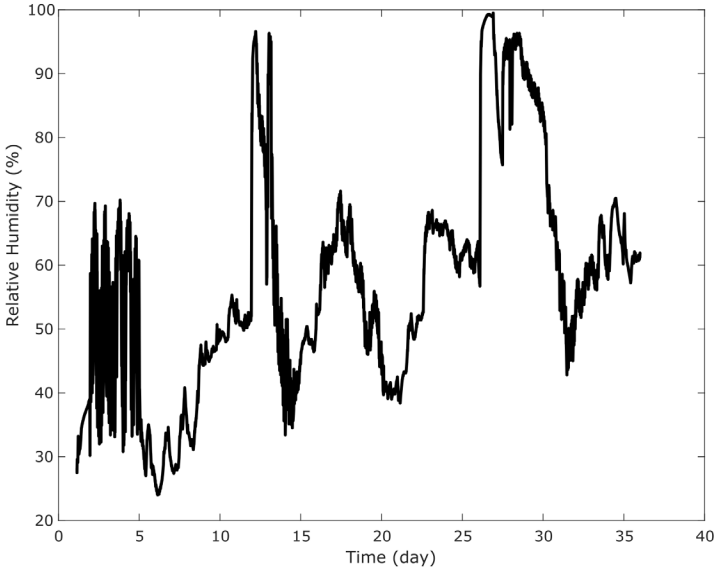

Figure 3.7 Relative humidity above the MSE wall backfill

3.3 Internal Measurements during Wetting-Drying Cycles

Moisture-related measurements within the backfill consisted of TDRs, standpipes located at the base of the facility, and fiber optics. The fiber optic measurements proved difficult to interpret but are included in the appendix for completeness, along with commentary on observations that could be made.

Typical TDR responses plotted as volumetric water content (VWC) versus time are shown in Figure 3.8. Two plots are shown to represent the response of a TDR placed in a sandbag near the surface (Figure 3.8a) and a TDR in backfill near the base (Figure 3.8b). Figure 3.8a shows that VWC in the top backfill layer increased almost immediately after rainfall initiation, which indicates passing of the wetting front at that elevation. Just 14 minutes passed between the beginning of the rainfall event and detection by this TDR. After the wetting front passes, VWC of the TDR in the sandbag remains at an elevated level (VWC~0.3) due to higher capillarity of the sand relative to the surrounding backfill. Later at 4 days, water in the surrounding sand bag seeps out and the measured VWC decreases accordingly. At initiation of the third rainfall event, the wetting front is once again detected and the response repeats again for the fifth and final rainfall.

Figure 3.8b shows the typical response of a TDR placed directly in contact with backfill in the lowest layer of the wall profile. After initiation of the first rainfall, 52 minutes later, VWC increases as the wetting front passes. After a rise to VWC=0.1, moisture content decreases gradually for the rest of day 1. Then 46 minutes after initiation of the second rainfall event on day 2, VWC again spikes and gradually decreases again. Over the next 10 days VWC decreases asymptotically to its initial value 0.06. These responses are repeated for rainfalls 3, and 4 on days 11 and 12 as well as rainfall event 5 on day 26 as VWC peaks in response to the passing wetting front and then gradually decreases during drying phases.

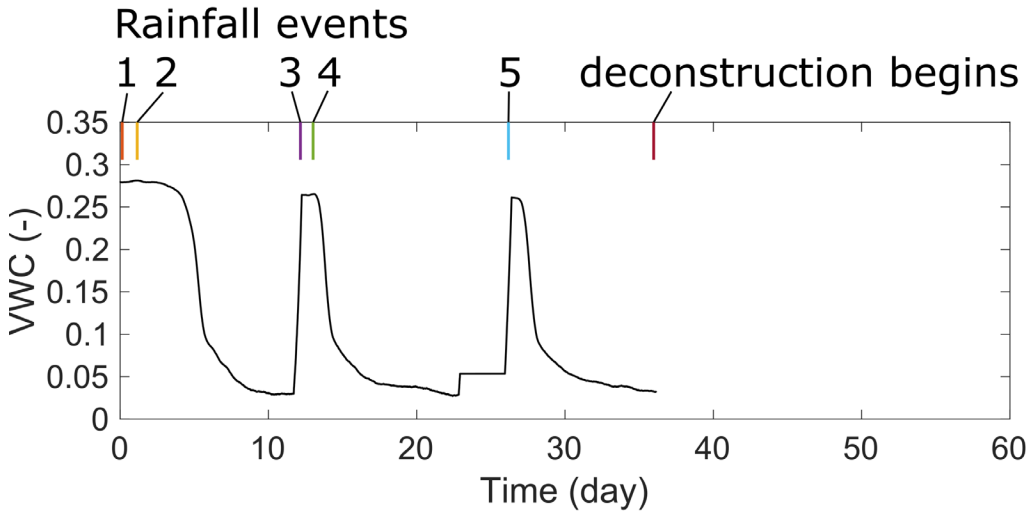

(a)

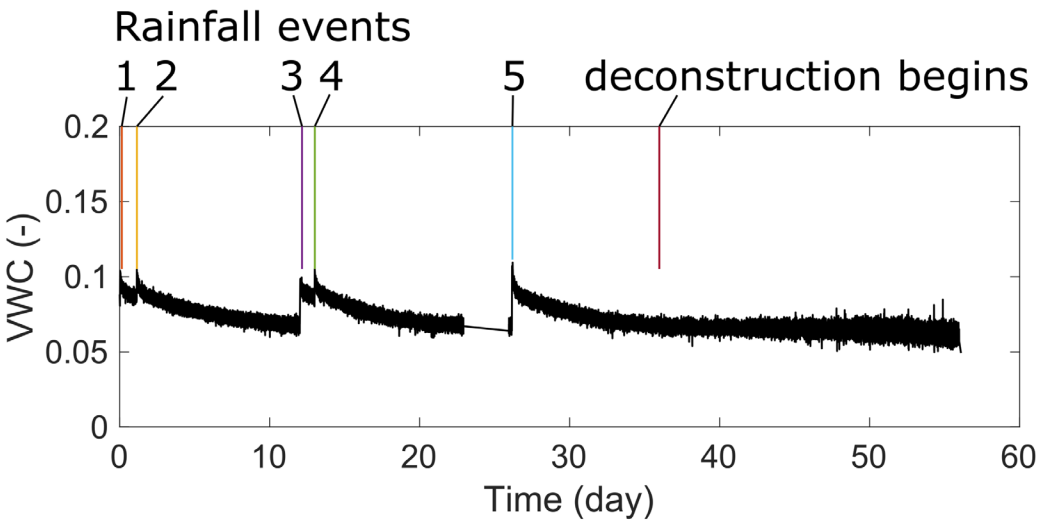

(b)

Figure 3.8 Typical TDR readings for a) TDR20 placed in sandbag in the top layer, and b) TDR5 placed in contact with RCA backfill in the bottom layer.

The combination of TDRs placed in sandbags and backfill provides quantitative data to track passage of wetting fronts through the reinforced wall backfill. All TDR readings are plotted in Figure 3.9 and distributed within the figure in their relative location in the RCA backfill. The majority of the TDR measurements follow the typical responses described in the previous paragraphs. This is especially true in the top two and lower two layers. Comparing the TDRs placed in the upper two layers shows the second layer generally drain slower than the top layer. Moisture content measurements during deconstruction confirmed the TDR measurements are accurate.

Even with the differing responses, consistent waterfront detection times are observed. Figure 3.10, for example, is a plot of wetting front elevation versus time for all five rainfall events. The results indicate linear progression of the wetting front as it passed through the RCA and reinforcement profile. The lines drawn on the figure show the wetting front reached the base of the facility between approximately 50-100 minutes. This absolute time and relative variation are expected for poorly graded gravels that are processed within the specification used in this study.

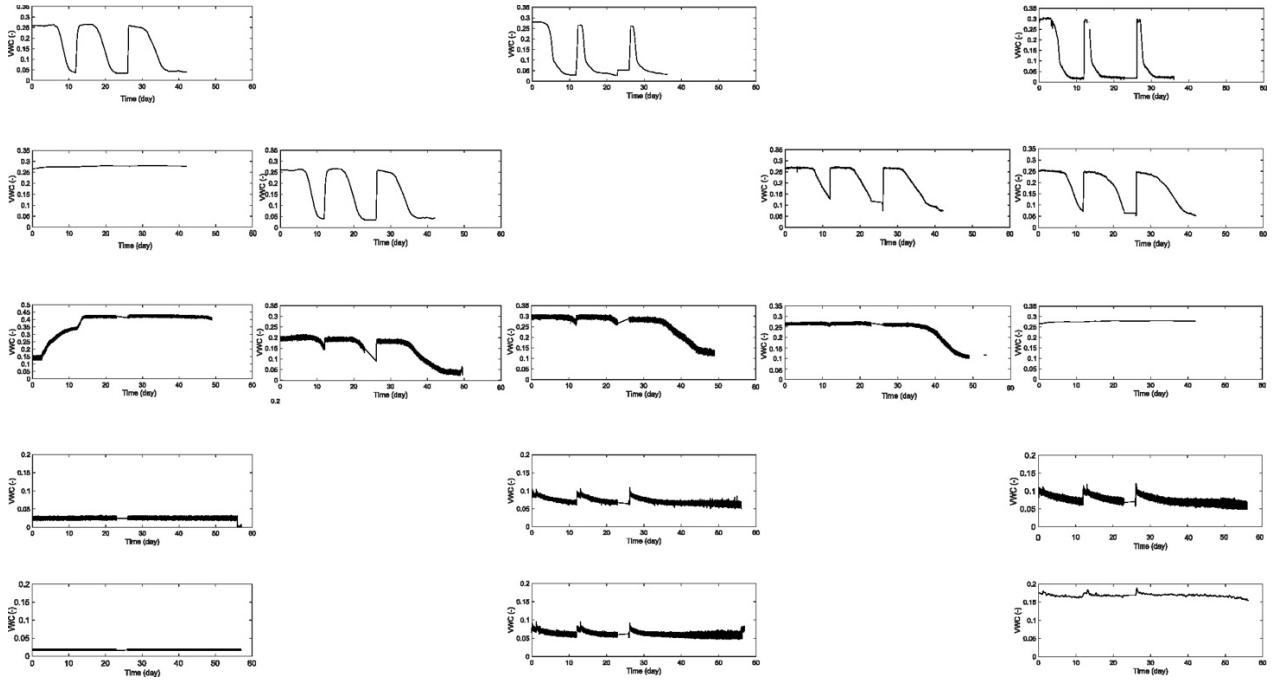

Figure 3.9 TDR readings throughout wall.

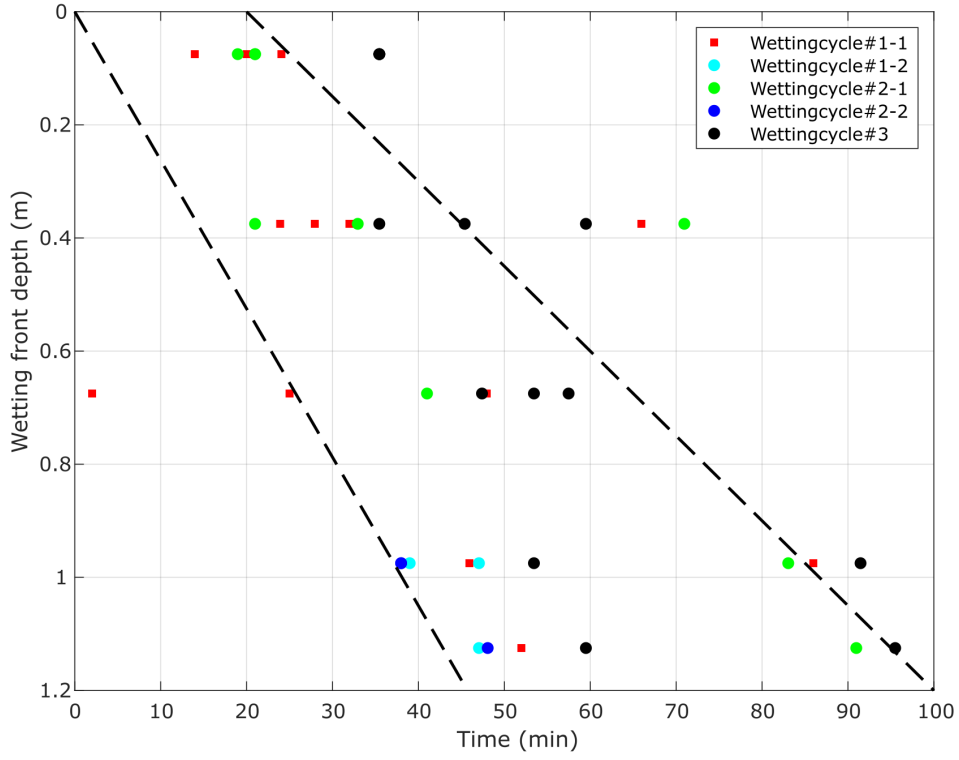

Figure 3.10 Wetting front versus time detected by TDRs

3.4 Measurements Obtained during Excavation

Measurements obtained during deconstruction and excavation included moisture content profiles, sand cone densities, and reinforcement samples for clogging and chemical analysis. The gravimetric moisture content measurement profile is plotted in Figure 3.11. Below 1m elevation measurements in the backfill just above and below the reinforcement are generally between 5-7% and average 6%. In the top layer drying to an average of 3.5% occurred due to surficial drying. Some outlier measurements also were recorded but there was no spatial significance to their distribution. The results show that moisture in the lower 7 layers is relatively constant due to capillarity while the top most layer experienced drying from the surface.

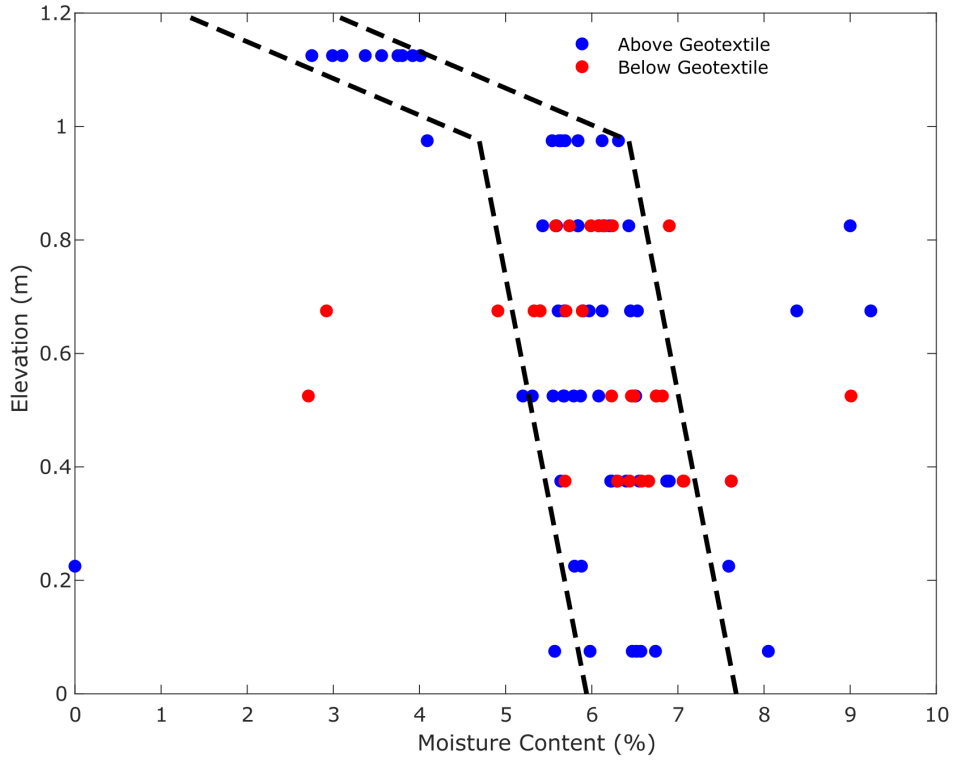

Figure 3.11 Moisture content measurements during excavation

3.5 Permittivity of Exhumed Geotextiles

The results of the permittivity tests are shown in Figures 3.12 and 3.13. In these figures, the permittivity ratio (Ψ_R) is calculated by dividing the permittivity of the exhumed geotextile by the permittivity of the virgin geotextile (Equation 1). Figure 3.12a shows results obtained from each layer of the large-scale wall experiment of the samples exhumed from the middle and Figure 3.12b shows the results from all of the samples exhumed from layer 5 of the large-scale wall experiment. Results for the L5-S5 are shown in both figures.

$$\Psi_R = \frac{\Psi_{used\ geotextile}}{\Psi_{virgin\ geotextile}} \quad (1)$$

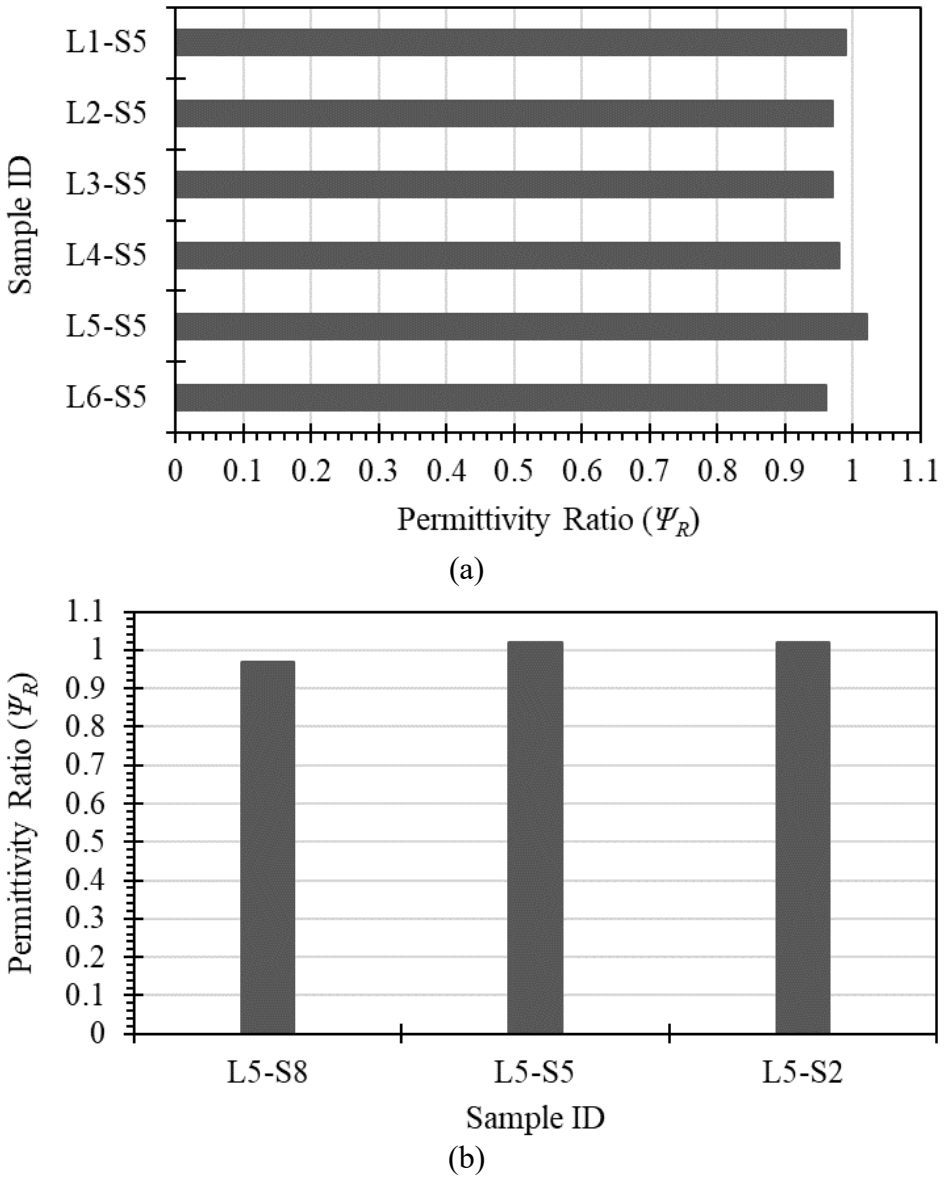

Figure 3.12 Results of permittivity tests on geotextile samples exhumed from large-scale wall (a) samples from the middle of all layers, (b) samples from the mid-section of layer 5.

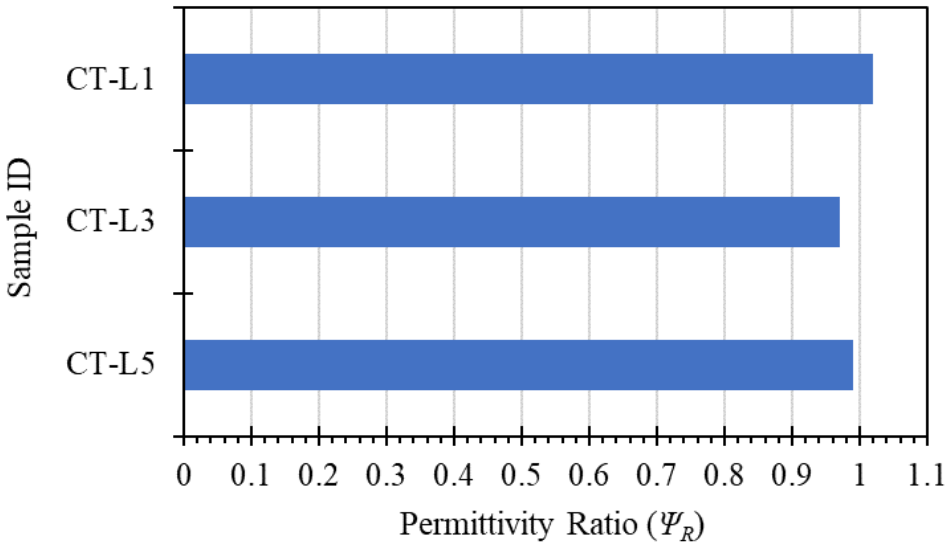

Figure 3.13 Results of permittivity tests on geotextile samples exhumed from column test.

As can be seen from these figures, calculated permittivity ratios for all samples fall in the range of 96% to 102% and have no particular order with respect to the location or layer number of the sample. Most of the observed variation (± 5%) can be attributed to the setup accuracy and operator error (Abbaspour et al., 2018). Based on this discussion, it appears that the loss in serviceability of the geotextile due to physical clogging in this study is non-existent or very insignificant. There is no analytical model for the loss of serviceability of the RCA/woven geotextile system due to physical clogging in the literature but if we use the model developed to calculate the loss of serviceability for the RCA/nonwoven geotextile (Abbaspour et al., 2018), the loss of serviceability will still be negligible, if not zero as shown in Table 3.1.

Table 3.1 Summary of the evaluation processes for a reduction in serviceability due to physical and chemical clogging phenomena in geotextile

Sample	Physical Clogging			Chemical Clogging	
	Ψ_R	$1-\Psi_R$	$R_{physical\ serviceability}$	S_{tufa}	$R_{chemical\ serviceability}$
L1-S5	99.0%	1.0%	Negligible	0.020%	Negligible
L2-S5	97.0%	3.0%	Negligible	0.011%	Negligible
L3-S5	97.0%	3.0%	Negligible	0.014%	Negligible
L4-S5	98.0%	2.0%	Negligible	N.D.	Zero
L5-S2	102.0%	-2.0%	Zero	N.D.	Zero
L5-S5	102.0%	-2.0%	Zero	N.D.	Zero
L5-S8	97.0%	3.0%	Negligible	0.016%	Negligible
L6-S5	96.0%	4.0%	Negligible	0.026%	Negligible
CT-L1	102.0%	-2.0%	Zero	N.T.	Not Tested
CT-L2	N.T.	N.T.	Not Tested	0.014%	Negligible
CT-L3	97.0%	3.0%	Negligible	N.T.	Not Tested
CT-L4	N.T.	N.T.	Not Tested	N.D.	Zero
CT-L5	99.0%	1.0%	Negligible	N.T.	Not Tested
CT-L6	N.T.	N.T.	Not Tested	0.025%	Negligible

Notes: N.D. = Not Detected; N.T. = Not Tested; Ψ_R = permittivity ratio between used geotextile and virgin geotextile (%); 1- Ψ_R = reduction in permittivity values (%); $R_{physical\ serviceability}$ = reduction in serviceability of the geotextile due to physical clogging (%) (Abbaspour et al., 2018; Abbaspour and Tanyu, 2019a); S_{tufa} = surface area of geotextile covered with tufa deposition (Abbaspour and Tanyu, 2021); $R_{chemical\ serviceability}$ = reduction in serviceability of the geotextile due to chemical clogging (%) (Abbaspour and Tanyu, 2021).

3.6 Microscopic Image Analysis

The results of image analyses were consistently below 0.01 and marked as not detected (as summarized in Table 3.1). Occasionally, values above 0.01% up to 0.032% were detected in the analysis, which can be associated with unfiltered noise and light reflection. Figure 3.14 and Figure 3.15 show two examples of as-is and cleaned geotextile samples under the microscope. Even though the after-cleaning, samples show signs of damage due to placement and compaction of RCA over geotextile, there is no indication of crystallization of any kind or deposition of RCA tufa as reported in the previous studies. Similar to physical clogging, even if the model developed for chemical clogging of the RCA/nonwoven geotextile (Abbaspour and Tanyu, 2021) were utilized, the results yield zero or negligible reduction in serviceability values. Therefore, it is determined that the samples analyzed in this study did not show any sign of chemical precipitations.

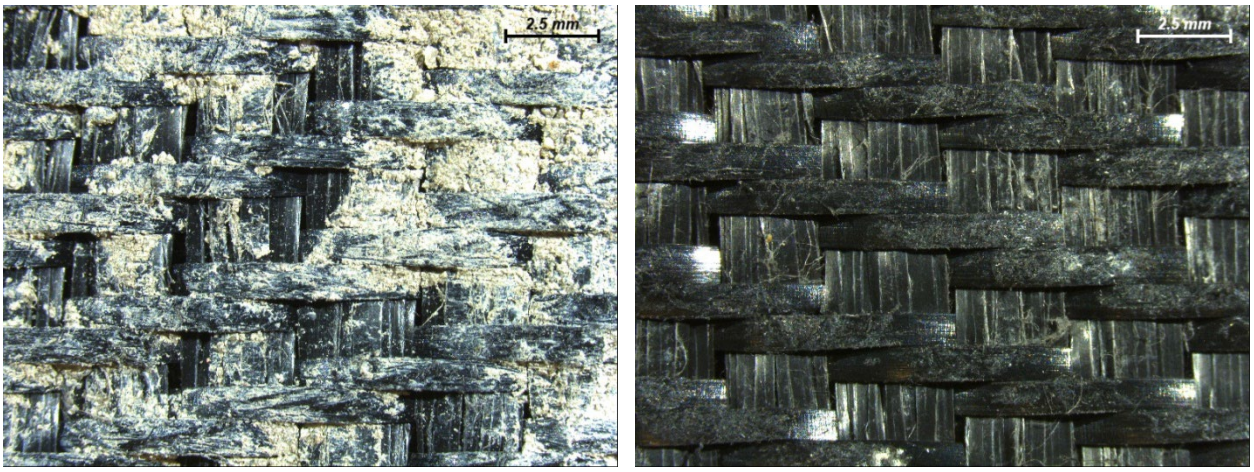

(a) (b)

Figure 3.14 Exhumed geotextile sample from the large-scale wall test (L5-S5) under the microscope, (a) before cleaning, (b) after cleaning

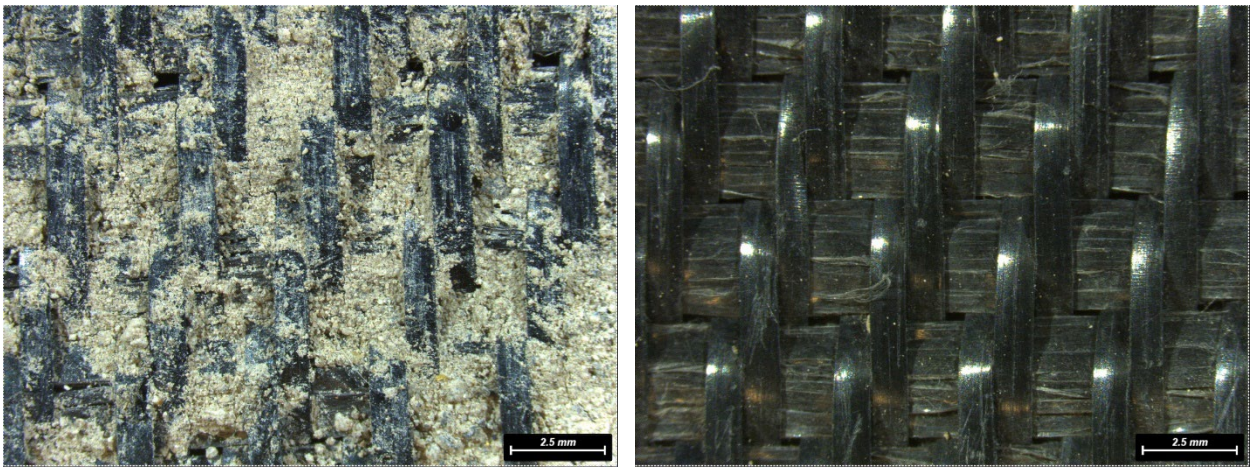

(a) (b)

Figure 3.15 Exhumed geotextile samples from column test (CT-L5) under the microscope, (a) before cleaning, (b) after cleaning

3.7 Chemical Analysis

The measured chemical properties of the outflow leachate from both the large-scale wall and the column tests are depicted in Figures 3.16 and 3.17. The pH values for both tests are very similar, especially after the first wetting-drying cycle. The pH of the outflow leachate in the column test is about 10.1 at the beginning of the testing but increases to values near 11 during the first day of the second cycle. The trend is followed by an increase to a pH value of about 12 after the second day of the second cycle which matches the pH values observed in the large-scale wall. The similarity in the pH values for both tests continues during the third cycle. The difference in the initial pH

value can be attributed to the pore moisture content of the RCA material in the two tests. As the column test is a much smaller sample than the large-scale wall, the material initially was most probably drier in the column test. Therefore, the pore water in the large-scale wall was in contact with the RCA matrix for a much longer period. With the addition of the rainwater, the existing pore water percolated out of the wall with higher pH than the outflow of the column test. As cycles repeated in a simultaneous fashion, it could be speculated that both tests reached a similar condition in terms of moisture content during the second cycle.

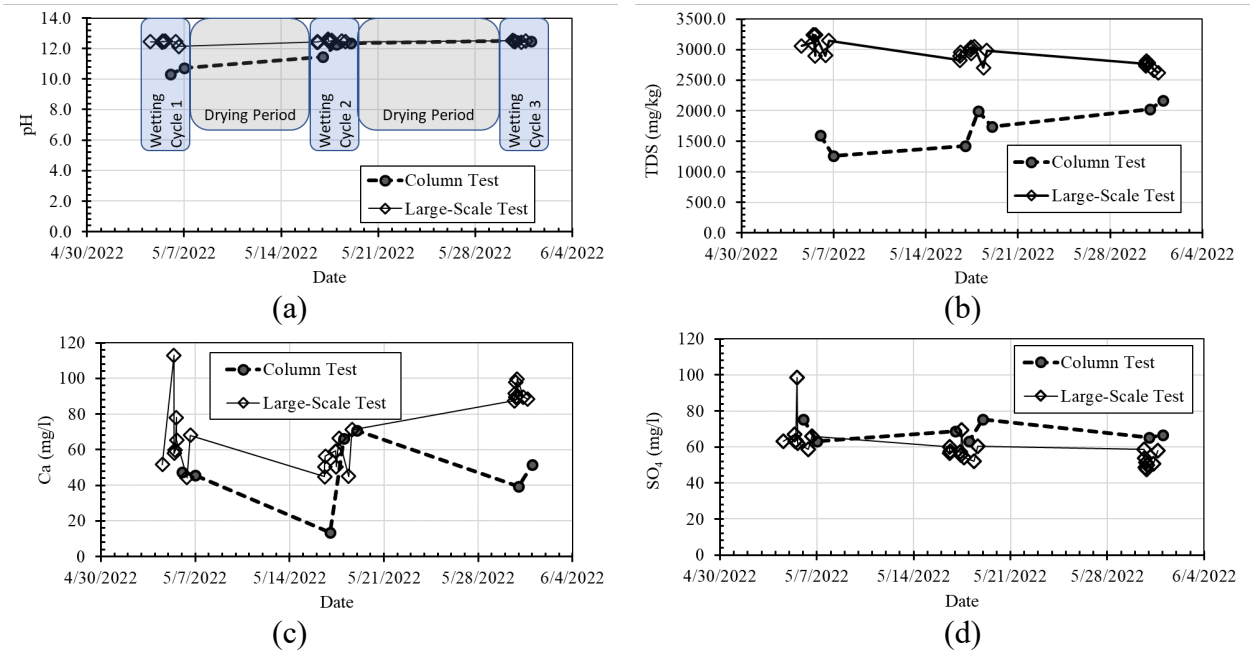

Figure 3.16 Outflow leachate characteristics measured during 3 wetting and drying cycles for large-scale wall and column tests (a) pH, (b) TDS, (c) leached concertation of calcium, (d) leached concertation of sulfate

Measured TDS values (a direct measurement of dissolved ion activities in the outflow leachate) are consistently higher from the large-scale wall in comparison to the column test. During the first cycle, the TDS of large-scale wall outflow is more than twice that of the column test. With the progress of the cycles, the TDS value of the large-scale wall reduces from 3000 mg/kg to about 2600 mg/kg at the end of the third cycle. This reducing trend can be attributed to the first flush phenomenon and can be expected to stabilize with the continuation of the infiltration (raining) cycles. The TDS values of the column test are about 1400 mg/kg on average for cycle one but steadily increase during cycles two and three to about 2200 mg/kg at the end of testing. The same explanation provided for the increase in pH values can be given for the increase in TDS values. In this case, it can be concluded that the effect of contact time between pore fluid and solid matrix exceeds the effect of the first flush, thus an increasing trend is observed. Once the system reaches equilibrium, as it appears at the end of the third cycle, it can be expected that the TDS values in the column test also follow a reducing trend similar to the large-scale wall. The difference in magnitude of the TDS values can be attributed to two factors: (i) the significantly higher RCA mass and (ii) the two-dimensional flow paths in the large-scale wall test. Both factors can lead to

higher contact time between effluent and RCA matrix as is evident in the duration of outflow from two tests as is evident (over 195 hours outflow in the large-scale wall as opposed to less than 48 hours flow in the column test).

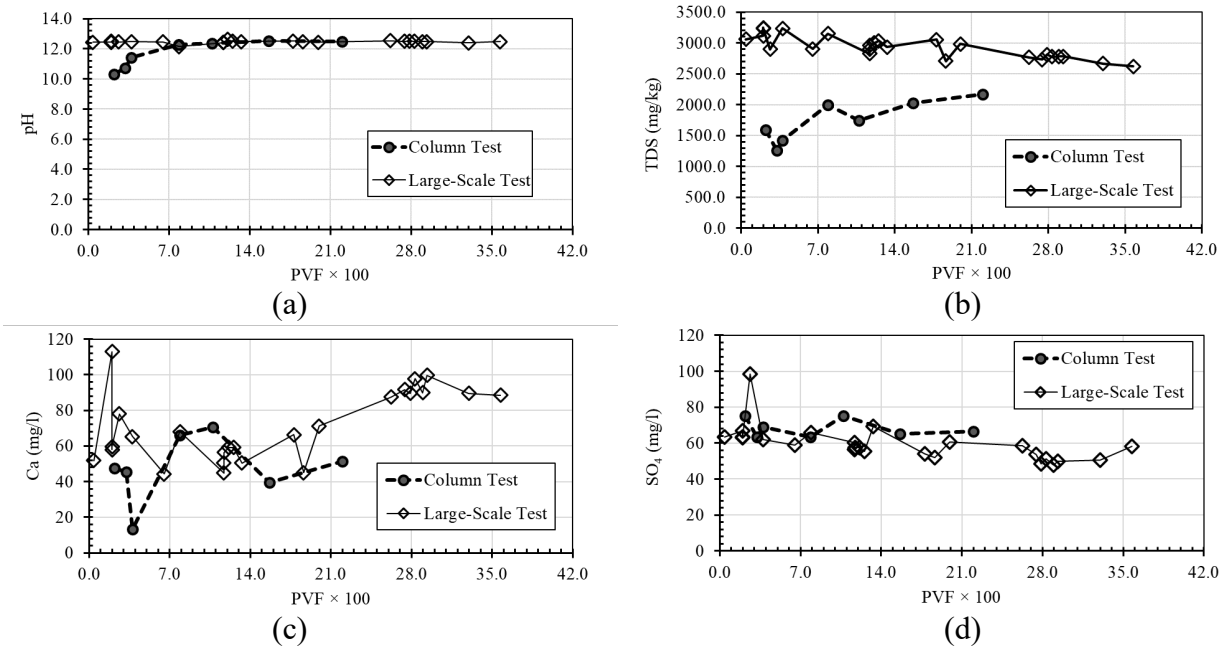

Figure 3.17 Outflow leachate characteristics vs. pore volume flow (PVF) for large-scale wall and column tests (c) leached concertation of calcium, (d) leached concertation of sulfate

TDS levels higher than 900mg/kg in the RCA leachate are an indication of a high probability of tufa precipitate formation as the solution is oversaturated with respect to the RCA tufa minerals (Abbaspour and Tanyu, 2021). A review of the leached concentrations of Ca and SO_4 ions also shows that the leachate from both large-scale wall and column tests is in metastable condition with respect to polymorphs of calcium carbonate (i.e. calcite and aragonite) and calcium sulfate (i.e. gypsum, selenite, and anhydrous) (Abbaspour and Tanyu, 2019b, 2020).

The nucleation process, which is the first and most important step in tufa growth, is a very time-dependent (meaning it cannot be expedited) and uncertain process. The lack of any observation of RCA tufa formation in this study may not mean that no initiation of nucleation within and around the geotextile fibers would not occur with time. This is especially important to note because the chemical characteristic of the leachate indicates the potential of tufa precipitation; however, such a condition could not be verified from the samples exhumed in this study. Therefore, it is not clear if the experiments were to be conducted for a longer duration, whether the nucleation would occur with the continuation of the testing program or not. In addition, the rate of growth after nucleation within a free-flow system (as created based on the selected RCA gradation in this study) is also uncertain. In order to obtain enough information to develop analytical models that can predict the service life of such systems, a much longer testing program is required similar to the study conducted on the nonwoven geotextile filter fabrics installed for highway underdrains (Abbaspour and Tanyu, 2019b).

CHAPTER 4: NUMERICAL SEEPAGE MODELING

In this chapter, wetting-drying cycles are simulated to understand the larger hydraulic behavior in the large-scale MSE wall experiments. First calibration of the Rainfall event #5 is presented followed by Rainfall events #1 and #2.

4.1 Model Inputs

This section describes all model inputs including the domain, boundary conditions, hydraulic functions, modeling steps and two-part calibration process. Numerical modeling was performed using the SEEP/W provided by Geoslope Incorporated within Geostudio ver2021.4. The program solves the time dependent partial differential equation for unsaturated flow using a finite element modeling scheme and has been used previously to simulate seepage through layered systems.

4.1.1 Model Domain

The idealized model domain and boundary conditions are shown in Figure 4.1. The numerical model is a rectangular domain that is 5.5 m wide by 1.2 m tall by 1.0 m deep (into the page). Typically square elements 0.01 x 0.01 m are implemented within the backfill. The geotextile elements were rectangular with a height of 0.002 m and width of 0.01 m. The resulting model domain has 69977 nodes and 69300 elements.

Boundary conditions applied to the model are indicated in Figure 4.1b. At the surface, either a flow boundary equivalent to the rainfall rate applied in the physical tests or a surface energy boundary is applied. The surface energy boundary used idealized laboratory conditions of 20^{o}C and 60% RH and wind of 1 m/s representing nominal average conditions between rainfall events. Along the sides and bottom there are no flow boundaries representing the bottom and back walls of the facility. No seepage was detected at the front face, and thus no flow boundary is also used to represent this condition. At the toe of the model domain, a drain is implemented to represent the water collection system.

The numerical model inputs for RCA backfill and geotextile reinforcement are plotted in Figure 4.2 including water retention curves (WRC) and unsaturated hydraulic conductivity curves. RCA WRC was based on unpublished reports that investigated the effect of finer particles on the unsaturated properties of RCA. RCA saturated conductivity was measured at 0.05 m/s and formed the anchor for the unsaturated conductivity curve that was estimated using the finite element program's automated protocols. Reinforcement WRC and conductivity curves were based on literature values from Lin (2019) and supplier issued information (Mirafi 2022). Both are typical or free draining materials used in reinforced structures.

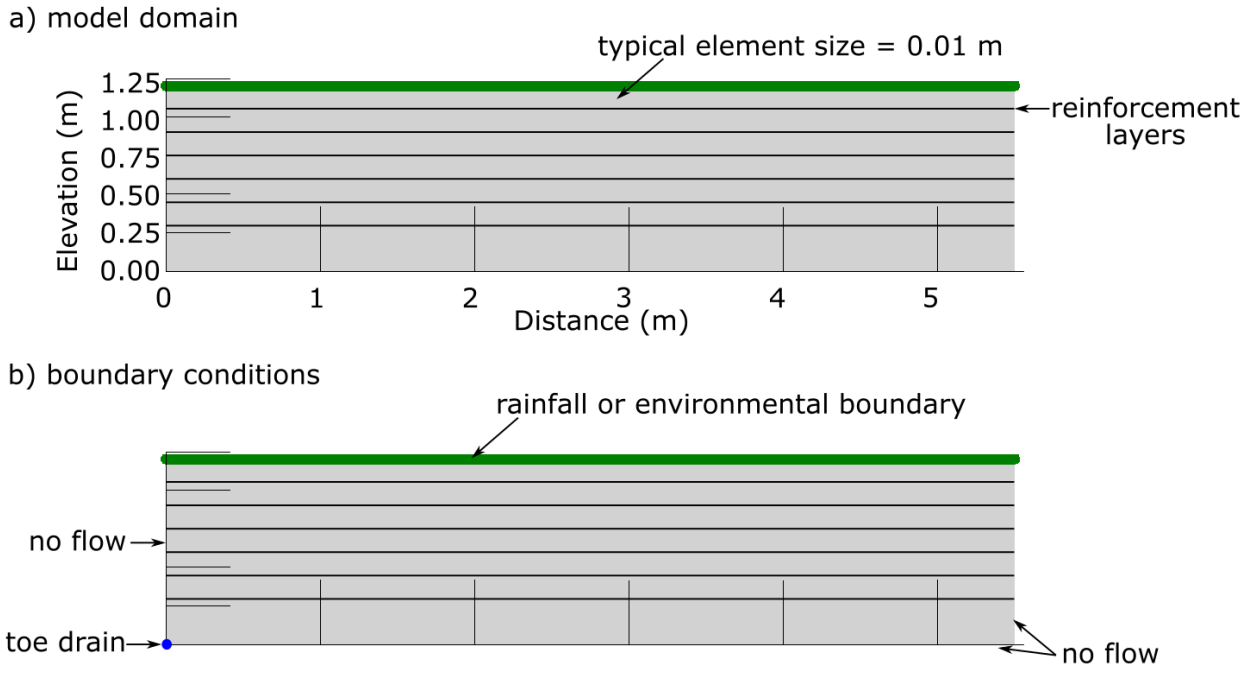

Figure 4.1 (a) Model domain and (b) boundary conditions.

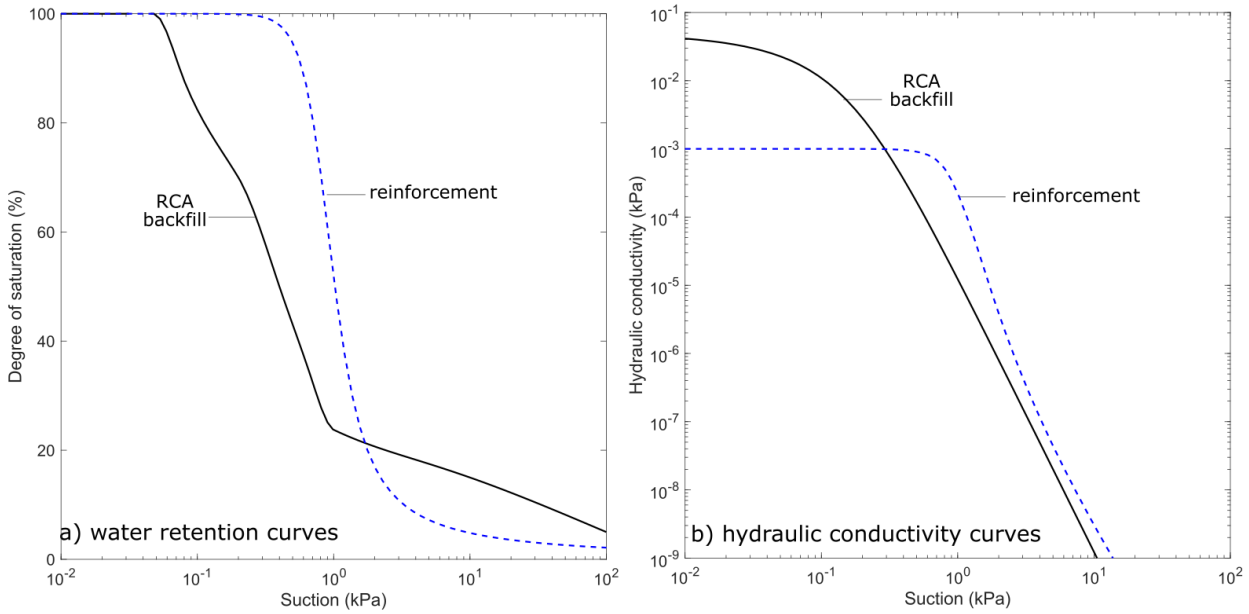

Figure 4.2 Hydraulic properties of reinforcement and RCA backfill: (a) water retention curves and (b) unsaturated hydraulic conductivity curves.

Model calibration was performed to match the numerical output to the physically measured data. The process also took advantage of the differing rainfall durations and reoccurrences. First, rainfall #5 and the final drying phase were used a baseline calibration. Then the same parameters were

input with the conditions applied for Rainfalls #1 and #2 and the subsequent drying phase. Comparisons were generated to visually confirm the numerical model was capturing the main hydraulic behavior observed in the physical tests. The primary comparisons used during calibration were: (i) VWC response of the lower two layers, (ii) wetting front progression with time, and (iii) relative pore volume fraction outflow versus time.

4.2 Results

4.2.1 Simulation of Rainfall Event #5

Modeling proceeded as described in the previous section. Rainfall #5 was applied as a positive flow boundary across the surface. The resulting VWC contours are given in Figure 4.3. The wetting front proceeds quickly through the profile as a horizontal front that reaches the base of the facility in 47 minutes. Moisture accumulates at the base of the model, shown at 50 minutes, and then drains out the toe illustrated by the sloping VWC contours at 60 minutes. Finally, 12 days after the rainfall event, moisture has migrated down through the profile (VWC contours return to green from yellow) and evaporation is occurring from the surface. All of these numerical observations agree with the physical model. Next quantitative comparisons are made between the physical and numerical results.

TDRs in the lower two levels provide direct comparison for VWC versus time. Figure 4.4 plots the numerical and physical comparison. TDR2 (Elev = 0.075 m) and TDR5 (Elev = 0.225 m) readings show good agreement in terms of both detecting the time of wetting front progression and the relative change in moisture content. All readings spike when the quickly moving wetting front passes their location. After passing VWC asymptotically reduces for the rest of the drying phase as moisture migrates downward and then out the toe drain. The numerical results return slightly quicker but achieve the same relative changes during rainfall #5 and the subsequent drying phase and are judged to be acceptable agreement.

Wetting front versus time for all the physical results as well as the numerical results for Rainfall #5 are plotted in Figure 4.5. Rainfall #5 wetting front reaches the base in 47 minutes, which is comparable to the lower bound of the physical test results. Very good agreement is noted in this type of material with high conductivity (Ksat=0.05 m/s). In the upper layers, progression occurs faster, however there is a physical explanation. While sensors in the lower layers are placed in contact with backfill, TDRs in the upper layers are placed inside bags of sand and their readings recorded every two minutes. Thus a delay is understandable compared with the instantaneous recording of the numerical results.

Finally the relative boundary measurements for Rainfall #5 are plotted in Figure 4.6 as Rainfall volume fraction versus time. In this way the relative outflow can be compared with the inflow both numerically and physically. As expected, the numerical results show a fraction of the inflow for this rainfall event exiting through the toe drain. Outflow begins immediately after the rainfall event begins and is mostly complete after a few days. Qualitative comparisons show the numerical and physical outflow results show the same shape. However, the physical results show that more outflow occurred compared with the allotted rainfall. This is perhaps unexpected but can be explained as moisture accumulation for the identical previous rainfall events.

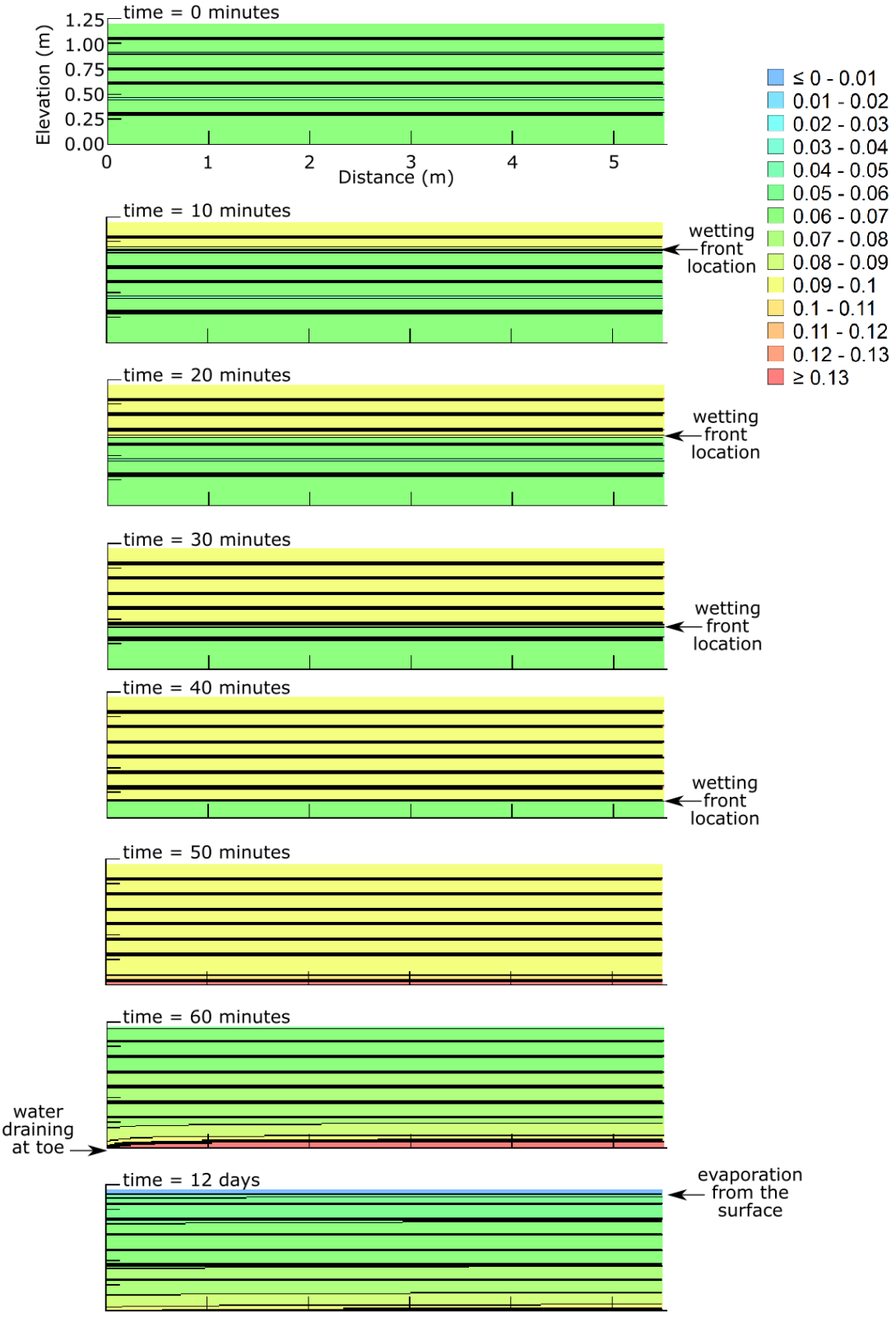

Figure 4.3 Volumetric water content contours during and after rainfall event #5

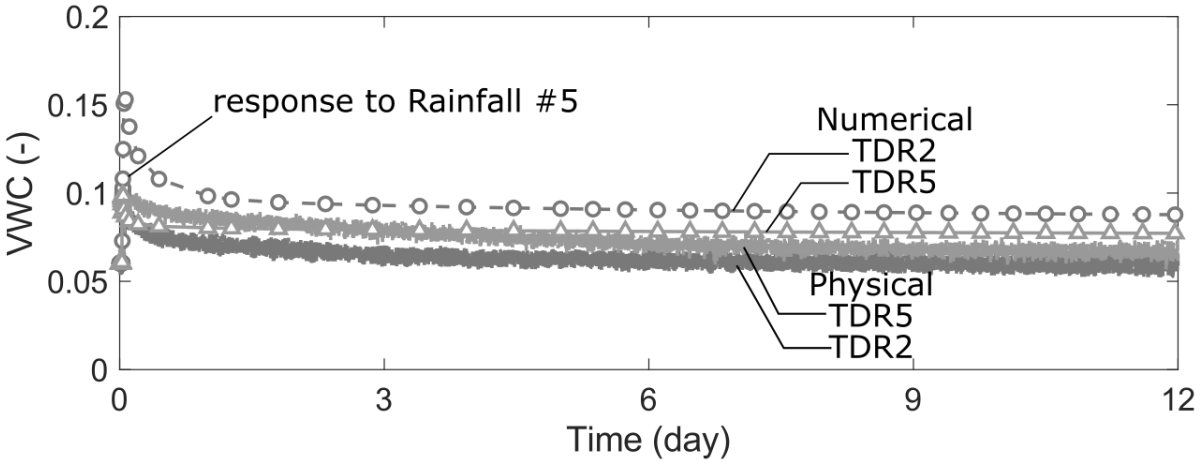

Figure 4.4 Rainfall #5 - VWC versus time comparison for physical and numerical results for TDR2 (Elev 0.075 m) and TDR5 (Elev 0.225 m)

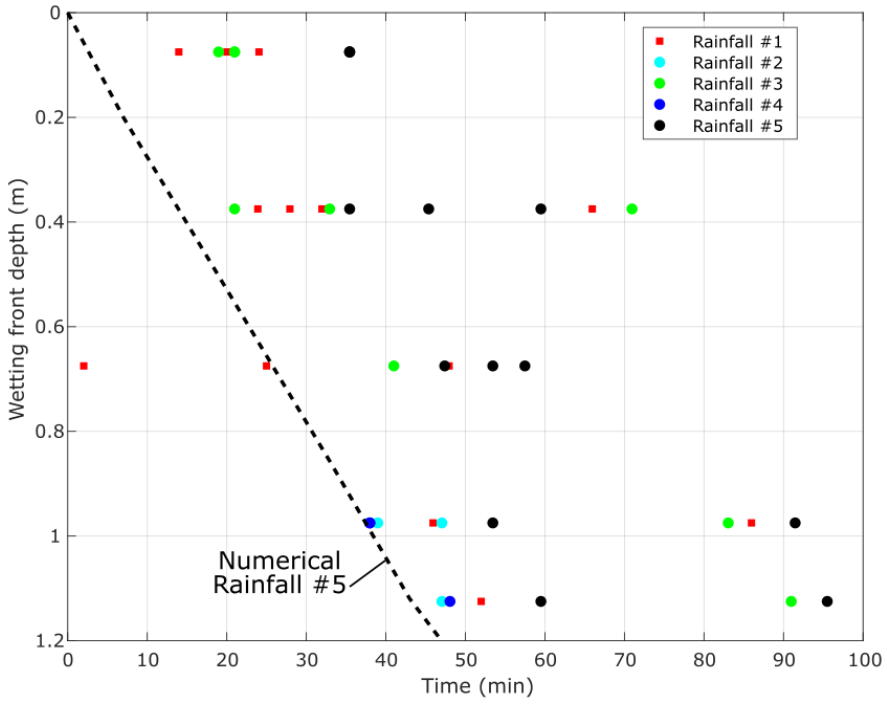

Figure 4.5 Wetting front progression versus time for all physical results and numerical results for Rainfall #5

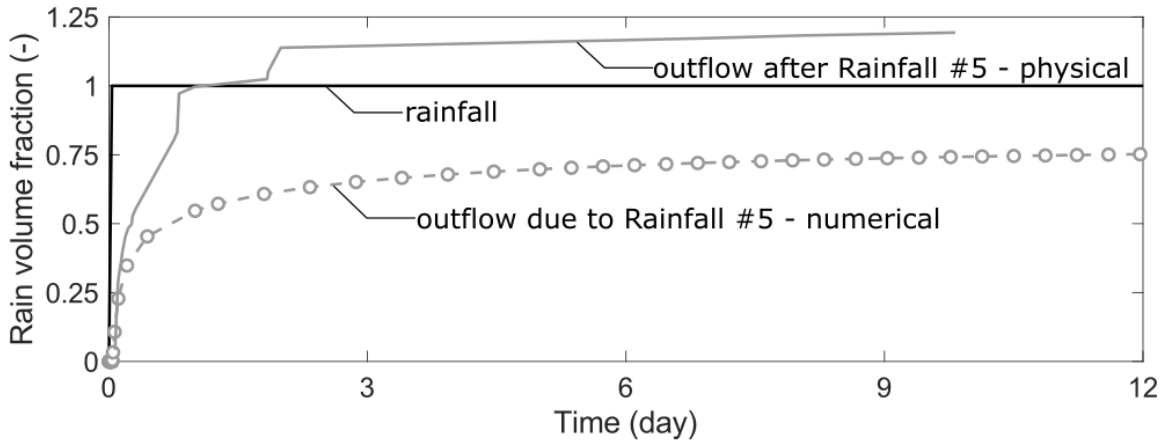

Figure 4.6 Rainfall #5 - rainfall volume fraction for inflow (rainfall) and outflow from toe drain comparison for model and physical test

4.2.2 Simulation of Rainfall Events #1 and #2

Rainfalls #1 and #2 fell one day from each other and thus provided a second, slightly more complicated, opportunity to compare isolated numerical and physical results. Similar to Rainfall #5, results are plotted as VWC versus time (Figure 4.7), wetting front progression versus time (Figure 4.8), and rain volume fraction versus time (Figure 4.9).

The VWC time series show consistent results for both numerical and physical representations in Figure 4.7. VWC spikes for both Rainfall #1 and #2 and then dissipates as moisture continues downward and outflow through the toe drain. Quantitatively and qualitatively the results compare very well.

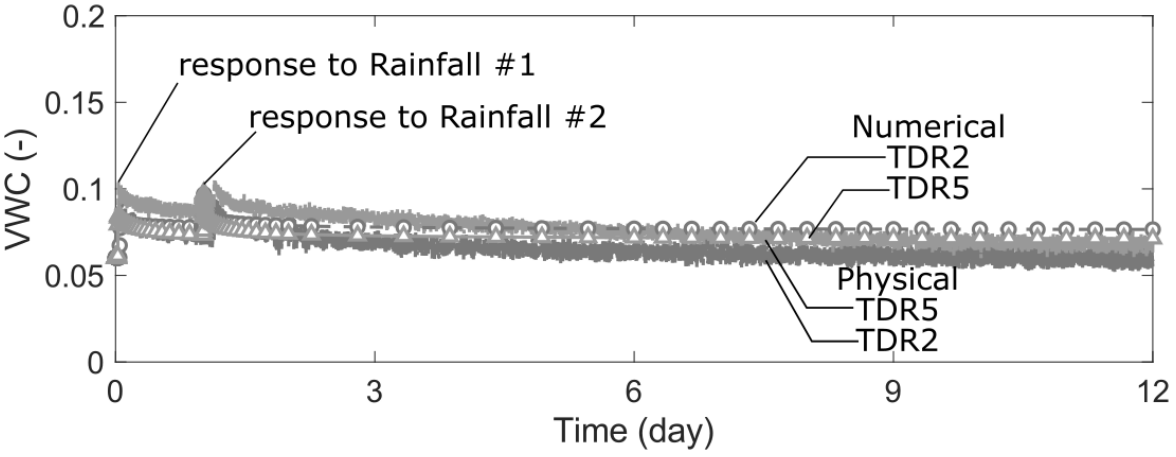

Figure 4.7 Rainfalls #1 and #2 - VWC versus time comparison for physical and numerical results for TDR2 (Elev 0.075 m) and TDR5 (Elev 0.225 m)

Wetting front progression for Rainfall #1 and #2 show distinctive responses due to their differing initiation points. Rainfall #1 fell on ground with a constant moisture content. The consequential wetting front proceeded linearly downward until depth of 0.8 m, which coincides with the end of rainfall. After that time, the driving gradients from the surface drop and wetting front slows for the remainder of Rainfall #1 response time. Rainfall #2 falls when some moisture has dissipated but is still the profile is initially elevated compared with the beginning of the model. Thus there is less storage available and the wetting front proceeds relatively quickly through the model profile. The numerical results are reasonable for the applied conditions and show acceptable agreement with the physical reality.

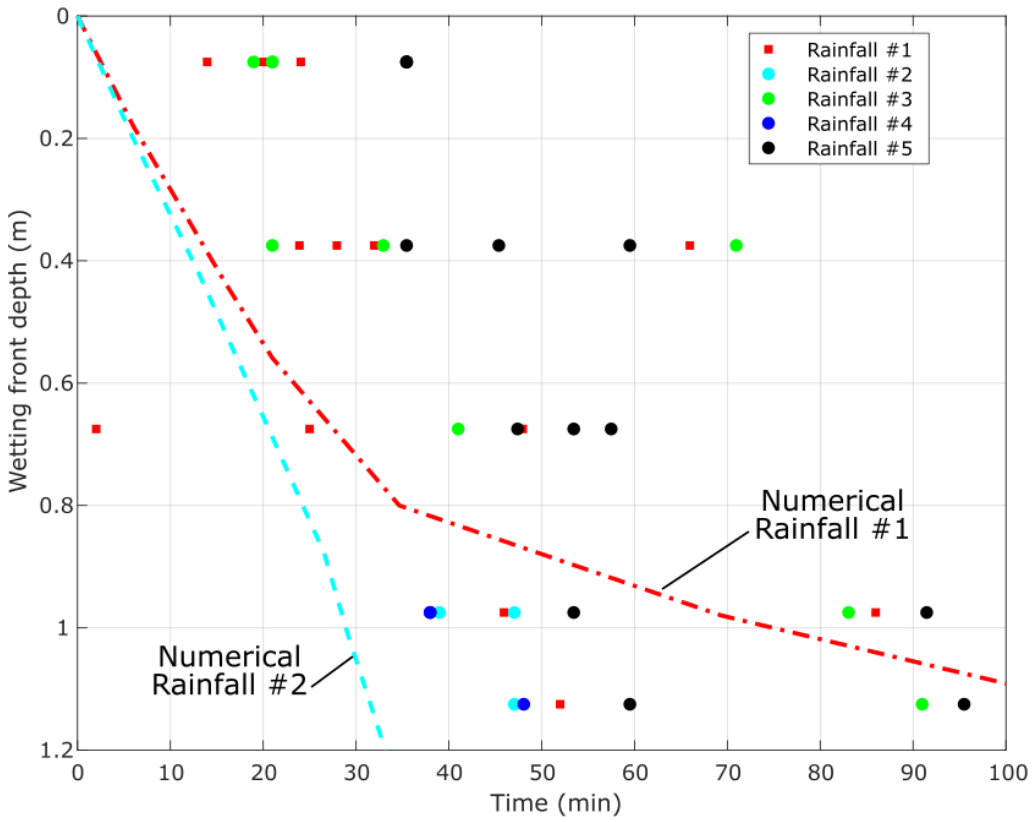

Figure 4.8 Wetting front progression versus time for all physical results and numerical results for Rainfalls #1 and #2

Finally outflow comparisons for Rainfalls #1 and #2 are plotted in Figure 4.9. Both the numerical and physical outflow shows only minor outflow in the day following Rainfall #1 as most moisture is taken up in storage. Both also show immediate response to Rainfall #2 with outflow continuing for days after rain initiation. By the end of 12 days outflow has tailed off in physical and numerical representations.

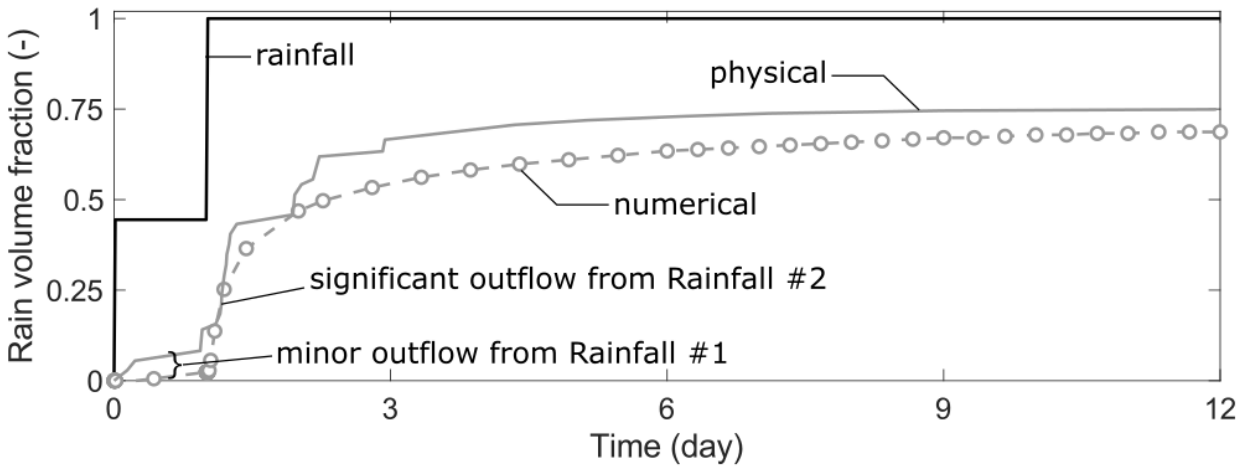

Figure 4.9 Rainfalls #1 and #2 - rainfall volume fraction for inflow (rainfall) and outflow from toe drain comparison for model and physical test

4.3 Modeling Summary

Numerical representation of the physical test results is presented in this chapter. The results are comparable for the scenarios considered in the controlled environment. They represent a unique numerical dataset for providing additional understanding of moisture migration within reinforced walls constructed with RCA backfill. For the cycles tested no excess moisture retention or positive pore pressure development was detected. The conceptualized numerical assumptions worked effectively to capture the main physical realities measured in the laboratory.

CHAPTER 5: SUMMARY AND RECOMMENDATIONS

5.1 Summary

The overall goal of this project is to facilitate use of recycled materials in reinforced backfills for mechanically stabilized earth (MSE) retaining wall construction. The previous Phase I effort was designed to address many of the critical aspects in beneficial use of recycled materials for construction applications, with emphasis on use of recycled concrete aggregate (RCA) and recycled asphalt pavement (RAP) in MSE wall construction. Results from the Phase I effort indicate that RCA and RAP are potentially suitable materials for use as MSE wall backfill from a mechanical property perspective, but that comprehensively assessing hydraulic performance for MSE applications requires more detailed investigation with careful consideration of scale and flow conditions.

The Phase II effort described in this report was conducted to evaluate the suitability of RCA in MSE wall applications from a hydraulic (drainage/clogging) perspective, and specifically when the system is reinforced with woven geotextiles. Previous studies from the GMU research team (e.g., Abbaspour et al., 2018; Abbaspour and Tanyu, 2019a; Abbaspour and Tanyu, 2019b; Tanyu and Abbaspour, 2020) show that hydraulic performance of RCA-geotextile systems can be affected by one of two major clogging phenomena (physical and chemical) depending on the environment and fluid flow conditions. Physical clogging is predominant in saturated fluid environments under continuous flow conditions, as the pore water more likely remains chemically undersaturated with respect to minerals that precipitate tufa. Such conditions inhibit precipitate formation or deposition and, in some cases, even lead to the dissolution of the readily soluble minerals in the RCA material. On the other hand, the relatively large seepage forces associated with saturated flow systems can cause fines within RCA to migrate onto the geotextile and reduce its ability to permeate water. Gradation of the RCA and permittivity of the geotextile are thus important factors affecting migration of fines and associated physical clogging. Chemical clogging (precipitate formation), on the other hand, tends to dominate in environments characterized by periodic flow conditions with repeated cycles of wetting and drying, which is more typical of MSE wall conditions in field applications. Calcareous tufa (calcium-based crystals that may grow on the geotextile) is derived by diagenetic calcite precipitation (Abbaspour and Tanyu, 2019b), followed by evaporative precipitate formations, dominantly gypsum, that becomes active due to wetting and drying cycles. Tufa deposition within the geotextile filaments can lead to a reduction in filtration capacity of the RCA/geotextile system.

The Phase II effort has been designed to closely replicate field conditions for RCA-geotextile systems in MSE wall applications in terms of scale (i.e., large-scale experiments), flow conditions (i.e., 2-D, 3-D flow), and wetting-drying cycles. Two sets of complementary experiments were designed to investigate hydraulic performance of RCA-woven geotextile systems: one that replicates a large-scale MSE wall structure through physical modeling conducted at the Royal Military College of Canada's MSE wall testing facility and the other as a series of large-scale column tests used to evaluate one-dimensional vertical flow conditions under conditions identical to the large-scale MSE wall. Numerical models were conducted to understand the larger hydraulic behavior in the wall experiments and to generalize the flow phenomena for different boundary conditions. In both experimental set-ups the following conditions were simulated:

- The gradation of the RCA was selected and processed to have minimum fines content. Based on previous findings, this was necessary to create a scenario where the potential for physical clogging does not become the leading mechanism for clogging, thereby maximizing the potential for understanding chemical clogging and the conditions that lead to it;

- Spacing between the reinforcement geotextiles were selected to be as close to each other as allowed in GRS-IBS systems, thereby providing a worst-case scenario in terms of potential clogging;

- The aggregate within the RCA was selected to contain calcium-based compounds, thereby providing a worst case scenario in terms of chemical clogging.

The one-dimensional column experiments were constructed in a 1-ft diameter circular column with a height of 4 ft. The large-scale MSE wall was constructed to the same height and 3.3 m × 6 m area. Both tests were constructed in 8 layers lifts of 150 mm thickness. Woven geotextile reinforced layers were used in 6 layers from the second to the seventh layer. Five rainfall events were periodically carried out over 36 days for both the MSE wall system and the column systems to simulate rainfall-induced wetting-drying events. Rainfall events ranged from 1-inch to 2.5 inches. The first two cycles were performed in 2 stages of 1.5 in and 1 in and the last wetting cycle was applied as one step of 2.5 inches of water. After each wetting cycle, the systems were left to drain for approximately 10 days. Internal moisture migration for the MSE wall system was monitored using TDRs as well as boundary measurements of outflow and temperature / relative humidity.

5.2 Conclusions

The following conclusions are made based on the observations from the study:

- The large-scale wall and column experiments showed good drainage performance during three wetting-drying cycles. No evidence of positive pore pressures was observed at the backfill surface, above the reinforcement layers, or at the impermeable base of the MSE wall. Wetting front mobility was unimpeded in the layered profile for all rainfall events. These observations are consistent even during Rainfall #5, which was the longest event. Uniform final moisture content profile was observed in all layers except the top (where evaporation occurred), which provides further evidence of the free draining nature of this backfill-reinforcement combination. The backfill specification used for the study appears acceptable from this perspective under the conditions tested.

- The calibrated numerical model provides further confirmation and confidence in the physical test results and provides an improved perspective of interior wall hydraulic behavior. The numerical results show that, with proper drainage at the toe of the structure, moisture migration was unhindered by the woven geotextile reinforcement, wetting front mobility was consistent across the range of rainfall event magnitudes, and no positive pore pressures were observed in the backfill.

- During the three cycles of wetting and drying, the woven geotextile used in the large-scale wall and column test did not experience any physical or chemical clogging. The lack of evidence for physical clogging, as determined from image analysis and permittivity testing of exhumed geotextiles, supports the validity of the selected gradation for the RCA used in this study. However, the lack of evidence for chemical clogging may need to be further evaluated in a follow-up study because of the key indicators observed during the experimentation, as noted below.

- The leachate samples collected from the large-scale wall test have higher TDS values and higher leached concentrations of Ca and SO_4 ions in comparison to the column test.

- The pH of the leachate from the column test is initially lower than the samples from the large-scale wall, but with the progress of the testing program, the pH values of both tests become similar at around 12. Leachate with a pH of around 12 potentially indicates that in the long run, some chemical precipitation may occur, especially if the structure does not perform as a free draining body.

- The differences in leaching characteristics of the large-scale wall and column tests can be attributed mainly to three parameters: (i) the initial moisture content of the material at the beginning of the tests, (ii) the larger quantity of RCA material in the large-scale wall, and (iii) the two-dimensional flow characteristics of large-scale wall vs. the one-dimensional nature of the flow in the column test.

- Leachate samples collected from both tests are supersaturated with respect to tufa minerals, with TDS levels significantly higher than 900 mg/kg. 900 mg/kg is the limit identified in the previous studies for the occurrence of tufa precipitation from RCA leachate.

- It is unclear if the testing program continued, whether the nucleation of RCA tufa would occur or not. It is also uncertain that if the nucleation occurs, what would be the rate of growth after nucleation within a system in a free-flowing material such as the selected RCA gradation.

5.3 Recommendations for Implementation

Based on the findings of this research, the Phase I research program, and our previous column-scale studies of physical and chemical clogging phenomena for RCA-geotextile systems the following recommendations are offered:

- The experimentation conducted in this study validates previous observations from one-dimensional column tests to be valid when more realistic two-dimensional flow conditions are considered for an MSE wall reinforced with woven geotextile. For the selected RCA gradation and woven geotextile, physical clogging is not likely to occur.

- Leachate data indicates that large-scale experimentation is important because some of the key indicators slightly differ between 1-D column tests and large-scale, multidimensional experimentation.

- Findings from this study demonstrate that with proper gradation, RCA could be considered as an infill for the MSE walls even if the reinforcements are woven geotextiles. Based on the observations from this study, it is recommended that further evaluation is conducted for an MSE wall reinforced with RCA and woven geotextile under actual field conditions and with a duration of at least two years in order to capture seasonal effects. Further study will also allow development of analytical models that can then be used to predict the service life of woven geotextile/RCA systems as it relates to chemical clogging.

- It is highly recommended and very important to recognize that RCA considered for geo-transportation infrastructure construction not be mixed with any other recycled materials (such as slag) without significant additional evaluations.

- It is a known fact that fines content affect the drainage properties of aggregates. This remains valid for RCA. It is recommended that when RCA is used adjacent to geotextiles, the selected gradation have a minimum fines content that results in a freely-draining material. The large-scale MSE wall and column tests conducted here show that gradation meeting AASHTO No. 8 and No. 89 appear to be appropriate selections for that purpose.

- Based on the findings of this research, it is recommended that DOTs consider constructing MSE type structures with RCA using geogrids that are not sensitive to high pH conditions.

- The research completed in this study provides an optimistic outcome. However, before the development of State wide transportation agency specifications, and to confirm the long-term suitability in terms of chemical clogging, it is recommended that a trial MSE structure be constructed in the field and subject to long-term environmental conditions using a woven geotextile similar to that used in this study and RCA meeting the AASHTO No. 8 or 89 gradations.

REFERENCES

AASHTO (American Association of State Highway and Transportation) (2010). LRFD Bridge Design Specifications, 5th Edition, American Association of State Highway and Transportation Officials, Washington, DC Officials, Washington, DC.

Abbaspour, A., Tanyu, B. f., 2021. Chemical clogging and geotextile serviceability in subdrains adjacent to recycled concrete. Geosynthetics International 28, 402–420. https://doi.org/10.1680/jgein.20.00051

Abbaspour, A., Tanyu, B.F., 2019a. Evaluate hydraulic compatibility of geotextile and RCA in underdrain systems under turbulent flow regime, in: Geosynthetics Conference 2019. IFAI, Houston, Texas, U.S.A.

Abbaspour, A., Tanyu, B.F., 2019b. Tufa precipitation from Recycled Concrete Aggregate (RCA) over geotextile: Mechanism, composition, and affecting parameters. Construction and Building Materials 196, 317–329. https://doi.org/10.1016/j.conbuildmat.2018.10.146

Abbaspour, A., Tanyu, B.F., 2020. CO2 Sequestration by Carbonation Processes of Rubblized Concrete at Standard Conditions and the Related Mineral Stability Diagrams. ACS Sustainable Chem. Eng. 8, 6647–6656. https://doi.org/10.1021/acssuschemeng.9b07690

Abbaspour, A., Tanyu, B.F., Aydilek, A.H., Dayioglu, A.Y., 2018. Methodology to evaluate hydraulic compatibility of geotextile and RCA in underdrain systems. Geosynthetics International 25, 67–84. https://doi.org/10.1680/jgein.17.00034

Abbaspour, A., Tanyu, B.F., Cetin, B., 2016. Impact of aging on leaching characteristics of recycled concrete aggregate. Environ Sci Pollut Res 23, 20835–20852. https://doi.org/10.1007/s11356-016-7217-9

Abdelouhab, A., Dias, D., Freitag, N. (2010). Numerical Analysis of the Behavior of Mechanically Stabilized Earth Walls Reinforced with Different Types of Strips. doi:10.1016/j.geotexmem.2010.10.011. Elsevier Ltd.

Abichou, T., Edil, T., Benson, C. (2004). "*Beneficial Use of Foundry By-Products in Highway Construction".* Geo Trans 2004. Geotechnical Engineering for Transportation Projects. ASCE 715-722

Abu-Farsakh, M., Coronel, J., (2006). "*Characterization of Cohesive Soil–Geosynthetic Interaction from Large Direct Shear Test*". 85th Transportation Research Board Annual Meeting, Washington, D.C

ACAA (American Coal Ash Association). (2015). About Coal Ash, What are CCPs?, Fly Ash. Retrieved July 27th, 2015 from: http://www.acaa-usa.org/About-Coal-Ash/What-are-CCPs/Fly-Ash

Adams, M., Nicks, J., Stabile, T., Schlatter, W., Hartmann, J., 2012. Geosynthetic reinforced soil integrated bridge system interim implementation guide (No. Publication No. FHWA-HRT-11-026). Federal Highway Administration (US), McLean, VA.

AFS (American Foundry Society). (n.d.). Introduction to Foundry Sand. Retrieved July 20th, 2015 from: http://www.afsinc.org/content.cfm?ItemNumber=7075

Akram, M. H., Gabr, M. A., (1997). "Filtration of Fly Ash Using Non-Woven Geotextiles; Effect of Sample Preparation Technique and Testing Method", Geotechnical Testing Journal, ASTM, Vol. 20, No. 3, pp. 263-271.

Allen, T., Christopher, B., Elias, V., DiMaggio, J. (2001) *"Development of the Simplified Method for Internal Stability Design of Mechanically Stabilized Earth Walls".* Technical Report, WA-RD 513.1, Washington State Department of transportation.

Anderson, K. W., Uhlmeyer, J. S., Russell, M. (2009). "*Use of Recycled Concrete Aggregate in PCCPs: Literature Search".* (June), 35: Washington Department of transportation, Office of Research & Library Services.

Anderson, P., Gladstone, R., Sankey, J. (2012). *"State of the Practice of MSE Wall Design for Highway Structures". Geotechnical Engineering* S*tate of the Art and Practice*, 1–21. doi:10.1061/ 9780784412138.0018

ARRA (Asphalt Recycling and Reclaiming Association). (2001). *Basic Asphalt Recycling Manual*. (Vol. 1)

ASTM D 4491 (2003). "Test Methods for Water Permeability of Geotextiles by Permittivity", American Society for Testing and Materials, West Conshohocken, Pennsylvania, USA.

ASTM D 5101 (2003). "Standard Test Method for Measuring the Soil-Geotextile System Clogging Potential by the Gradient Ratio", American Society for Testing and Materials, West Conshohocken, Pennsylvania, USA.

ASTM, D 1557 (2003). "Standard Test Methods for Laboratory Compaction Characteristics of Soil Using Modified Effort." American Society for Testing and Materials, West Conshohocken, Pennsylvania, USA.

ASTM, D 4751 (2003). "Test Method for Determining the Apparent Opening Size of a Geotextile", American Society for Testing and Materials, West Conshohocken, Pennsylvania, USA.

Aydilek, A. and Mijic, Z. (2015). "*Hydraulic and Environmental Behavior of Roadway Millings in Highway Shoulder Applications*". Environmental Geotechnics Report 15-8, University of Maryland, College Park, MD.

Aydilek, A. H. and Edil, T.B., (2002). "Filtration Performance of Woven Geotextiles with Wastewater Treatment Sludge." Geosynthetics International, IFAI, Vol. 9, No. 1, pp. 41-69.

Aydilek, A. H., and Edil, T.B., (2003). "Long-Term Filtration Performance of Nonwoven Geotextile-Sludge Systems", Geosynthetics International, IFAI, Vol. 10, No. 4.

Basma, A., Tuncer, E. (1992). *"Evaluation and Control of Collapsible Soils". Journal of Geotechnical Engineering*. ASCE 1992.118:1491.-1504.

Basudhar, P., Vashistha, A., Deb, K., Dey, A. (2006). *"Cost Optimization of Reinforced Earth Walls". Sprinter-Science.* doi:10.1007/s10706-007-9143-6

Benson, C., Tinjum, J., Nokkaew, K. (2012). *"Hydraulic Properties of Recycled Asphalt Pavements and Recycled Concrete Aggregate".* GeoCongress, ASCE 2012

Berg, R., Christopher, B., & Samtani, N. (2009). *"Design and Construction of Mechanically Stabilized Earth Walls and Reinforced Soil Slopes–Volume I". Federal Highway Administration (FHWA)*.

Bhatia, S.K., Moraille J., and Smith J.L., (1998). "Performance of Granular versus Geotextile Filters in Protecting Cohesionless Soils", Filtration and Drainage in Geotechnical and Geoenvironmental Engineering, ASCE, Geotechnical Special Publication 78, L.N. Reddi and M.V.S. Bonala, Eds., pp. 1-29.

Bilgin, O., Mansur, E. (2014). *"Effect of Reinforcement Type on the Design Reinforcement Length of Mechanically Stabilized Earth Walls".* Elsevier. Engineering Structures 59 (2014) 663-673

Bleakley, A., Cosentino, P., Kalajian, E., & Patel, M. (2014). *"Strength and Creep Characteristics of RAP-Sand Blend Backfill in Mechanically Stabilized Earth Walls".* (July 2013).

Transportation Research Board, Transportation Research Record. TRB Annual Meeting. (2014).

Bose, Bidula. (2012) *"Geo-Engineering Properties of Expansive Soil Stabilized with Fly Ash"*. Electronic journal of Geotechnical Engineering, Volume 17.

Bruinsma, J., Peterson, K. Snyder, M. (1997).*"Chemical Approach to Formation of Calcite Precipitation from Recycled Concrete Aggregate Base Layers".* Transportation Research Record 1577, Paper No. 971154, pp 10-17.

Butler, L., Wets, J., Tighe, S. (2011). *"Quantification of Recycled Concrete Aggregate (RCA) Properties for Usage in Bridges and Pavement: An Ontario Case Study".* 2011 Annual Conference of the Transportation Association of Canada: Innovative Developments in Sustainable Pavement Session, Edmonton, Alberta.

Caltrans (California Department of Transportation). (2004). California Department of Transportation, Bridge Design Specifications, Section 5 – Retaining Walls.

Cancelli, A., Rimoldi, P., Togni, S., (1992). "*Frictional Characteristics of Geogrids by Means of Direct Shear and Pull-out Tests*". Proceedings of the International Symposium on Earth Reinforcement Practice, Kyushu, vol. 1, pp. 29–34.

Cazzuffi, D., Picarelli, L., Ricciuti, A., Rimoldi, P., (1993). "*Laboratory investigations on the shear strength of geogrid reinforced soils".* ASTM Special Technical Publication 1190, 119–137

CDRA (Construction & Demolition Recycling Association) (n.d.). *"Asphalt Roofing Shingles Recycling: Introduction"*. Retrieved Aug 2nd, 2015 from: http://www.shinglerecycling.org/content/markets-recycling-asphalt-shingles

CDRA (Construction & Demolition Recycling Association) (n.d.). *"Markets for Recycled Concrete Aggregate"*. Retrieved July 30th, 2015 from: http://www.cdrecycling.org/end-markets

Chalermyanont, T., & Benson, C. H. (2004). "*Reliability-Based Design for Internal Stability of Mechanically Stabilized Earth Walls"*. *Journal of Geotechnical and Geoenvironmental Engineering*, *130*(February), 163–173. doi:10.1061/(ASCE)1090-0241(2004)130:2(163)

Cosentino, P. J., Kalajian, E. H., & Ho, R. K. (2001). Final Report - Developing Specifications for Using Recycled Asphalt Pavement as Base, Subbase or General Fill Materials.

CWC (Clean Washington Center) (n.d.). *"Beneficial Use of Spent Foundry Sand".* Retrieved Aug 3rd, 2015 from: http://www.cwc.org/industry/ibp951fs.pdf

Das, B. (2007). *Principles of Foundation Engineering* (7th edition, pp. 406 – 436). Stamford, CT: Cengage Learning

Edil, T.B., Tinjum, J. M., and Benson, C. H. (2012) Final Report - Recycled Unbound Materials, Technical Document, Report No. MN/RC 2012-35, Minnesota Department of Transportation.

Elias, V., Christopher, B., & Berg, R. (2001). *"Mechanically Stabilized Earth Walls and Reinforced Soil Slopes Design & Construction Guidelines"*. *Construction*, (132042). doi:FHWA-NHI-10-024 & FHWA-NHI-10-025

Elias, V., Fishman, K., Christopher, B., & Berg, R. (2009). *NHI Courses No. 132042 and 132043 CORROSION / DEGRADATION OF SOIL REINFORCEMENTS FOR. U.S Department of Transportation Federal Highway Administration*.

EPA (United States Environmental Protection Agency). (n.d.). Retrieved January 22th, 2015, from: http://www.epa.gov/climate/climatechange/wycd/ waste/downloads/concrete-chapter10-28-10.pdf

Fannin, R.J., Vaid, Y.P., and Shi, Y.C., (1994). "Filtration Behavior of Nonwoven Geotextiles", Canadian Geotechnical Journal, Vol.31, pp. 555-563.

Faure Y.H., Kehila, Y., Olivier F., and Paillez, S., (2000). "Behavior of Nonwoven Geotextiles for Filtrating Particles in Suspension", Filters and Drainage in Geotechnical and Geoenvironmental Engineering, W. Wolski and J. Mlynarek, eds., Balkema, Rotterdam, The Netherlands, pp. 59-66.

FHWA (Federal Highway Administration Agency). (1997). *"User Guideline for Waste and Byproduct Materials in Pavement Construction".* Report. Publication number: FHWA-RD-97-148. Retrieved July 28th 2015 from: http://www.fhwa.dot.gov/publications/research/infrastructure/structures /97148/fs1.cfm

FHWA (Federal Highway Administration Agency). (2004a). *"Transportation Applications of Recycled Concrete Aggregate".* FHWA State of the Practice National Review. U.S. Department of Transportation Federal Highway Administration.

FHWA (Federal Highway Administration Agency). (2004b). *"Fly Ash Finds Multiple Uses in Highway Construction". Technical Report*. U.S. Department of Transportation Federal Highway Administration. FHWA-IF-04-004

FHWA (Federal Highway Administration Agency). (2004c). *"Foundry Sand Facts for Civil Engineers". FOCUS,* Accelerating Infrastructure Innovations. U.S. Department of Transportation Federal Highway Administration. FHWA-HRT-04-024

Fowler, J., Bagby, R., and Trainer, E., (1996). "Dewatering Sewage Sludge with Geotextile Tubes" Proceedings of the 49th Canadian Geotechnical Conference, St. John's, New Foundland, Canada, 30 p.

Gabr, M. A., and Akram, M. H., (1996). "Clogging and Piping Criteria for Geotextile Filters for Fly Ash", Proceedings of the 3rd International Symposium on Environmental Technology, San Diego, California, USA, pp. 836-847

Gautreau, G., Abu-Farsakh, M, Zhang, Z. (2009). *"Bottom Ash Test and Evaluation". Technical Assistance Report #: 08-3TA, Louisiana Transportation Research Center.*

Giroud, J.P., (1996). "Granular Filters and Geotextile Filters." Proceedings of Geofilters '96, Montreal, QB, Canada, pp. 565-680.

Giroud, J.P., Delmas, P., and Artières, O., (1998). "Theoretical Basis for the Development of a Two-Layer Geotextile Filter" Proceedings of the Sixth International Conference on Geosynthetics, Atlanta, Georgia, USA, pp. 1037-1044.

Goodhue, M., Edil, T., Benson, C. (2001). *"Interaction of Foundry Sands with Geosynthetics". Journal of Geotechnical and Geoenvironmental Engineering / April 2001, 353-362*

Griffiths, C., Krstulovich, J. (2002). *"Utilization of Recycled Materials in Illinois Highway Construction".* Illinois Department of Transportation. Bureau of Materials and Physical Research, Report No. 142. Springfield, Illinois.

Gutt, W., Nixon, P. (1979). *"Use of Waste Materials I the Construction Industry".* Analysis of the RILEM Symposium by Correspondence. BORDAS-DUNOD 0025-5432/1979/255

Holtz, R., Christopher, B., Berg, R. (1998). *"Geosynthetic Design and Construction Guideline".* Participant notebook. Pdf. Publication no. FHWA HI-95-038. Course no. 13213. National Highway Institute.

Huang, W. (1990). *"The Use of Bottom Ash in Highway Embankments, Subgrades and Subbases". Joint Highway Research Project, Final Report, FHWA/IN/JHRP-90/4*

Juan, M., Gutierrez, P. (2009). *"Study on the Influence of Attached Mortar Content on the Properties of Recycled Concrete Aggregate"*. Construction and Building materials. Elsevier 23(2009) 872-877.

Kim, H., Lee, H. (2014) *"Coal Bottom Ash in Field of Civil Engineering: A Review of Advanced Applications and Environmental Considerations"*. KSCE Journal of Civil Engineering. Springer. doi:10.1007/s12205-015-0282-7

Soleimanbeigi, A., Tanyu, B.F., Aydilek, A.H., Florio, P., Abbaspour, A., Dayioglu, A.Y., Likos, W.J., 2019. Evaluation of recycled concrete aggregate backfill for geosynthetic-reinforced MSE walls. Geosynthetics International 26, 396–412. https://doi.org/10.1680/jgein.19.00025

Soleimanbeigi, A., William J. Likos, Tanyu, B.F., Aydilek, A.H., Florio, P., 2016. Recycled Materials as Backfill for Mechanically Stabilized Earth (MSE) Walls (Final Report). Recycled Materials Resource Center, University of Wisconsin-Madison.

Tanyu, B., Abbaspour, A., 2020. Evaluation of Use of Crushed Hydraulic Cement Concrete (CHCC) as an Additive to Base Course/Subbase Material (Final Report No. Final Report No. FHWA/VTRC 21-R12). Virginia Transportation Research Council, George Mason University, Charlottesville, VA. https://doi.org/10.13140/RG.2.2.32533.96483/2

VDOT, 2008. Road and Bridge Standards, 2015th ed. Virginia Department of Transportation, Richmond, VA.

VDOT, 2016. 2016 Road and Bridge Specifications. Virginia Department of Transportation, Richmond, VA.

Yoon, S., Balunaini, U., Yildirim, I., Prezzi, M., Siddiki, N. (2009). *"Construction of an Embankment with Fly and Bottom Ash Mixture: Field Performance Study"*. Journal of Materials in Civil Engineering. ASCE. June 2009. doi:10.1061/_ASCE_0899-1561_2009_21:6_271_

APPENDIX A – Fiber Optic Sensor Observations

Fiber optics were installed coincidental with four reinforcement layers along the profile. Fiber optic cable (45 m long) was placed in contact with the top of the geotextile reinforcement layers and run in a "zig zag" pattern to cover a uniform area of the backfill. A typical fiber optic layout is displayed in plan view in Figure A-1. Six linear segments (5.5 m) are defined by the length of the cable along the long axis of the geotextile. This new concept for moisture detection was tested in the wall, where the goal was to utilize the fiber optic as a distributed temperature sensor. With the average temperature in the laboratory being 21 °C and the average temperature of the rainfall being approximately 16 °C, this difference provided an initial temperature differential of 5 °C. In terms of fiber optic microstrain, 5 °C corresponds to 50 microstrain. Thus, the intent was to detect changes in microstrain resulting from passage of water through the backfill/geotextile interface.

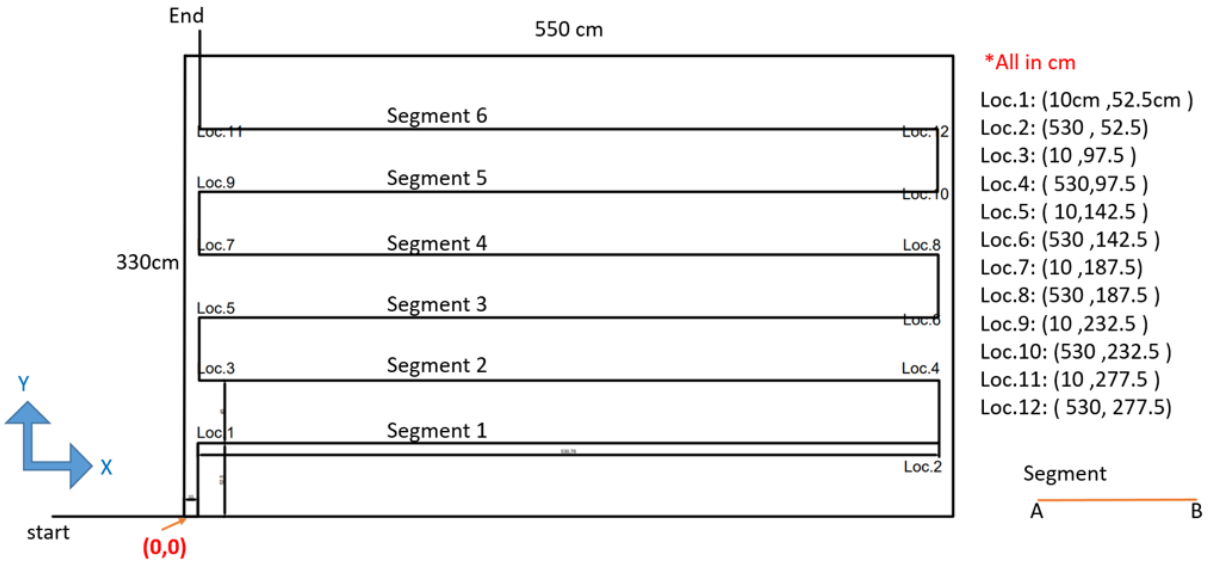

Figure A-1. Plan view of typical fiber optic sensor layout with Segments corresponding to plots in Figure 2.

The capability of the sensor to measure temperature change and infer moisture detection relies on differences in measurements between background data (i.e. several days after a rainfall) to the time immediately after rainfall. Unfortunately, the background and rainfall data were not detectably different. For example, Figure A-2a plots typical background data as (absolute) microstrain versus distance along the sensor with segments highlighted and Figure A-2b plots change in microstrain versus time. Both plots show less than 4-5 με over the time of measurements. Figure A-3 plots the change in microstrain versus time showing the same response as the background timing. This is typical of the rest of the sensors and rainfalls.

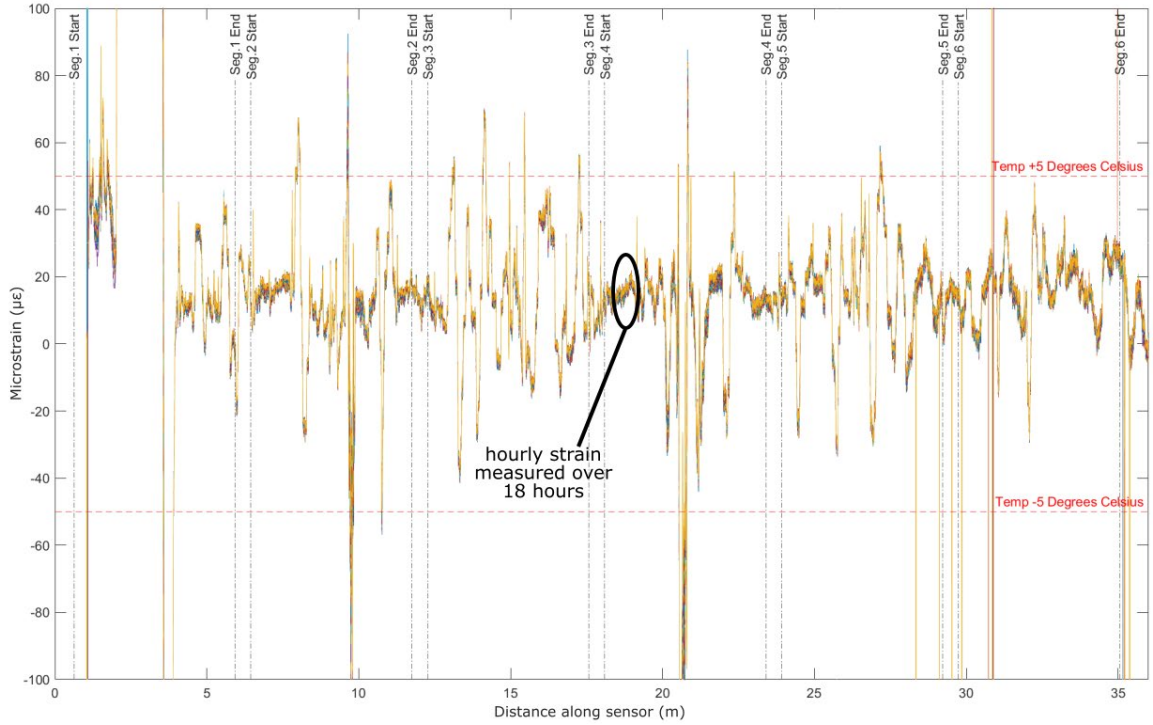

(a)

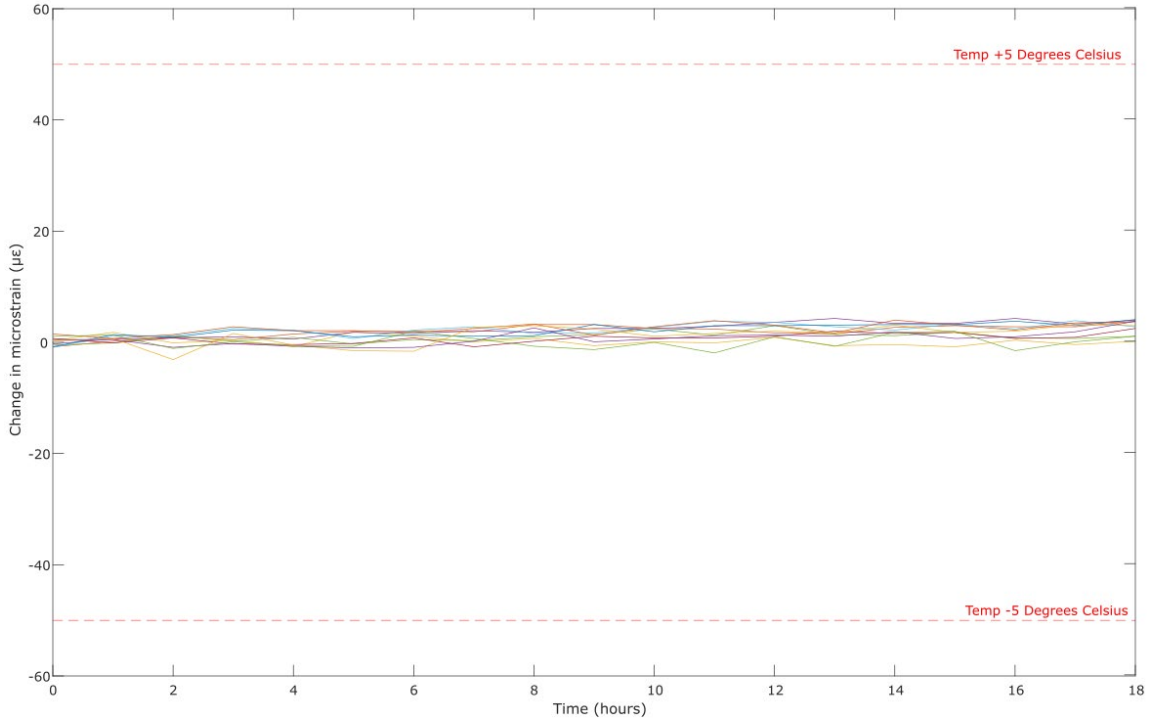

(b)

Figure A-2. Typical fiber optic measurements during a background period: (a) microstrain versus distance along sensor and (b) change in microstrain versus time.

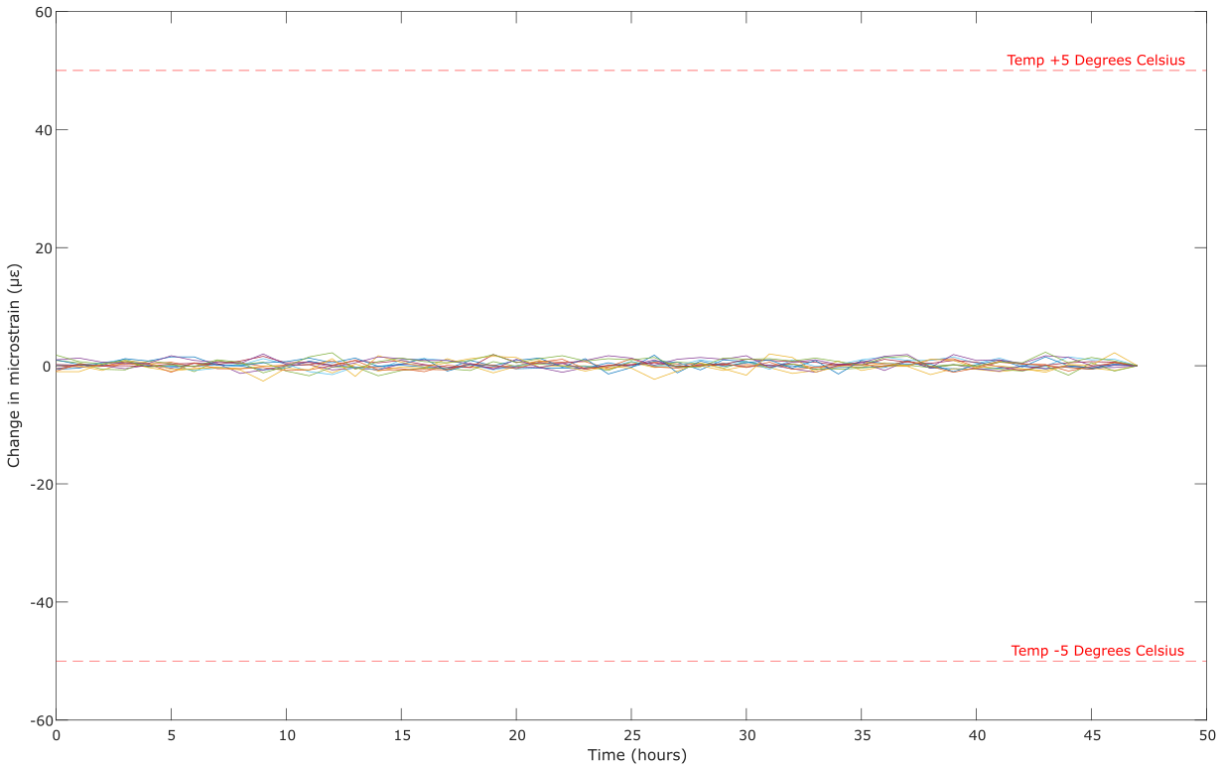

Figure A-3. Change in microstrain versus time after rainfall event 3 and 4.